

# Gauge-invariant theory of optical response to THz pulses in $s$ -wave and $(s+p)$ -wave superconducting semiconductor quantum wells

T. Yu\* and M. W. Wu†

*Hefei National Laboratory for Physical Sciences at Microscale, Department of Physics,  
and CAS Key Laboratory of Strongly-Coupled Quantum Matter Physics,  
University of Science and Technology of China, Hefei, Anhui, 230026, China*

(Dated: October 20, 2018)

We investigate the optical response to the THz pulses in the  $s$ -wave and  $(s+p)$ -wave superconducting semiconductor quantum wells by using the gauge-invariant optical Bloch equations, in which the gauge structure in the superconductivity is explicitly retained. By using the gauge transformation, not only can the microscopic description for the quasiparticle dynamics be realized, but also the dynamics of the condensate is included, with the superfluid velocity and the effective chemical potential naturally incorporated. We reveal that the superfluid velocity itself can contribute to the pump of quasiparticles (pump effect), with its rate of change acting as the drive field to drive the quasiparticles (drive effect). Specifically, the drive effect can contribute to the formation of the blocking region for the quasiparticle, which directly suppresses the anomalous correlation of the Cooper pairs. We find that both the pump and drive effects contribute to the oscillations of the Higgs mode with twice the frequency of the optical field. However, it is shown that the contribution from the drive effect to the excitation of Higgs mode is dominant as long as the driven superconducting momentum is less than the Fermi momentum. This is in contrast to the conclusion from the Liouville or Bloch equations in the literature, in which the drive effect on the anomalous correlation is overlooked with only the pump effect considered. Furthermore, in the gauge-invariant optical Bloch equations, the charge neutrality condition is *consistently* considered based on the two-component model for the charge, in which the charge imbalance of quasiparticles can cause the fluctuation of the effective chemical potential. It is predicted that during the optical process, the quasiparticle charge imbalance can be induced by both the pump and drive effects, leading to the fluctuation of the chemical potential. This fluctuation of the chemical potential is further demonstrated to directly lead to a relaxation channel for the charge imbalance even with the elastic scattering due to impurities. This is contrast to the previous understanding that in the isotropic  $s$ -wave superconductivity, the impurity scattering cannot cause any charge-imbalance relaxation. Furthermore, it is revealed that when the momentum scattering is weak (strong), the charge-imbalance relaxation is enhanced (suppressed) by the momentum scattering. Finally, we predict that in the  $(s+p)$ -wave superconducting (100) quantum wells, with the vector potential parallel to the quantum wells, the optical field can cause the total spin polarization of Cooper pairs, oscillating with the frequency of the optical field. The direction of the total Cooper-pair spin polarization is shown to be parallel to the vector potential.

PACS numbers: 74.40.Gh, 74.25.Gz, 74.25.N-, 73.21.Fg

## I. INTRODUCTION

In recent decades, the nonequilibrium property of superconductors has attracted much attention for providing new understandings in superconductivity<sup>1–8</sup> and/or exploring novel phases or regimes.<sup>9–14</sup> Among them, the optical response plays an important role in both linear<sup>15–19</sup> and nonlinear regimes.<sup>20–29</sup> The former has been well established from the understanding of the optical conductivity in the linear response of the superconducting state, which sheds light on the determination of the pairing symmetry of the superconducting order parameter.<sup>15–18</sup> The latter is inspired by the recently-developed THz technique, whose frequency lies around the superconducting gap.<sup>20–29</sup> With an intense THz optical field, the superconductor can be even excited to the states far away from the equilibrium, opening a window to reveal the dynamical properties of both the Bogoliubov quasiparticles and the condensate.<sup>20–29</sup>

In the linear regime, in the dirty limit at zero temperature, Mattis and Bardeen<sup>15</sup> revealed that the optical absorption is realized by breaking the Cooper pairs into the quasi-electron and quasi-hole when the photon energy is larger than twice the magnitude of the superconducting gap.<sup>16,17</sup> Nevertheless, in the early-stage work,<sup>15</sup> a physical optical conductivity is established only for a specific gauge with transverse vector potential and zero scalar potential.<sup>15–17</sup> A gauge-invariant description with charge conservation for the optical conductivity tensor is later established by Nambu based on the generalized Ward's identity,<sup>30,31</sup> in which the collective excitation is revealed to cancel the unphysical longitudinal current.<sup>16,17,19</sup> Furthermore, Ambegaokar and Kadanoff<sup>32</sup> showed that in the long wave limit, the collective mode can be actually described as a state in which the *superconducting phase* of the order parameter varies periodically in time and space.<sup>16,19,32–36</sup> Actually, without considering the response of the order parameter to the optical field, the absence of the charge conservation naturally arises be-

cause the particle number is not a conserved quantity in the mean-field description of the superconductor with a *global*  $U(1)$  symmetry spontaneously broken.<sup>16,19,30,33,34</sup>

When the photon energy is far below the superconducting gap, a simple physical picture for the optical response can be captured based on the two-fluid model, in which the optical conductivity at *finite* frequency  $\omega$  reads<sup>18,20–22,24</sup>

$$\sigma(\omega) = \frac{\rho_n e^2 \tau}{m^*} \frac{1}{1 + \omega^2 \tau^2} + i \left( \frac{\rho_n e^2 \tau}{m^*} \frac{\omega \tau}{1 + \omega^2 \tau^2} + \frac{\rho_s e^2}{m^*} \frac{1}{\omega} \right). \quad (1)$$

Here,  $\rho_n$  and  $\rho_s$  denote the normal-fluid and super-fluid densities in the *equilibrium* state, respectively;  $m^*$  is the effective mass of the electron; and  $\tau$  represents the momentum relaxation time. Based on Eq. (1), the optical absorption can be well understood from the electric current driven by the optical field.<sup>15–18</sup> In the clean limit, the optical conductivity is purely imaginary with the phase difference between the induced current and the optical field being exactly  $\pi/2$ , and hence no optical absorption is expected. Nevertheless, in the dirty sample, the real part of the optical conductivity arises due to the existence of the normal-fluid, which contributes to the electric current in phase to the optical field, and hence, the optical absorption. Thus, in the pump-probe measurement, after strongly excited by the pump field, the non-equilibrium normal-fluid and super-fluid densities can be estimated from the optical response to the probe field with photon energy far below the superconducting gap.<sup>20–22,24</sup> However, to the best of our knowledge, a microscopic theoretical-description for the evolution of the normal- and super-fluids from the equilibrium state to the non-equilibrium ones is still lacking.

In the nonlinear regime, in which the superconducting state can be markedly influenced by the optical field, the experimental<sup>25–29</sup> and theoretical<sup>13,14,37–46</sup> studies are still in progress. Very recently, it was reported in several experiments in the film of the conventional superconducting metal that the oscillations of the Higgs mode, i.e., the fluctuation of the order-parameter magnitude, can be excited by the intense THz field.<sup>25–29</sup> It is revealed that the oscillation frequency of the Higgs mode is twice the frequency of the THz field, no matter the photon energy is larger or smaller than twice the magnitude of the superconducting gap.<sup>28,29</sup> Moreover, a large THz third-harmonic generation was reported when the photon energy is tuned to be resonant with the superconducting gap.<sup>28,29</sup> Finally, it was discovered that there exists plateau for the Higgs mode after the THz pulse in most situations, whose value increases with the increase of the field intensity.<sup>26,27</sup> These observations indicate that there exists strong optical absorption with the quasiparticles considerably excited by the strong optical field.<sup>26–29</sup>

These experimental findings have been theoretically clarified based on the Liouville equation<sup>37,38,40</sup> or the Bloch equation<sup>28,29,39,41–44,46</sup> derived in the Anderson pseudospin representation<sup>47</sup> *in the clean limit*. Specifi-

cally, the optical absorption in the clean limit is naturally understood by the nonlinear term proportional to  $\mathbf{A}^2$ , with  $\mathbf{A}$  standing for the vector potential of the optical field. It is shown that this non-linear term contributes to the precessions between the quasi-electron and quasi-hole states,<sup>37,38</sup> which directly contribute to the excitation of the quasiparticles (pump effect).<sup>13,14,37–46</sup> Thus, the optical absorption is realized in the clean limit due to this pump effect, from which the Cooper pairs are broken into the quasi-electrons and quasi-holes.<sup>20–29</sup> Furthermore, because the frequency of  $\mathbf{A}^2$  is  $2\omega$ , the pump effect contributes to the oscillation of the Higgs mode with twice the frequency of the optical field.<sup>37–44,46</sup> Moreover, it is revealed that the Higgs mode can be resonant with the optical field when the photon energy equals to the superconducting gap, which is further shown to contribute to the large third harmonic generation.<sup>28,29,45</sup>

However, there still exist several difficulties inherited in the Liouville<sup>37,38,40</sup> or Bloch<sup>39,41–44,46</sup> equations used in the literature. Firstly, the anomalous correlation is calculated between the two electrons with momenta  $\mathbf{k}$  and  $-\mathbf{k}$ , no matter the optical field is slowly or rapidly varied. This means that it is preconceived that no center-of-mass momentum  $\mathbf{q}$  of the Cooper pairs can be excited.<sup>37–44,46</sup> Nevertheless, in the nonlinear regime, with a strong electric field applied, a large supercurrent is expected to be induced, which should arise from the center-of-mass momentum of the Cooper pairs. It has been well understood that in the static situation, a large  $\mathbf{q}$  contributes to the Doppler shift in the energy spectra of the elementary excitation, which can lead to the formation of the blocking region with the anomalous correlation of the Cooper pairs significantly suppressed.<sup>48–55</sup> Nevertheless, the induction of the center-of-mass momentum for the Cooper pairs and its further influence on the superconducting state are absent in the description of the Liouville equation or the Bloch equation in the Anderson pseudospin representation.<sup>37–44,46</sup> In fact, in the Liouville equation, the generalized coordinate, i.e., the momentum  $\mathbf{k}$ , is treated to be time-independent or fixed, whereas the velocity field  $\mathbf{v}(\mathbf{k}) = \mathbf{k} - (e/c)\mathbf{A}$  located at the generalized coordinate varies with time. This is similar to the Euler description in the fluid mechanics, in contrast to the Lagrangian description with time-dependent generalized coordinate.<sup>56</sup> Thus, the anomalous correlation is always described between  $\mathbf{k}$  and  $-\mathbf{k}$  in the Liouville or Bloch equations used in the literature.<sup>37–44,46</sup>

Secondly, the scattering effect, which is inevitable in the dirty superconducting metal,<sup>39,40</sup> cannot be simply included in the Liouville equation in the presence of the optical field.<sup>57</sup> Moreover, a simple inclusion of the elastic scattering with the Boltzmann description<sup>1,5</sup> in the Liouville equation does not influence the calculated results, because the pump effect is isotropic in the momentum space.<sup>37–46</sup> However, this is un-physical because the normal-fluid can still be scattered. Finally, the *gauge invariance*<sup>16,30,33</sup> in the Liouville or the Bloch equations used in the literature is not clearly addressed.<sup>37–44,46</sup> On

one hand, two quantities in the vector potential, scalar potential and superconducting phase are simultaneously taken to be zero.<sup>16,30,33</sup> Specifically, with the vector potential chosen, the resulted physical current is shown to be proportional to  $\mathbf{A}$ , which is *not* a gauge-invariant physical quantity unless a transverse gauge for  $\mathbf{A}$  is further restricted.<sup>15,16</sup> On the other hand, from different choices of gauge, different forms of the equation can be expected. Specifically, with only the scalar potential, the  $\mathbf{A}^2$ -term vanishes and the electric field contributes to the drive field; whereas with only the superconducting phase  $\mathbf{q} \cdot \mathbf{r}$ , its rate of change can also contribute to a drive field.<sup>16,30,33,58</sup>

In fact, as pointed out by Nambu,<sup>30</sup> the absence of the gauge invariance in the theoretical description is equivalent to the breaking of the charge conservation.<sup>16,19,33,34</sup> By restoring the gauge invariance, in the linear regime, Nambu revealed a collective excitation stimulated in the optical process,<sup>30</sup> which was further shown by Ambegaokar and Kadanoff<sup>32</sup> to be described by a state with the period variations in time and space for the superconducting phase in the long-wave limit.<sup>16,19,32–36</sup> The temporal and spacial variations of the superconducting phase can further contribute to the effective chemical potential and superconducting velocity.<sup>16,19,32–36</sup> Then, it is inspired by this scheme<sup>16,19,30,33,34</sup> that with the gauge invariance retained in the kinetic equation, the collective excitation can also arise naturally.<sup>45</sup> Specifically, by noting that in the mean-field description based on the Bogoliubov-de Gennes (BdG) Hamiltonian, only the dynamics of the quasiparticle is considered. It has been suggested that the “condensate” can respond to the dynamics of the quasiparticles from the consideration of the gauge structure in superconductor,<sup>30</sup> with the charge conservation restored by the fluctuation of the chemical potential.<sup>59–69</sup>

One way to understand the interplay between the particle charge and chemical potential is based on the two-component model for the charge.<sup>1–4,59–62</sup> In the two-component model, the electron charge is treated to be carried by the quasiparticle and condensate, respectively. This can be easily seen in the electrical injection process. In that process, the injection of one electron with charge  $e$  into the *conventional* superconductor can add a quasiparticle with charge  $e(u_{\mathbf{k}}^2 - v_{\mathbf{k}}^2)$  and one Cooper pair with charge  $2ev_{\mathbf{k}}^2$ , respectively. Here,  $u_{\mathbf{k}}$  and  $v_{\mathbf{k}}$  comes from the Bogoliubov transformation with  $u_{\mathbf{k}}^2 + v_{\mathbf{k}}^2 = 1$ , indicating the charge conservation in the electrical injection process.<sup>59–61</sup> Thus, the fluctuation of the quasiparticle charge is associated with the fluctuation of the condensate density.<sup>1–4,59–62</sup> This is consistent with the conjugacy relationship between the particle number and superconducting phase.<sup>30,34</sup>

Furthermore, in the dynamical process, the charges for the quasiparticle and condensate can both be deviated from their equilibrium values. This is referred to as the charge imbalance,<sup>1–4,59–61,70,71</sup> which has been measured for both the quasiparticle<sup>2,59,60,70,71</sup> and condensate.<sup>23</sup>

For the quasiparticle, due to the momentum-dependence of the charge, its non-equilibrium distribution can lead to the charge imbalance, whose creation and relaxation are intensively studied in the electrical experiment.<sup>1,59–61,70,71</sup> It is so far widely believed that for the isotropic  $s$ -wave superconductor, the *elastic* scattering due to the impurity cannot cause the relaxation of the charge imbalance.<sup>1,2,59,60</sup> This is because there exists the coherence factor  $(u_{\mathbf{k}}u_{\mathbf{k}'} - v_{\mathbf{k}}v_{\mathbf{k}'})$  in the scattering potential, where  $\mathbf{k}$  and  $\mathbf{k}'$  are the initial and final momenta during the scattering, due to which the elastic scattering cannot exchange the electron-like and hole-like quasiparticles.<sup>1,2,59,60</sup> However, in that relaxation process, the condensate is assumed to be in its equilibrium state, meaning that the charge conservation or neutrality is not explicitly considered in the literature. Moreover, the correlation between the quasi-electron and quasi-hole is often neglected.<sup>1–4,60,61</sup> Thus, it is essential to check the influence of the condensate on the charge-imbalance relaxation in the framework of charge neutrality. Furthermore, although the charge imbalance including its creation and relaxation is intensively studied in the electrical experiment,<sup>1–4,59–61,70,71</sup> it has yet been well investigated in the optical process.<sup>23</sup>

So far we have addressed the experimental and theoretical investigations on the optical response in the conventional superconductivity, in which the Cooper pairs do not carry any net spin. As the optical method is often used to create and manipulate the electron spins in semiconductors<sup>57,72–74</sup> or topological insulator<sup>75</sup> by inducing an effective spin-orbit coupling (SOC), it is intriguing to consider the possibility of the creation and manipulation for the Cooper-pair spin polarization. This is possible in the triplet superconductivity as the triplet Cooper pairs can carry net spin polarization.<sup>76–81</sup> It is noticed that the inclusion of the optical field can break the time-reversal symmetry. Previous works have shown that the breaking of the time-reversal symmetry by the Zeeman field<sup>82</sup> or the supercurrent<sup>83</sup> can induce the Cooper-pair spin polarization. In the former situation, for the conventional  $s$ -wave superconductor in proximity to a ferromagnet, the triplet Cooper pairing can be induced in the superconductor-ferromagnet interface.<sup>7,8,78,84–87</sup> Then Jacobsen *et al.* showed that in the superconductor-ferromagnet-superconductor Josephson junction, when there exists the SOC in the superconductor-ferromagnet interface, the net spin polarization of triplet Cooper pairs can be created, and a superconducting spin flow with spin-flip immunity can be realized.<sup>82</sup> In the latter situation, Tkachov pointed out that in noncentrosymmetric superconductors, a *nonunitary* triplet pairing<sup>9,76,88</sup> can be induced by the supercurrent, which contributes to the spin polarization of triplet Cooper pairs and can be detected by the magnetoelectric Andreev effect.<sup>83</sup> It is further noted that the optical field can also induce a supercurrent in noncentrosymmetric superconductivity, which is expected to dynamically generate the Cooper-pair spin polarization.

Recently, the proximity-induced superconductivity has been realized in InAs<sup>53,89,90</sup> and GaAs<sup>91-93</sup> heterostructures. Thus, based on the well-developed techniques in semiconductor optics,<sup>94-96</sup> the superconducting semiconductor quantum wells (QWs) can provide an ideal platform to study the optical response of superconductivity. Compared to the film of the superconducting metal, the QWs can be synthesized to be extremely clean. Furthermore, the material parameters in the QWs, e.g., the electron density, the strength of the SOC and the interaction strengths including the Coulomb, electron-phonon and electron-impurity interactions, can be easily tuned. Moreover, in the QWs, the simple Fermi surface and exactly-known interaction forms can significantly reduce the difficulties in the comparison between the theory and experiment. Finally, the predictions revealed in the superconducting QWs can still shed light on the optical response in the superconducting metal even with complex Fermi surfaces.

In the present work, we investigate the optical response to the THz pulses in both the  $s$ -wave and  $(s+p)$ -wave superconducting semiconductor QWs. The gauge-invariant optical Bloch equations are set up via the gauge-invariant nonequilibrium Green function approach,<sup>54,94,97-99</sup> in which the gauge-invariant Green function with the Wilson line<sup>94,98,100</sup> is constructed by using the gauge structure revealed by Nambu.<sup>30</sup> In the optical Bloch equations, the structure can be easily captured by a special gauge, in which the superconducting phase is chosen to be zero among the vector potential, scalar potential and superconducting phase. This gauge is referred to as the  $\mathbf{p}_s$ -gauge here, with  $\mathbf{p}_s$  being the superfluid momentum driven by the optical field. It is noted that this superfluid momentum directly contributes to the center-of-mass momentum of Cooper pairs. Furthermore, in the  $\mathbf{p}_s$ -gauge, not only can the microscopic description for the quasiparticle dynamics be realized, but also the dynamics of the condensate is included, with the superconducting velocity and the effective chemical potential naturally incorporated. Then in the derived gauge-invariant optical Bloch equations, this superconducting velocity  $\propto \mathbf{p}_s^2$  is shown to directly contribute to the pump of the quasiparticles (pump effect), whose rate of change  $\partial_t \mathbf{p}_s$  induces a drive field to drive the quasiparticle (drive effect). We find that both the pump and drive effects contribute to the oscillation of the Higgs mode with twice the frequency of the optical field. However, it is shown that the contribution from the drive effect to the excitation of Higgs mode is dominant as long as the superconducting momentum  $\mathbf{p}_s$  is smaller than the Fermi momentum  $k_F$ , thanks to the efficient suppression of the pump effect by the Pauli blocking. This is in sharp contrast to the results from the Liouville<sup>37,38,40</sup> or Bloch<sup>39,41-44,46</sup> equations in the literature, where only the pump effect is considered and the effects of the center-of-mass momentum on the superconducting state are overlooked. The influence of the electron-impurity scattering is also addressed, which is shown to further suppress the Cooper pairing on the

basis of the drive effect.

The physical picture for the suppression of the anomalous correlation of Cooper pairs by the optical field can be understood as follows. Thanks to the drive of the optical field, the electron states are drifted, obtaining exactly the center-of-mass momentum  $\mathbf{p}_s$  in the impurity-free situation. The drift states of electrons are schematically presented in Fig. 1 with the Fermi surface labeled by the red chain curve. In Fig. 1, without loss of generality, the superconducting momentum is taken to be along the  $\hat{x}$ -direction, i.e.,  $\mathbf{p}_s = p_s \hat{x}$ , with  $p_s < 0$ . It can be seen that with the drift of the electron states, a blue region labeled by “B” arises, in which the electrons deviate from their equilibrium states. Actually, these electrons are directly excited to be the quasiparticles, whose population can be close to one.<sup>48-51,54,55</sup> By using the terminology in the Fulde-Ferrell-Larkin-Ovchinnikov (FFLO) state,<sup>48-50</sup> this blue region populated by the quasiparticles is referred to as the blocking region.

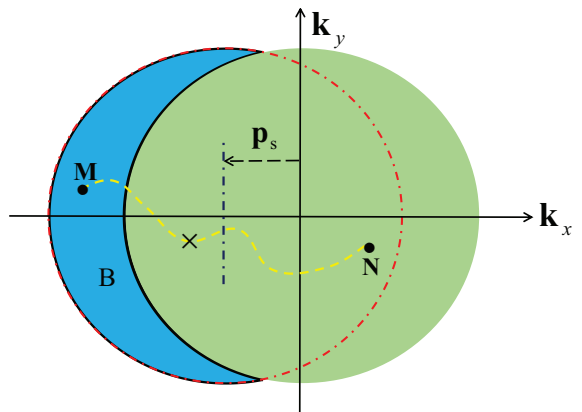


FIG. 1: (Color online) Schematic of the electron drift states in response to the optical field, with the Fermi surface labeled by the red chain curve. Here, the superconducting momentum  $\mathbf{p}_s = p_s \hat{x}$  with  $p_s < 0$ . With the drift of the electron states, a blue region labeled by “B” arises, in which the electrons deviate from their equilibrium states. Actually, these electrons are directly excited to be the quasiparticles, whose population can be close to one.<sup>48-51,54,55</sup> By using the terminology in the FFLO state,<sup>48-50</sup> this blue region populated by the quasiparticles is referred to as the blocking region. Furthermore, due to the induction of the center-of-mass momentum for the Cooper pairs by the applied optical field, the two electrons with momenta  $\mathbf{k} + \mathbf{p}_s$  and  $-\mathbf{k} + \mathbf{p}_s$  are paired together. Nevertheless, once the electrons are excited in the blocking region, they no longer participate in the Cooper pairing.<sup>48-51,54,55</sup> For instance, the electron labeled by “N” cannot pair with its corresponding one labeled by “M” in the blocking region, which has been excited to be the quasiparticle. Accordingly, the anomalous correlation is directly suppressed due to the drift of the electron states.

Furthermore, it is noted that the applied optical field breaks the time-reversal symmetry. Thus, the paired electrons do not necessarily come from two time-reversal partners with momenta  $\mathbf{k}$  and  $-\mathbf{k}$ . On the contrary, due to the induction of the center-of-mass momentum for the

Cooper pairs by the applied optical field, the two electrons with momenta  $\mathbf{k} + \mathbf{p}_s$  and  $-\mathbf{k} + \mathbf{p}_s$  are paired together. Nevertheless, once the electrons are excited in the blocking region, they no longer participate in the Cooper pairing.<sup>48–51,54,55</sup> One typical example is shown in Fig. 1, in which the electron labeled by “N” cannot pair with its old partner labeled by “M” in the blocking region, which has been excited to be the quasiparticle. Consequently, the anomalous correlation in the blocking region is significantly suppressed, directly leading to the suppression of the magnitude of the order parameter.<sup>50,54,55</sup> This is responsible for the oscillation of the Higgs mode. Nevertheless, at high frequency, this oscillation is suppressed due to the suppression of the drift effect and hence the range of the blocking region. This picture is consistent with the *static* case when the center-of-mass momentum of the Cooper pairs emerges due to either the spontaneous symmetry-breaking<sup>48–50</sup> or the supercurrent.<sup>51,54,55</sup>

In the derived optical Bloch equations, the charge neutrality condition is consistently considered based on the two-component model for the charge, in which the induction of the charge imbalance of quasiparticles can cause the fluctuation of the condensate chemical potential.<sup>1–4,59–61</sup> We predict that during the optical process, the charge imbalance can be created by both the pump and drive effects, with the former arising from the AC Stark effect and the latter coming from the breaking of Cooper pairs by the electrical field. The induction of the charge imbalance directly leads to the fluctuation of the chemical potential. This fluctuation is further found to directly provide a relaxation channel for the charge imbalance even with the elastic scattering due to impurities. This is in contrast to the previous understanding that in the isotropic *s*-wave superconductivity, the impurity scattering cannot cause any charge-imbalance relaxation.<sup>2,59,60</sup> Specifically, we reveal that when the momentum scattering is weak (strong), the charge-imbalance relaxation is enhanced (suppressed) by the momentum scattering.

We demonstrate that the fluctuation of the condensate chemical potential can *first* induce the quasiparticle correlation between the quasi-electron and quasi-hole, which *then* provides the charge-imbalance relaxation channel for the quasiparticle populations *in the presence of the elastic momentum scattering*. In the previous works, it was revealed that in the presence of the impurities, the charge-imbalance relaxation is induced by the direct scattering of quasiparticles between the electron- and hole-like branches,<sup>2,59,60</sup> during which the quasiparticle number is conserved. Nevertheless, this is demonstrated to be forbidden in the isotropic *s*-wave superconductors.<sup>2,59,60</sup> Differing from this charge-imbalance relaxation channel,<sup>2,59,60</sup> in this work, the charge-imbalance relaxation is actually caused by the direct annihilation of the quasiparticles in the quasi-electron and quasi-hole bands, in which the quasiparticle-number conservation is broken. These two charge-imbalance relaxation channels are schematically shown

in Fig. 2, labeled by “①” and “②”, respectively. Specifically, process ① represents the direct scattering of quasiparticles between the electron- and hole-like branches. Whereas in process ②, the quasi-electron and quasi-hole, labeled by “M” and “N”, become correlated due to the fluctuation of the effective chemical potential, which then annihilate into one Cooper pair due to the momentum scattering.

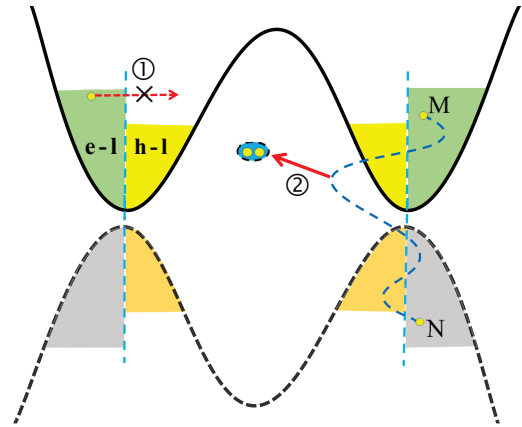


FIG. 2: (Color online) Schematic of the charge-imbalance relaxation channels. The upper and lower bands, plotted by the black solid and dashed curves, represent the quasi-electron and quasi-hole bands, respectively. In the quasi-electron (quasi-hole) band, the green (gray) and yellow (orange) regions denote the electron- (hole-) and hole-like (electron-like) quasi-electrons (quasi-holes), respectively. One sees that the quasi-electron number in the electron-like branch is larger than the one in the hole-like branch. In this situation, the charge imbalance is created with net negative charges. The two charge-imbalance relaxation channels labeled by “①” and “②” can be understood as follows. Process ① has been addressed in the previous works, representing the direct scattering of quasiparticles between the electron- and hole-like branches, which is actually forbidden in the elastic scattering process in the isotropic *s*-wave superconductor.<sup>2,59,60</sup> In process ②, the quasi-electron and quasi-hole, labeled by “M” and “N”, become correlated due to the fluctuation of the effective chemical potential, which then annihilate into one Cooper pair due to the momentum scattering. Here, one notes that the momenta of the correlated quasi-electron (“M”) and quasi-hole (“N”) are the same, in consistent with the Bogoliubov transformation [refer to Eq. (31) in the main text]. Thus, the annihilation of extra quasiparticles directly leads to the charge-imbalance relaxation.

Actually, it is overlooked in the previous studies<sup>2,59,60</sup> that the non-equilibrium effective chemical potential itself can induce the precession between the quasi-electron and quasi-hole states and hence the quasiparticle correlation.<sup>2,59,60</sup> The quasiparticle correlation is crucial to induce the quasiparticle-number fluctuation. As addressed in our previous work,<sup>54</sup> the induction of the quasiparticle correlation is related to the process of the condensation with two quasiparticles binding into one Cooper pair in the condensate, or vice versa.<sup>60,101,102</sup> These processes can directly cause *the annihilation of*

the extra quasiparticles in the quasi-electron or quasi-hole bands, inducing the charge-imbalance relaxation for the quasiparticles. Meanwhile, with the condensation or breaking of the Cooper pairs in the condensate, the fluctuation of the effective chemical potential is also induced. If only the induction of the quasiparticle correlation was not influenced by the momentum scattering, the charge-imbalance relaxation rate would be proportional to the electron-impurity scattering strength. Nevertheless, it is further revealed that the induction of the quasiparticle correlation can be suppressed by the impurity scattering. Thus, the competition between the relaxation channels due to the quasiparticle correlation and population leads to the non-monotonic dependence on the momentum scattering for the charge-imbalance relaxation.

Finally, we predict that in the  $(s+p)$ -wave superconducting InSb (100) QWs, with the vector potential being along the  $\hat{\mathbf{x}}$ -direction, the optical field can cause the spin polarization of Cooper pairs, which is also along the  $\hat{\mathbf{x}}$ -direction and oscillates with the frequency of the optical field. Specifically, in our previous work, it has been revealed that in InSb (100) QWs in proximity to an  $s$ -wave superconductor, due to the Rashba-like SOC, there exists  $p$ -wave triplet Cooper correlation in  $(p_x \pm ip_y)$ -type,<sup>103</sup> represented by  $[\mathbf{l}(\mathbf{k}) \cdot \boldsymbol{\sigma}]i\sigma_y$  with  $\boldsymbol{\sigma} = (\sigma_x, \sigma_y, \sigma_z)$  denoting the Pauli matrices. In the equilibrium state, the  $\mathbf{l}$ -vector of the triplet Cooper correlation is parallel to the effective magnetic field  $\boldsymbol{\Omega}(\mathbf{k})$  due to the SOC in the momentum space. Here, the  $\mathbf{l}$ -vector is defined from

$$[\mathbf{l}(\mathbf{k}) \cdot \boldsymbol{\sigma}]i\sigma_y = \begin{pmatrix} F_{\uparrow\uparrow}(\mathbf{k}) & F_{\uparrow\downarrow}(\mathbf{k}) \\ F_{\uparrow\downarrow}^*(\mathbf{k}) & F_{\downarrow\downarrow}(\mathbf{k}) \end{pmatrix}, \quad (2)$$

with  $F(\mathbf{k})$  representing the anomalous correlations of triplet Cooper pairs.<sup>9</sup>

Actually, the anomalous correlations  $F(\mathbf{k})$ , calculated by the optical Bloch equations in this work, are just the Fourier components of the wavefunction of triplet Cooper pairs in the spatial space.<sup>9</sup> By further considering the spin space, the wavefunction of the triplet Cooper pairs is expressed as<sup>9</sup>

$$F_t(\mathbf{r}) = F_{\uparrow\uparrow}(\mathbf{r})|\uparrow_1\rangle|\uparrow_2\rangle + F_{\downarrow\downarrow}(\mathbf{r})|\downarrow_1\rangle|\downarrow_2\rangle + F_{\uparrow\downarrow}(\mathbf{r})(1/\sqrt{2})(|\uparrow_1\rangle|\downarrow_2\rangle + |\downarrow_1\rangle|\uparrow_2\rangle). \quad (3)$$

Here,  $F_{\uparrow\uparrow}(\mathbf{r})$ ,  $F_{\downarrow\downarrow}(\mathbf{r})$  and  $F_{\uparrow\downarrow}(\mathbf{r})$  denote the wavefunctions of the triplet Cooper pairs with total spin  $S_z = 1, -1$  and  $0$ ,<sup>9</sup> respectively, with  $\mathbf{r}$  being the relative coordinate for the two electrons (labeled by “1” and “2”) in the Cooper pairs. Thus, with the  $\hat{\mathbf{z}}$ -direction of the spin operator chosen to be perpendicular to the QWs, in the equilibrium state of superconducting InSb (100) QWs,  $F_{\uparrow\downarrow}(\mathbf{r}) = 0$  and  $|F_{\uparrow\uparrow}(\mathbf{r})| = |F_{\downarrow\downarrow}(\mathbf{r})|$ .<sup>103</sup> From the Cooper-pair wavefunction, the total spin polarization of Cooper pairs is determined by

$$\mathbf{P}_C = \int d\mathbf{r} F_t^*(\mathbf{r}) \hat{\mathbf{S}} F_t(\mathbf{r}) \propto \sum_{\mathbf{k}} i\mathbf{l}(\mathbf{k}) \times \mathbf{l}^*(\mathbf{k}), \quad (4)$$

with  $\hat{\mathbf{S}} \equiv \hat{\mathbf{s}}_1 + \hat{\mathbf{s}}_2$  being the total spin operator by the sum of the spin operators  $\hat{\mathbf{s}}_1$  and  $\hat{\mathbf{s}}_2$  of two electrons.

When the optical field with the vector potential along the  $\hat{\mathbf{x}}$ -direction is applied to the superconducting system, the superconducting velocity is induced, which is shown to contribute to an effective SOC along the  $\hat{\mathbf{x}}$ -direction. This effective SOC can cause the precession of the  $\mathbf{l}$ -vectors, with a component perpendicular to  $\boldsymbol{\Omega}(\mathbf{k})$  induced. Thus, with the Cooper-pair spin vector defined as  $\mathbf{n}(\mathbf{k}) = i\mathbf{l}(\mathbf{k}) \times \mathbf{l}^*(\mathbf{k})$ ,<sup>76,83,88,104</sup> whose momentum integral contributes to the total Cooper-pair spin polarization  $\mathbf{P}_C$  [refer to Eq. (4)], the  $\hat{\mathbf{x}}$ -component of  $\mathbf{P}_C$  can be induced. Specifically, the  $\hat{\mathbf{x}}$ -component of the Cooper-pair spin polarization is  $\mathbf{P}_C^x = (1/\sqrt{2}) \int d\mathbf{r} \{ F_{\uparrow\downarrow}^*(\mathbf{r}) [F_{\uparrow\uparrow}(\mathbf{r}) + F_{\downarrow\downarrow}(\mathbf{r})] + \text{h.c.} \}$ . Accordingly, one finds that the excitation of the  $\hat{\mathbf{x}}$ -component of the Cooper-pair spin polarization is the reflection of the optical-induction of the triplet Cooper-pair wavefunction  $F_{\uparrow\downarrow}(\mathbf{r})$  with  $S_z = 0$ . Actually, the Fourier component of  $F_{\uparrow\downarrow}(\mathbf{r})$  is exactly  $\mathbf{l}_z(\mathbf{k})$ .<sup>76,83,88,104</sup> Furthermore, we reveal that the Cooper-pair spin polarization is proportional to the superconducting velocity, which oscillates with the frequency of the optical field.

This paper is organized as follows. We first focus on the  $s$ -wave superconducting semiconductor QWs in Sec. II, whose framework is then generalized to the  $(s+p)$ -wave one in (100) QWs in Sec. III. Specifically, for the  $s$ -wave [( $s+p$ )-wave] superconducting QWs, we present the Hamiltonian in Sec. II A (Sec. III A); then in Sec. II B (Sec. III B), the optical Bloch equations are derived via the gauge-invariant non-equilibrium Green function approach; the numerical results are presented in Sec. II C (Sec. III C). We conclude and discuss in Sec. IV.

## II. $s$ -WAVE SUPERCONDUCTING QWs

In this section, we investigate the optical response to the THz pulses in the  $s$ -wave superconducting QWs, which can be realized in the GaAs QWs in proximity to an  $s$ -wave superconductor with negligible SOC. We first present the Hamiltonian, in which the gauge structure is emphasized (Sec. II A). Then the optical Bloch equations via the nonequilibrium Green function method with the generalized Kadanoff-Baym (GKB) ansatz are set up, in which the gauge invariance is retained explicitly by using the gauge-invariant Green function (Sec. II B).<sup>54,94,97–99</sup> Finally, we numerically calculate the optical response by solving the optical Bloch equations including the THz-field-induced oscillations of the Higgs mode and THz-field-induced charge imbalance, in which a novel charge-imbalance relaxation channel due to the elastic momentum scattering is revealed (Sec. II C).

### A. Hamiltonian and Gauge Structure

In the  $s$ -wave superconducting QWs with negligible SOC, the Hamiltonian is composed by the free BdG

Hamiltonian  $H_0$  and the interaction Hamiltonian including the electron-electron Coulomb, electron-phonon and electron-impurity interactions  $H_{ee}$ ,  $H_{ep}$  and  $H_{ei}$ . Specifically,  $H_0$  is written as ( $\hbar \equiv 1$  throughout this paper)

$$H_0 = \int \frac{d\mathbf{r}}{2} \Psi^\dagger \begin{pmatrix} \zeta_{\mathbf{k}}^-(x) + e\phi(x) & |\Delta| e^{i\zeta(x)} \\ |\Delta| e^{-i\zeta(x)} & -\zeta_{\mathbf{k}}^+(x) - e\phi(x) \end{pmatrix} \Psi, \quad (5)$$

in which  $\zeta_{\mathbf{k}}^\pm(x) = [\mathbf{k} \pm \frac{e}{c} \mathbf{A}(x)]^2 / (2m^*) - \mu$  with  $x \equiv (t, \mathbf{r})$  being the time-space point,  $\mathbf{A}(x)$  denoting the vector potential and  $\mu$  representing the chemical potential of the system;  $\Psi(x) = (\psi_\uparrow(x), \psi_\downarrow(x))^T$  is the particle field operator in the Nambu space;  $\phi(x)$  denotes the scalar potential;  $\Delta$  and  $\zeta(x)$  stand for the  $s$ -wave order parameter and the superconducting phase. The electron-electron, electron-phonon and electron-impurity interactions are written as

$$H_{ee} = \int \frac{d\mathbf{r}d\mathbf{r}'}{2} U(\mathbf{r} - \mathbf{r}') [\Psi^\dagger(\mathbf{r})\tau_3\Psi(\mathbf{r})] [\Psi^\dagger(\mathbf{r}')\tau_3\Psi(\mathbf{r}')] \quad (6)$$

$$H_{ep} = \frac{1}{2} \int d\mathbf{r}d\mathbf{r}' g^\lambda(\mathbf{r} - \mathbf{r}') \Psi^\dagger(\mathbf{r})\tau_3\Psi(\mathbf{r})\chi(\mathbf{r}'), \quad (7)$$

$$H_{ei} = \frac{1}{2} \int d\mathbf{r} \Psi^\dagger(\mathbf{r})V(\mathbf{r})\tau_3\Psi(\mathbf{r}), \quad (8)$$

respectively. Here,  $\boldsymbol{\tau} \equiv (\tau_1, \tau_2, \tau_3)$  represent the Pauli matrices in the Nambu space;  $U(\mathbf{r})$  and  $V(\mathbf{r})$  denote the screened Coulomb potentials whose expressions have been derived in Ref. 103;  $\chi(\mathbf{r})$  is the phonon field operator; and  $g^\lambda(\mathbf{r} - \mathbf{r}')$  stand for the electron-phonon interactions due to the deformation potential in the LA branch and piezoelectric coupling including LA and TA branches, with  $\lambda$  denoting the corresponding phonon branch.<sup>105,106</sup> Their Fourier components  $g^\lambda(\mathbf{p})$  are explicitly given in Refs. 105,106.

The gauge structure in the  $s$ -wave superconductivity was first revealed by Nambu.<sup>30,33,58</sup> By performing the gauge transformation, i.e.,

$$\Psi(x) \rightarrow e^{i\tau_3\Lambda(x)/2} \Psi(x), \quad (9)$$

the gauge invariance of the BdG Hamiltonian [Eq. (5)] requires the vector potential, scalar potential and superconducting phase transforming as<sup>30,33,58</sup>

$$\mathbf{A}(x) \rightarrow \mathbf{A}(x) + (c/2e)\nabla\Lambda(x), \quad (10)$$

$$\phi(x) \rightarrow \phi(x) - (1/2e)\partial_t\Lambda(x), \quad (11)$$

$$\zeta(x) \rightarrow \zeta(x) + \Lambda(x). \quad (12)$$

From Eqs. (10-12), one can construct the gauge-invariant physical quantities<sup>30,33,58</sup>

$$\mathbf{p}_s(x) = (1/2)\nabla\zeta(x) - (e/c)\mathbf{A}(x), \quad (13)$$

$$\mu_{\text{eff}}(x) = (1/2)\partial_t\zeta(x) + e\phi(x), \quad (14)$$

which represent the superconducting momentum and effective chemical potential. It is noted that the above two

gauge-invariant quantities are related by the acceleration relation<sup>30,33,58</sup>

$$\partial_t \mathbf{p}_s = \nabla \mu_{\text{eff}} + e\mathbf{E}, \quad (15)$$

which is valid under any circumstances. Thus, with an optical field applied to the superconducting system, Eq. (15) shows that in the homogeneous limit, a time-dependent superconducting momentum can be induced, which is always a transverse physical quantity in the presence of the optical field.<sup>15,30</sup>

## B. Optical Bloch Equations

In this section, we derive the optical Bloch equations in the  $s$ -wave superconducting QWs via the nonequilibrium Green function method with the GKB ansatz.<sup>54,73,94,97</sup> From Sec. II A, one notices that there exists a nontrivial gauge structure in the BdG Hamiltonian. To account for this gauge structure, the gauge-invariant Green function is used to obtain the gauge-invariant kinetic equations.<sup>94,98,99</sup>

### 1. Gauge-invariant Green function

The optical Bloch equations can be constructed from the “lesser” Green function  $G_{12}^< \equiv i\langle \Psi_2^\dagger \Psi_1 \rangle$ , in which  $1 \equiv x_1 = (t_1, \mathbf{r}_1)$  represents the time-space point and  $\langle \dots \rangle$  denotes the ensemble average.<sup>54,73,94</sup> With the gauge transformation in Eq. (9), the “lesser” Green function transforms as  $G_{12}^< \rightarrow e^{i\tau_3\Lambda(x_1)/2} G_{12}^< e^{-i\tau_3\Lambda(x_2)/2}$ . As in the kinetic equations *in the quasiparticle approximation*,<sup>94</sup> only the center-of-mass coordinates are retained, the gauge structure cannot be easily realized in the kinetic equations constructed from  $G_{12}^<$ .<sup>94,98</sup> Nevertheless, the gauge invariance can be retained by introducing the Wilson line to construct the gauge-invariant Green function,<sup>94,98,100</sup> which is constructed as

$$\tilde{G}_{12}^< = P e^{-ie \int_{x_1}^R A_j dx^j \tau_3} G_{12}^< e^{-ie \int_R^{x_2} A_j dx^j \tau_3}. \quad (16)$$

In Eq. (16),  $A_j dx^j \equiv \phi dt - (1/c)\mathbf{A} \cdot d\mathbf{r}$ ,  $R \equiv (\mathbf{R}, T) = ((\mathbf{r}_1 + \mathbf{r}_2)/2, (t_1 + t_2)/2)$  are the center-of-mass coordinates, and “ $P$ ” indicates that the line integral is path-dependent. Then by the gauge transformation in Eq. (9), the gauge-invariant Green function is transformed as  $\tilde{G}_{12}^< \rightarrow e^{i\tau_3\Lambda(R)/2} \tilde{G}_{12}^< e^{-i\tau_3\Lambda(R)/2}$ , in which the transformed phase only depend on the center-of-mass coordinates.

Finally, by choosing the path to be the straight line connecting  $x_1$  and  $x_2$ ,<sup>94,98</sup> the gauge-invariant Green function reads

$$\begin{aligned} \tilde{G}_{12}^< &= \exp \left[ ie \int_0^{\frac{1}{2}} d\lambda A_j(T + \lambda\tau, \mathbf{R} + \lambda\mathbf{r}) x^j \tau_3 \right] \\ &\times G_{12}^< \exp \left[ ie \int_{-\frac{1}{2}}^0 d\lambda A_j(T + \lambda\tau, \mathbf{R} + \lambda\mathbf{r}) x^j \tau_3 \right], \quad (17) \end{aligned}$$

in which  $x = (\tau, \mathbf{r}) = (t_1 - t_2, \mathbf{r}_1 - \mathbf{r}_2)$  are the relative coordinates.

## 2. Derivation on the optical Bloch equations

In this part, we derive the optical Bloch equations in the  $s$ -wave superconducting QWs, with special attention paid to the gauge structure. Accordingly, we do not specify any gauge in the beginning of the derivation, and finally choose a special gauge for the convenience of physical analysis and numerical calculation. Thus, in the derived equations, there exist  $\mathbf{A}(\mathbf{r}, t)$ ,  $\phi(\mathbf{r}, t)$  and  $\zeta(\mathbf{r}, t)$ , which are not physical quantities.

We begin from the two Dyson equations,<sup>54,73,94</sup>

$$i\partial_{t_1} G_{12}^< - H_{\mathbf{k}_1} G_{12}^< = \int d3(\Sigma_{13}^R G_{32}^< + \Sigma_{13}^< G_{32}^A), \quad (18)$$

$$-i\partial_{t_2} G_{12}^< - G_{12}^< \overleftarrow{H}_{\mathbf{k}_2} = - \int d3(G_{13}^R \Sigma_{32}^< + G_{13}^< \Sigma_{32}^A), \quad (19)$$

in which “ $R$ ” and “ $A$ ” label the retarded and advanced Green functions, and  $\Sigma$  are the self-energies contributed by the electron-electron and electron-impurity interactions.<sup>54,73,94</sup> In Eqs. (18) and (19),

$$H_{\mathbf{k}_1} = \begin{pmatrix} \frac{(\mathbf{k}_1 - \frac{e}{c}\mathbf{A}_1)^2}{2m^*} - \mu + e\phi_1 & |\Delta|e^{i\zeta_1} \\ |\Delta|e^{-i\zeta_1} & -\frac{(\mathbf{k}_1 + \frac{e}{c}\mathbf{A}_1)^2}{2m^*} + \mu - e\phi_1 \end{pmatrix}, \quad (20)$$

and

$$H_{\mathbf{k}_2} = \begin{pmatrix} \frac{(\mathbf{k}_2 + \frac{e}{c}\mathbf{A}_2)^2}{2m^*} - \mu + e\phi_2 & |\Delta|e^{i\zeta_2} \\ |\Delta|e^{-i\zeta_2} & -\frac{(\mathbf{k}_2 - \frac{e}{c}\mathbf{A}_2)^2}{2m^*} + \mu - e\phi_2 \end{pmatrix}. \quad (21)$$

We first present the derivation of the free terms in the kinetic equations including the coherent, pump, drive and diffusion terms, in which the gauge-invariant scheme is used. Specifically, from the left-hand side of Eqs. (18) and (19), one obtains the equations for the gauge-invariant Green function  $\tilde{G}_{12}^<$ . Then by using the gradient expansion, the kinetic equations are derived from the Fourier component of the gauge-invariant Green function  $\tilde{G}(\mathbf{k}, \omega; \mathbf{R}, T) = \int d\mathbf{r} d\tau e^{i\omega\tau - i\mathbf{k}\cdot\mathbf{r}} \tilde{G}_{12}^<$ . Finally, after the integration over the frequency, one obtains the optical Bloch equations for the  $2 \times 2$  density matrix in the Nambu space

$$\tilde{\rho}_{\mathbf{k}}(\mathbf{R}, T) = \int \frac{d\omega}{2\pi} \tilde{G}(\mathbf{k}, \omega; \mathbf{R}, T), \quad (22)$$

whose diagonal terms represent the distributions of electron and hole, and off-diagonal terms denote the anomalous correlations. Finally, the optical kinetic equations are written as

$$\begin{aligned} \frac{\partial \tilde{\rho}_{\mathbf{k}}}{\partial T} + i \left[ \left( \frac{\mathbf{k}^2}{2m^*} - \mu + e\phi \right) \tau_3, \tilde{\rho}_{\mathbf{k}} \right] + i \left[ \begin{pmatrix} 0 & |\Delta|e^{i\zeta(R)} \\ |\Delta|e^{-i\zeta(R)} & 0 \end{pmatrix}, \tilde{\rho}_{\mathbf{k}} \right] + i \left[ \frac{1}{2m^*} \left( \frac{e}{c}\mathbf{A} \right)^2 \tau_3, \tilde{\rho}_{\mathbf{k}} \right] + \frac{1}{2} \left\{ e\mathbf{E}\tau_3, \frac{\partial \tilde{\rho}_{\mathbf{k}}}{\partial \mathbf{k}} \right\} \\ - i \left[ \frac{1}{8m^*} \tau_3, \frac{\partial^2 \tilde{\rho}_{\mathbf{k}}}{\partial \mathbf{R}^2} \right] + \frac{1}{2} \left\{ \frac{\mathbf{k}}{m^*} \tau_3, \frac{\partial \tilde{\rho}_{\mathbf{k}}}{\partial \mathbf{R}} \right\} + \left[ \frac{e\mathbf{A}}{2m^*c} \tau_3, \frac{\partial \tilde{\rho}_{\mathbf{k}}}{\partial \mathbf{R}} \tau_3 \right] + \left[ \frac{e}{4m^*c} \nabla \cdot \mathbf{A} \tau_3, \tilde{\rho}_{\mathbf{k}} \tau_3 \right] = \frac{\partial \tilde{\rho}_{\mathbf{k}}}{\partial t} \Big|_{\text{HF}} + \frac{\partial \tilde{\rho}_{\mathbf{k}}}{\partial t} \Big|_{\text{scat}}, \quad (23) \end{aligned}$$

with  $\mathbf{E} = -\nabla_{\mathbf{R}}\phi - (1/c)\partial_T\mathbf{A}$ . Here,  $[A, B] = AB - BA$  and  $\{A, B\} = AB + BA$  represent the commutator and anti-commutator, respectively. It is noted that in the equation, the gradient expansion has been performed to the second order in  $\mathbf{R}$ , i.e., the sixth term on the left-hand side in Eq. (23), to retain the gauge-invariance structure in the optical kinetic equations.

In Eq. (23), on the left-hand side, the second and third terms represent the coherent terms contributed by the kinetic energy and the order parameter, respectively; the fourth term describes the pump term, as addressed in the Liouville equation in the literature;<sup>13,14,37-46</sup> the fifth term is the drive term, which can directly induce the center-of-mass momentum of the Cooper pairs [Eq. (15)];<sup>16,30,33</sup> the diffusion terms are contributed by the sixth to the ninth terms. On the right-hand side of the equation,  $\partial_t \tilde{\rho}_{\mathbf{k}}|_{\text{HF}}$  and  $\partial_t \tilde{\rho}_{\mathbf{k}}|_{\text{scat}}$  represent the

Hartree-Fock (HF) term contributed by the Coulomb interaction and scattering term due to the electron-impurity and electron-phonon interactions, which are derived from the right-hand side of Eqs. (18) and (19). The gauge-invariant versions of the scattering terms are complex.<sup>94,98,99</sup> Nevertheless, these terms can be approximated by the ones without gauge-invariant treatments as long as the applied field is not very strong with *the driven center-of-mass momentum of the system being much smaller than the Fermi momentum*  $k_{\text{F}}$ .<sup>58,94,99</sup> In this situation, the energy spectra is not significantly disturbed. The gauge structure of Eq. (23) is then checked by the gauge transformation  $\tilde{\rho}_{\mathbf{k}} \rightarrow e^{i\tau_3\Lambda(R)/2} \tilde{\rho}_{\mathbf{k}} e^{-i\tau_3\Lambda(R)/2}$ . The same gauge structures as Eqs. (10), (11) and (12) are obtained for the vector potential, scalar potential and superconducting phase.

For the convenience of the physical analysis and nu-



merical calculation, a specific gauge is chosen. It is noted that generally one cannot choose two quantities in the vector potential, scalar potential and superconducting phase to be zero. Nevertheless, in the Liouville and Bloch equations used in the literature, both the scalar potential and superconducting phase are taken to be zero.<sup>13,14,37-46</sup> Here, we choose a special gauge referred to as the  $\mathbf{p}_s$ -gauge, in which the superconducting phase  $\zeta$  is zero.<sup>33,107</sup> This can be realized by the gauge transformation  $\tilde{\rho}_{\mathbf{k}} \rightarrow e^{-i\tau_3\zeta(R)/2} \tilde{\rho}_{\mathbf{k}} e^{i\tau_3\zeta(R)/2} \equiv \rho_{\mathbf{k}}$  in Eq. (23). Then by using the definition of the superconducting momentum [Eq. (13)] and effective chemical potential [Eq. 14], the optical Bloch equations become

$$\begin{aligned} \frac{\partial \rho_{\mathbf{k}}}{\partial T} + i \left[ \left( \frac{\mathbf{k}^2}{2m^*} - \Phi \right) \tau_3, \rho_{\mathbf{k}} \right] + i \left[ \begin{pmatrix} 0 & |\Delta| \\ |\Delta| & 0 \end{pmatrix}, \rho_{\mathbf{k}} \right] \\ + i \left[ \frac{\mathbf{p}_s^2}{2m^*} \tau_3, \rho_{\mathbf{k}} \right] + \frac{1}{2} \left\{ \left( \frac{\partial \mathbf{p}_s}{\partial T} - \nabla_{\mathbf{R}} \mu_{\text{eff}} \right) \tau_3, \frac{\partial \rho_{\mathbf{k}}}{\partial \mathbf{k}} \right\} \\ + \frac{1}{2} \left\{ \frac{\mathbf{k}}{m^*} \tau_3, \frac{\partial \rho_{\mathbf{k}}}{\partial \mathbf{R}} \right\} - i \left[ \frac{\tau_3}{8m^*}, \frac{\partial^2 \rho_{\mathbf{k}}}{\partial \mathbf{R}^2} \right] - \left[ \frac{\mathbf{p}_s}{2m^*} \tau_3, \frac{\partial \rho_{\mathbf{k}}}{\partial \mathbf{R}} \tau_3 \right] \\ - \left[ \frac{1}{4m^*} \nabla_{\mathbf{R}} \cdot \mathbf{p}_s \tau_3, \rho_{\mathbf{k}} \tau_3 \right] = \frac{\partial \rho_{\mathbf{k}}}{\partial t} \Big|_{\text{HF}} + \frac{\partial \rho_{\mathbf{k}}}{\partial t} \Big|_{\text{scat}}, \quad (24) \end{aligned}$$

where  $\Phi = \mu - \mu_{\text{eff}}$  is the total chemical potential in the system including the contribution from the rate of change of the superconducting phase.

It is noted that in Eq. (24), the electric force  $e\mathbf{E}$  is replaced by  $\partial_T \mathbf{p}_s - \nabla_{\mathbf{R}} \mu_{\text{eff}}$  according to the acceleration relation [Eq. (15)]. Accordingly, in Eq. (24), only the gauge invariant physical quantities  $\mathbf{p}_s$  and  $\mu_{\text{eff}}$  appear. In fact, in the gauge-invariant framework, from any specific gauge at the beginning of the derivation, one can obtain Eq. (24) with the existence of both the pump and drive terms.<sup>94</sup> Moreover, in Eq. (24), with  $\mathbf{p}_s$  and  $\mu_{\text{eff}}$  describing the kinetics of the condensate, Eq. (24) not only describes the dynamics of the quasiparticle, but also includes the influence of the condensate. This is consistent with the two-component description for the charge, in which there exists interplay between the quasiparticle and condensate.<sup>1-4,59-61</sup>

When considering the optical excitation by the THz pulses in the superconductor, Eq. (24) can be significantly simplified. Often the spacial dependence in the optical field can be neglected, and hence Eq. (24) can be solved in the homogeneous limit. Specifically, with  $\Phi$ ,  $\mathbf{p}_s$  and  $\rho_{\mathbf{k}}$  being independent on  $\mathbf{R}$ , the optical Bloch equations [Eq. (24)] are reduced to

$$\begin{aligned} \frac{\partial \rho_{\mathbf{k}}}{\partial T} + i \left[ \left( \frac{\mathbf{k}^2}{2m^*} - \Phi \right) \tau_3, \rho_{\mathbf{k}} \right] + i \left[ \begin{pmatrix} 0 & |\Delta| \\ |\Delta| & 0 \end{pmatrix}, \rho_{\mathbf{k}} \right] \\ + i \left[ \frac{\mathbf{p}_s^2}{2m^*} \tau_3, \rho_{\mathbf{k}} \right] + \frac{1}{2} \left\{ \frac{\partial \mathbf{p}_s}{\partial T} \tau_3, \frac{\partial \rho_{\mathbf{k}}}{\partial \mathbf{k}} \right\} = \frac{\partial \rho_{\mathbf{k}}}{\partial t} \Big|_{\text{HF}} + \frac{\partial \rho_{\mathbf{k}}}{\partial t} \Big|_{\text{scat}}. \quad (25) \end{aligned}$$

It is addressed that Eq. (25) is different from the Liouville<sup>37,38,40</sup> or Bloch<sup>28,29,39,41-44,46</sup> equations used in the literature in several aspects. Firstly, the momenta of the two electrons participating in the anomalous correlation are no longer  $\mathbf{k}$  and  $-\mathbf{k}$  during the evolution. This is

because in the optical kinetic equation here, similar to the Boltzmann equation,<sup>5,67-69,94,108</sup> the Lagrangian description is used, in which the generalized coordinate evolves with time.<sup>56</sup> Thus, with the anomalous correlation represented by  $\langle c_{\mathbf{k}(T)} c_{\mathbf{k}'(T)} \rangle$  in which  $c_{\mathbf{k}}$  is the annihilation operator of the electron, the center-of-mass momentum of the Cooper pairs  $\mathbf{p}_s = [\mathbf{k}(T) + \mathbf{k}'(T)]/2$ . Then, with  $\partial_T \mathbf{k}(T) = \partial_T \mathbf{k}'(T) = e\mathbf{E}$ , the acceleration relation in the homogeneous limit [Eq. (15)] can be directly recovered. One sees that it is natural to include the contribution of the center-of-mass momentum in the anomalous correlation in our description. Secondly, in the homogeneous limit, with  $\mathbf{p}_s$  and  $\partial_T \mathbf{p}_s$  being transverse in the presence of the optical field [Eq. (15)], the obtained electrical current is perpendicular to the propagation direction of the optical field. Moreover, the obtained physical quantities are naturally gauge-invariant due to the gauge invariance in  $\mathbf{p}_s$  and  $\partial_T \mathbf{p}_s$ . Furthermore, the effective chemical potential naturally arises from the gauge-invariant treatment in the derivation, which corresponds to the collective excitation, evolving with time in the homogeneous limit.<sup>30,32,35,36</sup> Finally, the scattering term can be simply included in our description which is similar to its setup in the Boltzmann equation,<sup>5,67-69,94,108</sup> with the details addressed as follows.

In Eq. (25),  $\partial_t \rho_{\mathbf{k}}|_{\text{HF}}$  and  $\partial_t \rho_{\mathbf{k}}|_{\text{scat}}$  are derived in the GKB ansatz.<sup>54,103</sup> For the HF term, it is written as

$$\partial_t \rho_{\mathbf{k}}|_{\text{HF}} = i \sum_{\mathbf{k}'} \left[ U_{\mathbf{k}-\mathbf{k}'} \tau_3 (\rho_{\mathbf{k}'} - \rho_{\mathbf{k}'}^0) \tau_3, \rho_{\mathbf{k}} \right]. \quad (26)$$

In Eq. (26), it is assumed that the renormalization energy due to the Coulomb interaction has been included in the free BdG Hamiltonian [Eq. (5)], and hence the density matrix in the equilibrium state  $\rho_{\mathbf{k}}^0$  appears in the HF self-energy. Accordingly, the fluctuation of the order parameter is represented by

$$\delta \Delta(\mathbf{k}) = \sum_{\mathbf{k}'} U_{\mathbf{k}-\mathbf{k}'} (\rho_{\mathbf{k}',12} - \rho_{\mathbf{k},12}^0), \quad (27)$$

which can be treated as the Higgs mode when the phase fluctuation can be neglected.<sup>13,14,37-46</sup>

For the scattering terms, both the electron-impurity and electron-phonon interactions are considered, which are written as

$$\begin{aligned} \partial_t \rho_{\mathbf{k}}|_{\text{ei}} &= -\pi n_i \sum_{\mathbf{k}'} \sum_{\eta_1 \eta_2 = \pm} |V_{\mathbf{k}-\mathbf{k}'}|^2 \delta(E_{\mathbf{k}'\eta_1} - E_{\mathbf{k}\eta_2}) \\ &\times [\tau_3 \Gamma_{\mathbf{k}'\eta_1} \tau_3 \Gamma_{\mathbf{k}\eta_2} \rho_{\mathbf{k}} - \tau_3 \rho_{\mathbf{k}'} \Gamma_{\mathbf{k}'\eta_1} \tau_3 \Gamma_{\mathbf{k}\eta_2} + \text{H.c.}], \quad (28) \\ \partial_t \rho_{\mathbf{k}}|_{\text{ep}} &= -\pi \sum_{\mathbf{k}' k_z} \sum_{\eta_1 \eta_2 = \pm} |g_{\mathbf{k}-\mathbf{k}', k_z}^\lambda|^2 \delta(E_{\mathbf{k}'\eta_1} - E_{\mathbf{k}\eta_2} + \omega_{\mathbf{k}-\mathbf{k}'}) \\ &\times (1 + n_{\mathbf{k}-\mathbf{k}'}) [\tau_3 \rho_{\mathbf{k}'}^\lambda \Gamma_{\mathbf{k}'\eta_1} \tau_3 \Gamma_{\mathbf{k}\eta_2} \rho_{\mathbf{k}}^\lambda - \tau_3 \rho_{\mathbf{k}}^\lambda \Gamma_{\mathbf{k}'\eta_1} \tau_3 \Gamma_{\mathbf{k}\eta_2} \rho_{\mathbf{k}'}^\lambda \\ &+ \text{H.c.}] + [\omega_{\mathbf{k}-\mathbf{k}'}^\lambda \rightarrow -\omega_{\mathbf{k}-\mathbf{k}'}^\lambda; (1 + n_{\mathbf{k}-\mathbf{k}'}) \rightarrow n_{\mathbf{k}-\mathbf{k}'}]. \quad (29) \end{aligned}$$

In Eq. (28),  $n_i$  is the impurity density;  $E_{\mathbf{k}\pm} = \pm E_{\mathbf{k}}$  in which  $E_{\mathbf{k}} = \sqrt{\zeta_{\mathbf{k}}^2 + |\Delta|^2}$  with  $\zeta_{\mathbf{k}} \equiv \varepsilon_{\mathbf{k}} - \mu = \mathbf{k}^2/(2m^*) -$

$\mu$ ;  $\Gamma_{\mathbf{k}\pm} = 1/2 \pm (1/2)\mathcal{U}_{\mathbf{k}}^\dagger \tau_3 \mathcal{U}_{\mathbf{k}}$  represent the projection operators. Here,

$$\mathcal{U}_{\mathbf{k}} = \begin{pmatrix} u_{\mathbf{k}} & v_{\mathbf{k}} \\ -v_{\mathbf{k}} & u_{\mathbf{k}} \end{pmatrix} \quad (30)$$

is the unitary transformation matrix from the particle space to the quasiparticle one with  $u_{\mathbf{k}} = \sqrt{1/2 + \zeta_{\mathbf{k}}/(2E_{\mathbf{k}})}$  and  $v_{\mathbf{k}} = \sqrt{1/2 - \zeta_{\mathbf{k}}/(2E_{\mathbf{k}})}$ . In Eq. (29),  $\omega_{\mathbf{k}}^\lambda$  is the  $\lambda$ -branch-phonon energy with momentum  $\mathbf{k}$ ;  $n_{\mathbf{k}}$  represents the phonon distribution function;  $\rho_{\mathbf{k}}^\zeta \equiv \rho_{\mathbf{k}} + 1/2 \pm 1/2$ .

Finally, we point out that the structures of the pump, drive and scattering terms in Eq. (25) can be analyzed more clearly in the quasiparticle space, in which the optical Bloch equations are set up by the Bogoliubov transformation  $\rho_{\mathbf{k}}^h = \mathcal{U}_{\mathbf{k}} \rho_{\mathbf{k}} \mathcal{U}_{\mathbf{k}}^\dagger$ . These detailed analysis are presented in Appendix A.

### 3. Charge neutrality condition

Equation (23) provides the microscopic description for the quasiparticle dynamics. Moreover, in the  $\mathbf{p}_s$ -gauge, both the superfluid momentum  $\mathbf{p}_s$  and the effective chemical potential  $\mu_{\text{eff}}$  which are associated with the dynamics of the condensate, appear in Eq. (23), although  $\mathbf{p}_s$  and  $\mu_{\text{eff}}$  still needs to be determined. Thus, the two-component picture naturally arises in our description, in which there exists the interplay between the quasiparticle and condensate.<sup>1-4,59-61</sup> Actually, this can be directly seen from the modified Bogoliubov transformation in which the creation and annihilation of the Cooper-pair operators  $S$  and  $S^\dagger$  are added,<sup>60,101,102</sup>

$$\begin{pmatrix} c_{\mathbf{k}\uparrow} \\ \hat{S} c_{-\mathbf{k}\downarrow}^\dagger \end{pmatrix} = \mathcal{U}_{\mathbf{k}} \begin{pmatrix} \alpha_{\mathbf{k}\uparrow} \\ \beta_{\mathbf{k}\downarrow}^\dagger \end{pmatrix}. \quad (31)$$

Here,  $\alpha_{\mathbf{k}\uparrow}^\dagger$  ( $\beta_{\mathbf{k}\downarrow}^\dagger$ ) is the creation operator for the quasi-electron (quasi-hole). From Eq. (31), one has  $\alpha_{\mathbf{k}\uparrow}^\dagger = u_{\mathbf{k}} c_{\mathbf{k}\uparrow}^\dagger - v_{\mathbf{k}} \hat{S}^\dagger c_{-\mathbf{k}\downarrow}$  and  $\beta_{\mathbf{k}\downarrow}^\dagger = v_{\mathbf{k}} c_{\mathbf{k}\uparrow} + u_{\mathbf{k}} \hat{S} c_{-\mathbf{k}\downarrow}^\dagger$ . By noting that  $\hat{S}$  annihilates one Cooper pair with charge  $2e$ , one obtains that  $\alpha_{\mathbf{k}\uparrow}^\dagger$  ( $\beta_{\mathbf{k}\downarrow}^\dagger$ ) corresponds to create a quasi-electron (quasi-hole) with charge  $e$  ( $-e$ ). Furthermore, one observes that the creation of one quasi-electron and one quasi-hole is associated with the creation and annihilation of the Cooper pair with probability  $v_{\mathbf{k}}^2$  and  $u_{\mathbf{k}}^2$ , respectively. Thus, the net creation of the Cooper pair is  $v_{\mathbf{k}}^2 - u_{\mathbf{k}}^2$ , which is positive (negative) when  $|\mathbf{k}| < k_F$  ( $|\mathbf{k}| > k_F$ ). Accordingly, when  $|\mathbf{k}| < k_F$ , both quasiparticles and Cooper pairs are created; whereas when  $|\mathbf{k}| > k_F$ , the quasiparticles are created by breaking Cooper pairs.

The above physical picture suggests that in the dynamical process, to maintain the charge neutrality or charge conservation, the Cooper pair condensate has to respond to the dynamics of the quasiparticles.<sup>61,63-69</sup>

That is to say, in the dynamical process, once the charge imbalance for the quasiparticle is created, the chemical potential of the condensate reacts to screen the extra charge due to the charge imbalance. Hence it is suggested that in Eq. (25), the effective chemical potential  $\mu_{\text{eff}}$  is determined from the charge neutrality condition, which actually has been used in the dynamical problem in superconductivity.<sup>61,63-69</sup> Specifically, in the quasiparticle space, the particle number with momentum  $\mathbf{k}$  is expressed as

$$n_{\mathbf{k}} = 2v_{\mathbf{k}}^2 + \frac{\zeta_{\mathbf{k}}}{E_{\mathbf{k}}} [\rho_{11}^h(\mathbf{k}) + \rho_{11}^h(-\mathbf{k})] - \frac{\Delta}{E_{\mathbf{k}}} [\rho_{12}^h(\mathbf{k}) + \rho_{21}^h(\mathbf{k})], \quad (32)$$

with  $v_{\mathbf{k}}^2$  treated as the distribution function of the condensate.<sup>61,63-69</sup> When the system is *near zero temperature and the equilibrium state*, to keep charge neutrality, the chemical potential for the condensate is suggested to be varied  $\mu \rightarrow \Phi$ .<sup>62,67-69</sup> Then the time evolution of the effective chemical potential can be obtained by solving the self-consistent equation with the quasiparticle density matrix obtained from Eq. (23),<sup>62,67-69</sup>

$$\sum_{\mathbf{k}} n_{\mathbf{k}} \equiv n_0 = \sum_{\mathbf{k}} \left[ 1 - \frac{\varepsilon_{\mathbf{k}} - \Phi}{\sqrt{(\varepsilon_{\mathbf{k}} - \Phi)^2 + \Delta^2}} + \frac{\zeta_{\mathbf{k}}}{E_{\mathbf{k}}} [\rho_{11}^h(\mathbf{k}) + \rho_{11}^h(-\mathbf{k})] - \frac{\Delta}{E_{\mathbf{k}}} [\rho_{12}^h(\mathbf{k}) + \rho_{21}^h(\mathbf{k})] \right]. \quad (33)$$

Here,  $n_0$  is the total electron density. From Eq. (33), it can be seen that not only the non-equilibrium quasi-electron and quasi-hole distributions but also the correlation between quasi-electron and quasi-hole states contribute to the charge imbalance.

The superfluid momentum  $\mathbf{p}_s$  can be obtained from Eq. (15) in the homogeneous limit with the electrical field in the optical pulse known. With the propagation direction of the optical field assumed to be perpendicular to the QWs, i.e., the  $\hat{\mathbf{z}}$ -direction, the direction of the electrical field is taken to be along the  $\hat{\mathbf{x}}$ -direction without loss of generality. Thus,

$$\mathbf{p}_s = (e/\omega) E_0 \hat{\mathbf{x}} \sin(\omega t) \exp[-t^2/(2\sigma_t^2)], \quad (34)$$

$$\partial_t \mathbf{p}_s \approx e E_0 \hat{\mathbf{x}} \cos(\omega t) \exp[-t^2/(2\sigma_t^2)]. \quad (35)$$

Here,  $E_0$  is the strength of the *effective* electrical field in the superconductor<sup>32</sup> and  $\sigma_t$  represents the duration time of the optical pulse. In the numerical calculation,  $-2.5\sigma_t \leq t \leq 5\sigma_t$ .

Finally, we address that Eqs. (25), (33-35) provide the consistent equations to solve the optical response to the THz pulses. Here, the condensate is assumed to react to the quasiparticles *simultaneously* due to the charge neutrality.<sup>60,101,102</sup> In our previous work in the study of the quasiparticle spin dynamics *with small spin imbalances*, it is assumed that the condensation rate is *slower* than the spin relaxation one and hence the framework with the quasiparticle-number conservation is used.<sup>54</sup> Therefore, different assumptions for the condensate dynamics can lead to different schemes. Nevertheless, for

the problem near the equilibrium, the induced change imbalance is expected to be small and these two schemes can even give similar physical results.

### C. Numerical Results

In this subsection, we present the numerical results by solving the optical Bloch equations [Eqs. (25), (33-35)] in a specific material GaAs QW in proximity to an  $s$ -wave superconductor. All parameters used in our computation are listed in Table I.<sup>109</sup>

TABLE I: Parameters used in the computation for GaAs QWs in proximity to an  $s$ -wave superconductor.<sup>109</sup>

$m^*/m_0$	0.067	$a$ (nm)	8
$\kappa_0$	12.9	$n_0$ (cm <sup>-2</sup> )	$5 \times 10^{11}$
$\sigma_t$ (ps)	4	$T_e$ (K)	2
$d$ (g/cm <sup>3</sup> )	5.31	$v_{sl}$ (m/s)	5290
$\Xi$ (eV)	8.5	$v_{st}$ (m/s)	2480
$e_{14}$ (10 <sup>9</sup> V/m)	1.41		

In Table I, for the material parameters,  $\kappa_0$  stands for the relative dielectric constant;  $a$  denotes the well width; and  $d$  is the mass density of the crystal. For the parameters associated with the electron-phonon interaction,  $\Xi$  denotes the deformation potential;  $e_{14}$  represents the piezoelectric constant;  $v_{sl}$  and  $v_{st}$  are the velocities of LA and TA phonons, respectively.<sup>105,106</sup> Finally,  $T_e$  is the environment temperature.

With these parameters, we directly estimate the contribution of the electron-AC-phonon interaction in the scattering term at  $T_e = 2$  K, compared to the one of the electron-impurity interaction with the typical impurity density  $\tilde{n}_i = 0.1n_0$ . In Eq. (29), at low temperature,  $n_{\mathbf{k}} \approx 0$ . Thus, the electron-AC-phonon interaction is approximately determined by its strength  $\sum_{k_z} |g_{\mathbf{k}-\mathbf{k}',k_z}^\lambda|^2$ . We explicitly calculate the electron-AC-phonon interaction strength  $\sum_{k_z} |g_{\mathbf{k}-\mathbf{k}',k_z}^\lambda|^2$  due to the deformation potential in the LA branch and piezoelectric coupling including LA and TA branches, which are found to be about three orders of magnitude smaller than  $\tilde{n}_i |V_{\mathbf{k}-\mathbf{k}'}|^2$ . Thus, the electron-AC-phonon interaction is negligible in our computation.

#### 1. Excitations of Higgs mode

Recently, it was reported in several experiments in the conventional superconducting metals that the Higgs mode can be excited by the intense THz field, which oscillates with twice the frequency of the THz field.<sup>25-29</sup> These experiments also show that there exists plateau

for the Higgs mode after the THz pulse in most situations, whose value increases with the increase of the field intensity.<sup>26,27</sup> Previously, the oscillation of the Higgs mode has been explained by the pump effect from the Anderson pseudo-spin picture, in which the drive effect on the superconducting state is absent.<sup>13,14,37-44,46</sup> Here, we aim to distinguish the contribution of the pump and drive effects to the evolution of the Higgs mode in GaAs QW in proximity to an  $s$ -wave superconductor.

*a. Different pump regimes* Before we present the numerical results, we first analyze the behavior of the pump effect from a simplified model, from which different regimes are divided according to the pump strength. In the pump term in Eq. (25),  $\frac{\mathbf{p}_s^2}{2m^*} = \frac{1}{4m^*} \left( \frac{e}{\omega_L} \tilde{E}_0 \right)^2 (1 - \cos 2\omega t)$  with  $\tilde{E}_0 \equiv E_0 \exp[-t^2/(2\sigma_t^2)]$  slowly varying with time. The analytical calculation is simplified for high optical frequency  $\omega$ , with which the rotation-wave approximation<sup>94</sup> can be applied with  $\frac{\mathbf{p}_s^2}{2m^*} \approx \frac{1}{4m^*} \left( \frac{e}{\omega_L} \tilde{E}_0 \right)^2 \equiv \eta$ . In this situation, in the free situation without the drive and HF terms, the optical Bloch equations in the quasiparticle space read [refer to Eq. (A1)]

$$\frac{\partial \rho_{\mathbf{k}}^h}{\partial T} + i \left[ \begin{pmatrix} E_{\mathbf{k}} + \frac{\zeta_{\mathbf{k}}}{E_{\mathbf{k}}} \eta & -\frac{\Delta}{E_{\mathbf{k}}} \eta \\ -\frac{\Delta}{E_{\mathbf{k}}} \eta & -E_{\mathbf{k}} - \frac{\zeta_{\mathbf{k}}}{E_{\mathbf{k}}} \eta \end{pmatrix}, \rho_{\mathbf{k}}^h \right] = 0. \quad (36)$$

With the initial state being the equilibrium distribution, the population for the quasi-electron is

$$\rho_{\mathbf{k},11}^h = f_{\mathbf{k}}^0 + \left[ \frac{1}{2} - f_{\mathbf{k}}^0 \right] \left( \frac{\Delta \eta}{E_{\mathbf{k}} \mathcal{E}_{\mathbf{k}}} \right)^2 (1 - \cos 2\mathcal{E}_{\mathbf{k}} T). \quad (37)$$

Here,  $f_{\mathbf{k}}^0 = \{\exp[E_{\mathbf{k}}/(k_B T_e)] + 1\}^{-1}$  represents the equilibrium distribution for the quasi-electron with  $k_B$  being the Boltzmann constant;  $\mathcal{E}_{\mathbf{k}} = \sqrt{(\varepsilon_{\mathbf{k}} - \mu + \eta)^2 + \Delta^2}$ , from which it can be seen that  $\eta$  directly contributes to the AC stark effect in the energy spectrum.<sup>57,72</sup>

According to the behavior of  $(E_{\mathbf{k}} \mathcal{E}_{\mathbf{k}})^2$ , which is further expressed as

$$(E_{\mathbf{k}} \mathcal{E}_{\mathbf{k}})^2 \equiv F(\mathbf{k}) = [(\zeta_{\mathbf{k}} + \eta/2)^2 - (\eta^2/4 - \Delta^2)]^2 + \Delta^2 \eta^2, \quad (38)$$

one can separate different pump regimes. When  $\eta < 2\Delta$ , the minimum value of  $F(\mathbf{k})$  lies at  $\zeta_{\mathbf{k}} = 0$ , indicating that the quasi-electron distribution evolves around  $|\mathbf{k}| = k_F$ . This regime with  $\eta < 2\Delta$  is referred to as the weak-pump regime. Whereas when  $\eta > 2\Delta$ , the minimum values of  $F(\mathbf{k})$  are realized when  $\zeta_{\mathbf{k}} = -\eta/2 \pm \sqrt{\eta^2/4 - \Delta^2}$ , which is smaller than zero. This indicates that during the pump process, the quasi-electron population mainly arises at  $|\mathbf{k}| < k_F$  and hence the hole-like quasi-electrons are mainly pumped. This regime with  $\eta > 2\Delta$  is referred to as the strong-pump regime. Actually, in the experiments, with  $\Delta = 2.6$  meV for the metal NbN and  $\omega = 2\Delta$ ,  $\eta \sim 17.6$  meV when the peak electric field is 50 kV/cm, indicating that the experiments lie in the strong-pump regime.<sup>26-29</sup>

*b. Weak-pump regime* We first focus on the weak-pump regime. In Figs. 3(a), (b) and (c), the temporal evolutions of the Higgs mode  $|\delta\Delta|$  are plotted in the clean (blue solid curves) and dirty (red chain and green dashed curves) samples with different pump frequencies of the optical field  $\omega = \Delta$ ,  $2\Delta$  and  $4\Delta$ , respectively ( $\Delta = 0.8 \text{ meV} \approx 1.15 \text{ THz}$ ). The electric field strength  $E_0 = 0.2 \text{ kV/cm}$ . Thus, for  $\omega = \Delta$ ,  $\eta = 0.18 \text{ meV}$  is

much smaller than  $2\Delta$ , indicating that the system lies in the weak-pump regime. With this electric field strength, the temporal evolutions of the superconducting momentum  $\mathbf{p}_s$ , which are driven by the optical field [Eq. (34)], are presented in Fig. 3(d) with  $\omega = \Delta$  (the red chain curve) and  $2\Delta$  (the blue solid curve), respectively. It can be seen in Fig. 3(d) that when  $\omega > \Delta$ , the induced supercurrents by the THz pulse is small in magnitude with

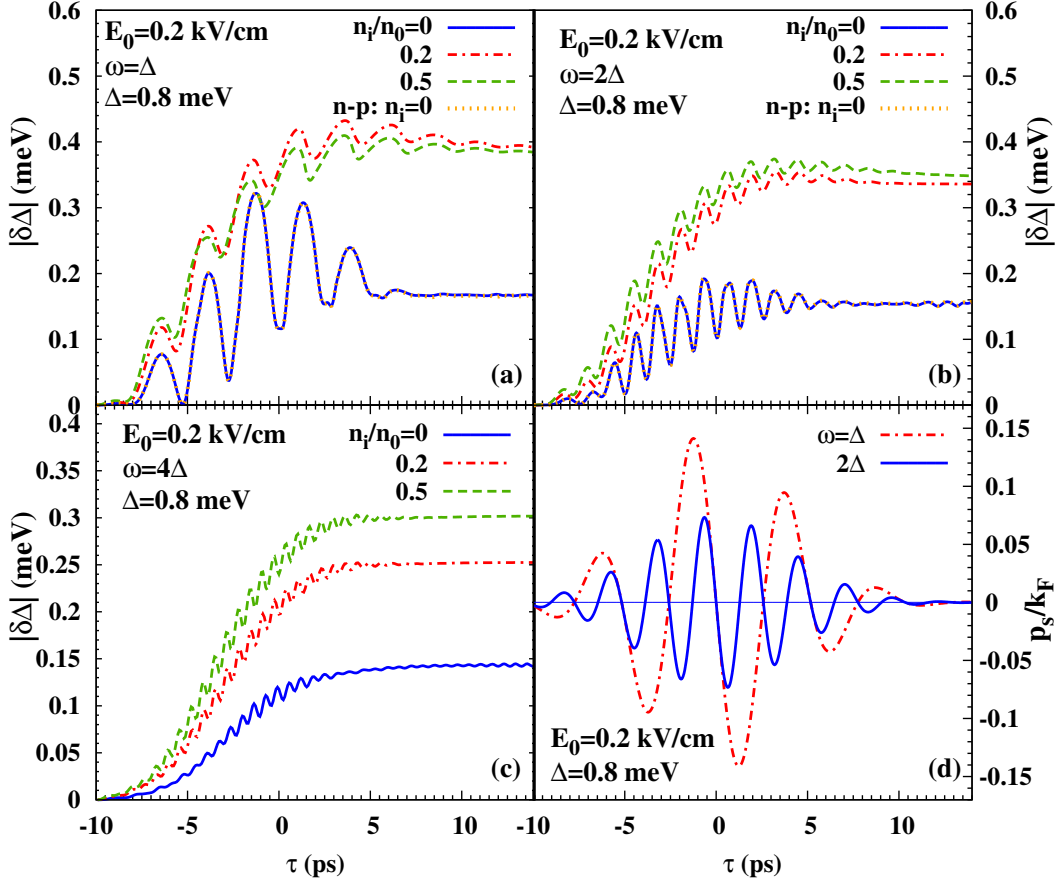


FIG. 3: (Color online) Temporal evolutions of the Higgs mode  $|\delta\Delta|$  with different pump frequencies of the THz pulse  $\omega = \Delta$  [(a)],  $2\Delta$  [(b)] and  $4\Delta$  [(c)], respectively. Here,  $\Delta = 0.8 \text{ meV}$  and the electric field strength  $E_0 = 0.2 \text{ kV/cm}$ . With this electric field, the superconducting momentum  $\mathbf{p}_s$  is presented in (d) when  $\omega = \Delta$  and  $2\Delta$ . It can be seen that  $|\mathbf{p}_s| < 0.15k_F$  when  $\omega > \Delta$ . In (a) and (b), it can be seen that without the pump effect, the Higgs modes, plotted by the yellow dotted curves, coincide with the ones with both the pump and drive effects, represented by the blue solid curves. Moreover, in (a), (b) and (c), it is found that there always exist plateaus after the THz pulse, which are suppressed with the increase of the optical-field frequency. Finally, it is shown in (a) [or (b), (c)] by the blue solid, red chain and green dashed curves that with the increase of the impurity density, the oscillation amplitude of the Higgs mode is suppressed and the amplitude of the plateau of the Higgs mode increases.

$|\mathbf{p}_s| < 0.15k_F$ . By comparing the oscillation frequencies of the Higgs mode [Figs. 3(a), (b) and (c)] with the ones of the supercurrent [Fig. 3(d)], one finds that the Higgs mode oscillates with twice the frequency of the

THz field when both the pump and drive effects exist. Then, the contributions of the pump and drive effects to the Higgs mode are compared in Figs. 3(a) and (b) in the impurity-free situation. It can be seen that without the

pump effect, the Higgs modes, plotted by the yellow dotted curves, coincide with the one with both the pump and drive effects, represented by the blue solid curves. This shows that the pump effect is marginal for the excitation of Higgs mode in the weak-pump regime. Moreover, it is found that there always exist plateaus for the Higgs mode after the THz pulse, which are suppressed with the increase of the optical-field frequency, as shown in

Figs. 3(a), (b) and (c). Finally, the role of the electron-impurity scattering is addressed. It is shown in Fig. 3(a) [or (b), (c)] by the blue solid, red chain, and green dashed curves that with the increase of the impurity density, the oscillation amplitude of the Higgs mode is suppressed and the plateau value of the Higgs mode increases. These rich features can be understood as follows.

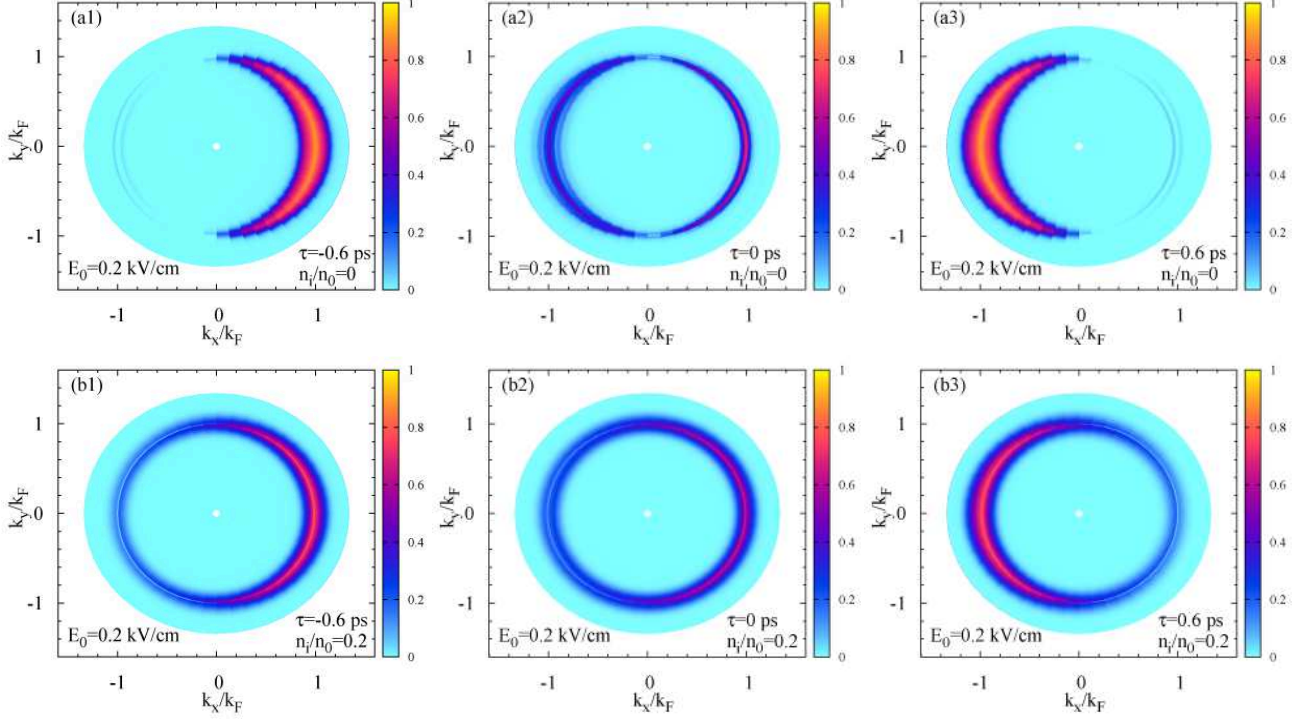


FIG. 4: (Color online) Quasi-electron distributions  $\rho_{\mathbf{k},11}^h$  in the momentum space at  $\tau = -0.6, 0$  and  $0.6$  ps in the clean [(a1), (a2) and (a3) with  $n_i = 0$ ] and dirty [(b1), (b2) and (b3) with  $n_i = 0.2n_0$ ] samples.  $\omega = 2\Delta$  with  $\Delta = 0.8$  meV. The electric field strength  $E_0 = 0.2$  kV/cm, with which  $\mathbf{p}_s \approx 0.13k_F, 0$  and  $-0.13k_F$  at  $\tau = -0.6, 0$  and  $0.6$  ps, respectively.

We first address the role of the drive effect on the anomalous correlation. It has been well investigated that in the *static* case when the center-of-mass momentum  $\mathbf{q}$  of the Cooper pairs emerges, which can originate from the spontaneous symmetry-breaking, e.g., in the FFLO state<sup>48–50,110</sup> or with a supercurrent,<sup>51,54,55</sup> a blocking region occupied by the quasiparticles can appear, in which the anomalous correlation for the Cooper pair can be significantly suppressed.<sup>48–51,54,55</sup> Then it is expected that when the *time-dependent* supercurrent emerges with the excitation of the center-of-mass momentum of Cooper pairs, the blocking region can be dynamically excited, in which the Cooper-pair anomalous correlation is also suppressed. Specifically, in Fig. 1, a comprehensive physical picture has been presented, in which one finds that

the driven blocking region, shown by the blue region in crescent form, directly suppresses the anomalous correlation between two electrons (labeled by “M” and “N”). In our calculation, with the drive of the electron and hole (particle space) in the opposite directions [refer to  $\tau_3$  in the drive term in Eq. (25)], the blocking region for the quasiparticles surely appears, with typical examples presented in Fig. 4 with  $E_0 = 0.2$  kV/cm at different times  $\tau = -0.6, 0$  and  $0.6$  ps, respectively.

In Figs. 4(a1), (a2) and (a3) when  $n_i = 0$ , one sees that when  $\tau = -0.6$  ps [Fig. 4(a1)] and  $0.6$  ps [Fig. 4(a3)] with finite  $\mathbf{p}_s \approx 0.13k_F\hat{\mathbf{x}}$  and  $-0.13k_F\hat{\mathbf{x}}$  [refer to Fig. 3(d)], the blocking regions in the crescent shape appear, whose positions are consistent with the sign of the center-of-mass momentum  $\mathbf{p}_s$  of the Cooper pairs; whereas when

$\tau = 0$  ps [Fig. 4(a2)], with zero center-of-mass momentum, the blocking region tends to disappear, but there still exists significant quasiparticle population. Furthermore, it is observed in Figs. 4(a1) and (a3) that inside the blocking region, the quasi-electron population is close to one. In the blocking region, the anomalous correlation

$$\begin{aligned} C(\mathbf{k}) &= u_{\mathbf{k}}v_{\mathbf{k}}(\rho_{\mathbf{k},11}^h - \rho_{\mathbf{k},22}^h) + u_{\mathbf{k}}^2\rho_{\mathbf{k},12}^h - v_{\mathbf{k}}^2\rho_{\mathbf{k},21}^h \\ &\approx u_{\mathbf{k}}v_{\mathbf{k}}(\rho_{\mathbf{k},11}^h - \rho_{\mathbf{k},22}^h) \end{aligned} \quad (39)$$

is significantly suppressed with  $\rho_{\mathbf{k},11}^h \lesssim 1$  and  $\rho_{\mathbf{k},22}^h = 1 - \rho_{-\mathbf{k},11}^h \lesssim 1$ .<sup>50,54</sup> Then due to the suppression of the anomalous correlation, from Eq. (27), the Higgs mode is significantly excited. Furthermore, the suppression of the anomalous correlation does not depend on the sign of the center-of-mass momentum of Cooper pairs. Accordingly, although the center-of-mass momentum of Cooper pairs oscillates with the frequency of the optical field, the Higgs mode originating from the suppression of the anomalous correlation oscillates with twice the frequency of the optical field. It is noted that in the weak-pump regime, the quasi-electrons are mainly pumped around the Fermi surface in the absence of the drive effect; whereas the blocking region also arises around the Fermi surface but due to the drive effect. Thus, thanks to the Pauli blocking effect, the emergence of the blocking region can efficiently suppress the pump effect. Consequently, in the weak-pump regime, the pump effect plays a marginal role and the drive effect is dominant in the excitation of the Higgs mode [refer to the blue solid and yellow dotted curves in Figs. 3(a) and (b)].

We then focus on the influence of the electron-impurity scattering on the Higgs mode dynamics. In Figs. 4(b1), (b2) and (b3) with  $n_i = 0.2n_0$ , by comparing with the impurity-free situation in Figs. 4(a1), (a2) and (a3), it is observed that the electron-impurity scattering has significant influence on the formation of the blocking region.<sup>111</sup> Specifically, on one hand, the electron-impurity scattering can suppress the range of the blocking region and hence its oscillation. This is because the drift effect of the electron and hole, which contributes to the formation of the blocking region, can be suppressed by the electron-impurity scattering.<sup>112-114</sup> Thus, the suppression of the oscillation of the blocking region tends to suppress the oscillation amplitude of the Higgs mode. On the other hand, the electron-impurity scattering tends to destroy the blocking region by averaging the quasi-electron distribution. Accordingly, from Eq. (39), the emergence of the significant quasiparticle population in the unblocking region further suppresses the anomalous correlation. This tends to enhance the magnitude of the Higgs mode.

To make the above physical picture clearer, in Fig. 5, we further plot the anomalous correlations before [(a),  $\tau = -10$  ps] and after [(b), (c) and (d),  $\tau = 10$  ps] the THz pulses with  $E_0 = 0.2$  kV/cm and  $\omega = 2\Delta \approx 2.3$  THz. In Figs. 5(b), (c) and (d), the impurity densities are set to be  $n_i = 0, 0.2n_0$  and  $0.5n_0$ , respectively. In these figures, it can be seen that the anomalous correla-

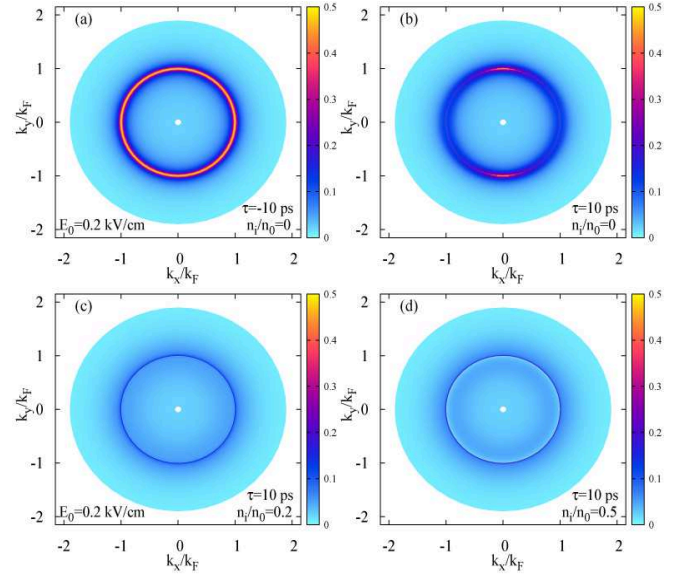


FIG. 5: (Color online) Anomalous correlations in the momentum space before [ $\tau = -10$  ps, (a)] and after [ $\tau = 10$  ps, (b), (c) and (d)] the THz pulses with  $E_0 = 0.2$  kV/cm and  $\omega = 2\Delta \approx 2.3$  THz. In (b), (c) and (d), the impurity densities  $n_i = 0, 0.2n_0$  and  $0.5n_0$ .

tion is significant only around the Fermi surface.<sup>50,54,110</sup> We first address the influence of the THz pulse on the anomalous correlation in the impurity-free situation. By comparing the anomalous correlation in Figs. 5(a) and (b), it can be seen that in the impurity-free situation, the anomalous correlation is suppressed by the THz pulse only in the blocking region and the anomalous correlation becomes anisotropic in the momentum space. This is consistent with the previous works in the static situation, in which the anomalous correlation is suppressed only in the blocking region.<sup>48,50,54</sup> Then the influence of the impurity can be seen by comparing Fig. 5(c) [or (d)] with (b). It is shown in Fig. 5(c) [(d)] that the anomalous correlation becomes isotropic due to the momentum scattering with  $n_i = 0.2n_0$  ( $0.5n_0$ ). This confirms the conclusion from Eq. (39) that the existence of the impurity tends to average the quasiparticle population and hence the anomalous correlation around the Fermi surface. Furthermore, one observes that in Figs. 5(c) [or (d)], the anomalous correlation is further suppressed compared to the free situation in (b), which shows that the electron-impurity scattering can further suppress the superconductivity after the THz pulse. Thus, with the increase of the impurity density, the plateau of the Higgs mode increases [refer to the red and blue solid curves in Figs. 3(a), (b) and (c)].

The further suppression of the superconductivity due to the impurity after the THz pulse can be understood from another point of view. We find that with the increase of the impurity density, the quasiparticle density increases during the temporal evolutions, shown in Fig. 14 in Appendix B. This can be understood from the

fact that in the presence of impurities, the optical absorption is significantly enhanced because the driven electrical current is no longer in phase to the driven field.<sup>112–114</sup> The enhancement of the optical absorption by the impurities further suppresses the anomalous correlation [refer to Eq. (39)]. With the increase of the quasiparticle density, the normal-fluid and super-fluid densities are expected to deviate from their equilibrium values. Thus, to further understand the non-equilibrium superconducting state after the pulse, the normal-fluid and super-fluid densities are also estimated in Appendix B, which are often estimated in the pump-probe experiments.<sup>20–22,24</sup> It is emphasized that this estimation is performed by assuming that the system is *in the Fermi-distribution with an effective temperature*, and hence the two-fluid description is expected to be effective.<sup>1,18,20–22,24</sup>

*c. Strong-pump regime* We then extend our calculation to the strong-pump regime. It is noted that a strong electrical field in the intense THz pulse can destroy the superconductivity (refer to Fig. 15). Here, we take  $E_0 = 0.5$  kV/cm and  $\Delta = 0.4$  meV. Then with  $\omega = 2\Delta$ , it is obtained that  $\eta \approx 1.1$  meV, which is larger than  $2\Delta$ . With these parameters, we show that in the superconducting GaAs QWs, even in the strong-pump regime, the pump effect still plays a marginal role in the excitation of the Higgs mode. This can be seen in Fig. 6 that in the clean (dirty) sample, the Higgs mode calculated with both the pump and drive effects, represented by the blue dashed (red solid) curve, almost coincides with the one calculated without the pump effect, denoted by the yellow dashed (green chain) curve.

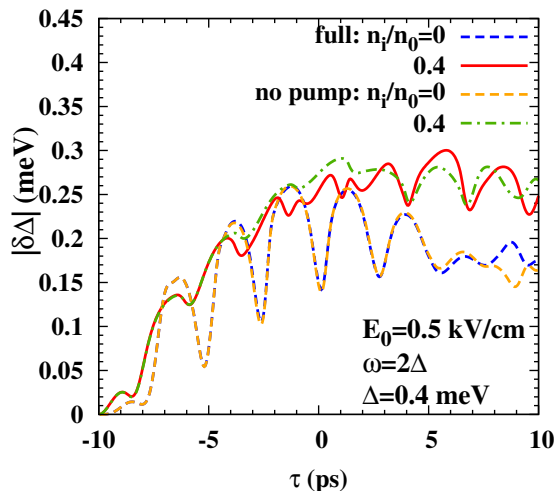


FIG. 6: (Color online) Temporal evolutions of the Higgs mode in the strong-pump regime. With  $E_0 = 0.5$  kV/cm and  $\omega = 2\Delta = 0.8$  meV, one obtains that  $\eta \approx 1.1$  meV, which is larger than  $2\Delta$ . It can be seen that in the clean (dirty) sample, the Higgs mode calculated with both the pump and drive effects, represented by the blue dashed (red solid) curve, almost coincides with the one calculated without the pump effect, denoted by the yellow dashed (green chain) curve.

Above we have shown that in both the weak- and strong-pump regimes, with relatively small superconducting momenta  $|\mathbf{p}_s| \ll k_F$ , the pump effect always plays a marginal role in the excitation of the quasiparticle due to the effect of Pauli blocking. Actually, it can be estimated that as long as  $|\mathbf{p}_s| \lesssim k_F$ , the pump effect cannot be efficient (shown below). This is exactly the situation in the conventional superconducting metals with large Fermi surfaces, although intense THz fields are applied.<sup>26–29</sup> Previously, the explanation of the Higgs-mode oscillation is based on the pump effect.<sup>25–29,37–39,45</sup> Our results suggest that it is the drive effect that is really responsible.

Finally, we remark that only when  $|\mathbf{p}_s| \gtrsim k_F$ , the pump effect can contribute to the excitation of the Higgs mode, as estimated as follows. In the strong-pump regime ( $\eta \gtrsim 2\Delta$ ), the hole-like quasiparticle is dominantly pumped around some special momenta labeled by  $\mathbf{k}_0$  [refer to Eqs. (37) and (38)], which are determined by

$$\mathbf{k}_0^2/(2m^*) - \mu \approx -\eta. \quad (40)$$

Actually, Eq. (40) is established only when  $|\mathbf{p}_s| \lesssim \sqrt{2}k_F$  with  $\mathbf{k}_0^2/(2m^*) \approx \mu - \eta > 0$  satisfied. When  $|\mathbf{p}_s| \lesssim \sqrt{2}k_F$ ,  $\mathbf{k}_0$  is away from the Fermi surface by  $\Delta k \equiv k_F - |\mathbf{k}_0|$ . It is noted that the boundary of the blocking region *in the clean limit* is away from the Fermi surface by about  $|\mathbf{p}_s|$ . Thus, when  $2\Delta k \gtrsim |\mathbf{p}_s|$ , the pumped hole-like quasiparticles lie out of the blocking region, which cannot be efficiently blocked. This requires that  $|\mathbf{p}_s| \gtrsim k_F$ . Whereas when  $|\mathbf{p}_s| \gtrsim \sqrt{2}k_F$ , Eq. (40) is no longer established. In this situation,  $\mathbf{p}_s^2/(4m^*) \gtrsim \mu$ , i.e., the effective chemical potential contributed by the AC Stark effect can be even larger than the one of the system. In this situation, the pump effect becomes extremely strong and the quasiparticles can be efficiently pumped in the whole momentum space. From above analysis, it is estimated that when  $|\mathbf{p}_s| \gtrsim k_F$ , the pump effect can have contribution to the excitation of the Higgs mode. Moreover, one sees that one way to realize the significant pump effect is to efficiently suppress the drive effect and hence the range of the blocking region.

## 2. Charge Imbalance: Creation and Relaxation

The charge imbalance created by the electrical method and its relaxation has been intensively studied.<sup>1–4,59–62</sup> It is believed that for the isotropic *s*-wave superconductor, the *elastic* scattering due to the impurity cannot cause the relaxation of the charge imbalance.<sup>1–4,59–61</sup> This is because the elastic scattering cannot exchange the electron-like and hole-like quasiparticles due to coherence factor ( $u_{\mathbf{k}}u_{\mathbf{k}'} - v_{\mathbf{k}}v_{\mathbf{k}'}$ ) in the electron-impurity scattering potential [refer to Eq. (A2)].<sup>1–4,59–61</sup> Nevertheless, in the previous studies,<sup>1–4,59–61</sup> the charge neutrality condition is not explicitly considered in the relaxation process of the charge imbalance. In other words, the studies<sup>1–4,59–61</sup>

are actually performed in the framework of quasiparticle-number conservation.<sup>54</sup> Actually, to maintain the charge neutrality, the Cooper pair condensate has to respond to the dynamics of the quasiparticles.<sup>61,63–69</sup> In this part, we investigate the creation of the charge imbalance by the optical pulse and its relaxation via the optical Bloch equations [Eqs. (25), (33–35)] in the framework of charge neutrality. The physical picture for the charge neutrality condition has been addressed explicitly in Sec. II B 3.

*a. Optical creation of charge imbalance* Although in the excitation of the Higgs mode, the pump effect is shown to play a marginal role (Sec. II C 1), it is found that both the pump and drive effects can be important in the creation of the charge imbalance. Their contributions can be even distinguished in the time domain. This is presented in Fig. 7, in which the temporal evolution of the effective chemical potential  $\mu_{\text{eff}}$  is plotted by the red solid curve with the typical impurity density  $n_i = 0.2n_0$  when  $E_0 = 0.2$  kV/cm and  $\omega = 2\Delta = 1.6$  meV. It can be seen that during the evolution, the effective chemical potential, represented by the red solid curve, is first negative when  $\tau < 3$  ps, then becomes positive when  $\tau > 3$  ps and finally decays to zero after the pulse. From Eq. (33) with  $\Phi = \mu - \mu_{\text{eff}}$ , one observes that the negative effective chemical potential means the increase of the total chemical potential and hence the condensate density; at the same time, the hole-like quasiparticle charge becomes larger than the electron-like one. It is noted that the total density of quasiparticles increases during the pulse (refer to Fig. 14). Thus, with the induction of the negative effective chemical potential, both the condensate and quasiparticle densities are increased to maintain the charge neutrality. This is in contrast to the common belief that the quasiparticle densities increase through the breaking of the Cooper pairs. Whereas with the positive effective chemical potential, the electron-like quasiparticle charge becomes larger than the hole-like one in accompany with the decrease of the condensate density.

Furthermore, in Fig. 7, when only the drive (pump) effect exists, as shown by the blue solid (yellow dotted) curve, the effective chemical potential is positive (negative). Moreover, one observes that the red solid curve can be treated as the simple summation of the blue solid and yellow dotted ones. This indicates that the positive and negative parts of the effective chemical potential mainly come from the drive and pump effects, respectively. It is noticed that in the physical situation with both the pump and drive effects, for the pump effect, the excitation of quasiparticle population is efficiently suppressed by the drive effect (Sec. II C 1). Nevertheless, as addressed in Eq. (33), both the quasiparticle population and the correlation between the quasi-electron and quasi-hole can contribute to the charge imbalance. Then it is speculated that the charge imbalance due to the pump effect mainly comes from the induction of the correlation between the quasi-electron and quasi-hole, which cannot be suppressed by the Pauli blocking. Moreover, the fact that the charge imbalance is the simple superposition of the

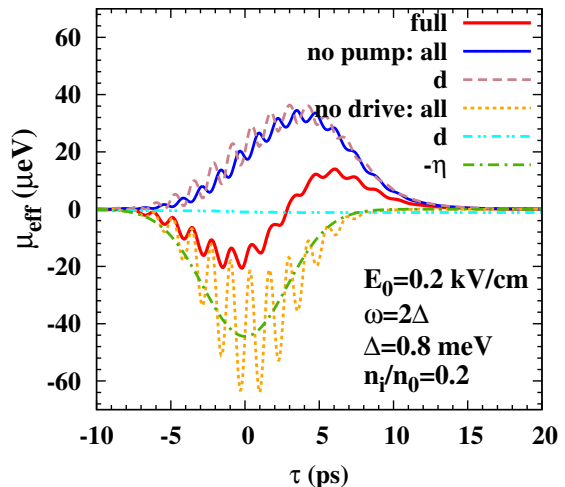


FIG. 7: (Color online) Temporal evolution of the effective chemical potential in the condensate in the presence of the optical pulse with the typical impurity density  $n_i = 0.2n_0$ .  $E_0 = 0.2$  kV/cm and  $\omega = 2\Delta$  with  $\Delta = 0.8$  meV. The red solid curve shows that during the evolution, the effective chemical potential is first negative when  $\tau < 3$  ps, then becomes positive when  $\tau > 3$  ps and finally decays to zero after the pulse. The blue solid (yellow dotted) curve represents the calculated effective chemical potential when only the drive (pump) effect exists. The cyan double-dot-dashed (purple dashed) curve is calculated with only the diagonal elements in the quasiparticle density matrix retained when only the pump (drive) effect exists. Finally, the chemical potential induced by the AC Stark effect, i.e.,  $\eta$ , is presented by the green chain curve, which depicts the envelope of the yellow dotted curve.

ones due to the pump and drive effects indicates that the charge imbalance due to the drive effect is contributed by a different channel from the pump effect. Thus, it is further speculated that the charge imbalance contributed by the drive effect comes from the induction of the quasiparticle population. Both speculations are directly confirmed by the numerical calculation. This can be seen in Fig. 7 by the cyan double-dot-dashed (purple dashed) curve that when only the pump (drive) effect exists, the quasiparticle populations have no (dominant) contribution to the charge imbalance. Thus, the optical excitation of the charge imbalance can be understood by separately studying the charge imbalance due to the pump and drive effects. It is emphasized that the obtained picture can be applied to both the weak and strong-pump regimes because in both situations, the induction of the quasiparticle due to the pump effect is suppressed (this is confirmed by the numerical calculations directly).

We first analyze the charge imbalance due to the pump effect by analytically calculating its contribution to the effective chemical potential. From Eqs. (36) and (37),



one obtains

$$\rho_{\mathbf{k},12}^h + \rho_{\mathbf{k},21}^h = \frac{E_{\mathbf{k}}^2 + \zeta_{\mathbf{k}}\eta}{\Delta\eta} \left( \frac{\Delta\eta}{E_{\mathbf{k}}\mathcal{E}_{\mathbf{k}}} \right)^2 (1-2f_{\mathbf{k}}^0) (1-\cos 2\mathcal{E}_{\mathbf{k}}T). \quad (41)$$

Then the net charge contributed by the correlation between the quasi-electron and quasi-hole is

$$\delta Q_c = - \sum_{\mathbf{k}} \frac{\Delta^2\eta}{E_{\mathbf{k}}\mathcal{E}_{\mathbf{k}}^2} (1-2f_{\mathbf{k}}^0)(1-\cos 2\mathcal{E}_{\mathbf{k}}T) \approx - \sum_{\mathbf{k}} \frac{\Delta^2\eta}{E_{\mathbf{k}}^3}. \quad (42)$$

By further noticing that  $2\delta v_{\mathbf{k}}^2 = -(\Delta^2/E_{\mathbf{k}}^3)\delta\mu_{\text{eff}}$  in Eq. (32), the charge neutrality condition requires that  $\delta\mu_{\text{eff}} \approx -\eta$ . This relation is directly confirmed by the green chain curve in Fig 7, in which  $\eta$  depicts the envelope of the yellow dotted curve. Actually, this simple relation provides a simple physical picture for the pump-induced charge imbalance, in which the AC Stark effect directly modifies the total chemical potential.

For the drive effect, the induced positive effective chemical potential indicates that the charge carried by the electron-like quasiparticle is larger than the hole-like one. The physics picture is qualitatively analyzed based on the optical Bloch equations in the quasiparticle space [Eq. (A1)] as follows. In the free situation with only the drive term retained, Eq. (A1) is written as

$$\frac{\partial \rho_{\mathbf{k}}^h}{\partial T} + \frac{1}{2} \left\{ eE_x \tilde{\tau}_3, \frac{\partial \rho_{\mathbf{k}}^h}{\partial k_x} \right\} + \frac{1}{2} \left\{ eE_x \tilde{\tau}_3, \left[ \rho_{\mathbf{k}}^h, \frac{\partial \mathcal{U}_{\mathbf{k}}}{\partial k_x} \mathcal{U}_{\mathbf{k}}^\dagger \right] \right\} = 0, \quad (43)$$

in which  $\tilde{\tau}_3(\mathbf{k}) \equiv \mathcal{U}_{\mathbf{k}}\tau_3\mathcal{U}_{\mathbf{k}}^\dagger = (v_{\mathbf{k}}^2 - v_{-\mathbf{k}}^2)\tau_3 - 2u_{\mathbf{k}}v_{\mathbf{k}}\tau_1$  with both the diagonal and off-diagonal terms retained. In Eq. (43), the second term is the conventional drive term for the quasiparticle in the Boltzmann equation,<sup>1,3,5,54</sup> whereas the third term is contributed by the Berry phase.<sup>115-117</sup> By defining  $q_{\mathbf{k}}^* = e(\zeta_{\mathbf{k}}/E_{\mathbf{k}})(\rho_{\mathbf{k},11}^h + 1 - \rho_{-\mathbf{k},22}^h)$ , which is the net charge for the quasiparticle with the momentum  $\mathbf{k}$ ,<sup>1,2</sup> and further neglecting the quasiparticle correlation, it is obtained from Eq. (43) that

$$\begin{aligned} \frac{\partial q_{\mathbf{k}}^*}{\partial T} + 2eE_x \left( \frac{\zeta_{\mathbf{k}}}{E_{\mathbf{k}}} \right)^2 \frac{\partial q_{\mathbf{k}}^*}{\partial k_x} - 2eE_x \frac{\zeta_{\mathbf{k}}}{E_{\mathbf{k}}} \frac{k_x}{m^*} \frac{\Delta^2}{E_{\mathbf{k}}^3} q_{\mathbf{k}}^* \\ + eE_x \frac{k_x}{m^*} \frac{\Delta^2}{E_{\mathbf{k}}^3} \frac{q_{\mathbf{k}}^* + q_{-\mathbf{k}}^*}{2} = e^2 E_x \frac{k_x}{m^*} \frac{\zeta_{\mathbf{k}}}{E_{\mathbf{k}}} \frac{\Delta^2}{E_{\mathbf{k}}^3}. \end{aligned} \quad (44)$$

Although Eq. (44) is complex, one important feature is that there exists a source term for  $q_{\mathbf{k}}^*$  on the right-hand side of the equation. This source term, which originates from the Berry-phase effect, is proportional to  $\Delta^2$ . This indicates that the charge-conservation of the *quasiparticle* is absent due to the existence of the superconducting order parameter. This is consistent with the conclusion in the Blonder-Tinkham-Klapwijk model when studying the Andreev reflection, which reveals that the order parameter itself directly breaks the charge conservation of quasiparticles.<sup>118</sup> One notices that in the situation with relatively small impurity density, only the blocking region should be considered. Actually, this source term

directly contributes to the formation of the blocking region. From the source term, it can be seen that with  $E_x > 0$  ( $E_x < 0$ ), the quasiparticle charges increase when  $k_x < 0$  ( $k_x > 0$ ). It is further noted that the source term is proportional to  $k_x$ , which is larger for the electron-like quasiparticle than the hole-like one. Then *in the blocking region*, the electron-like quasiparticle charge can be created faster than the hole-like one, which directly contributes to the charge imbalance with more electron-like quasiparticles.

We emphasize that the optical excitation of the charge imbalance is a unique feature for the superconductor with nonzero order parameter, which cannot be realized in the normal state. When the order parameter is close to zero, on one hand, the pump term tends to zero and hence there cannot exist significant correlation between the quasi-electron and quasi-hole states; on the other hand, the source term in Eq. (44) becomes close to zero and hence no significant quasiparticles can be created from the condensate. Experimentally, the effective chemical potential induced by the optical field in the charge imbalance can be directly measured either through the voltage between the quasiparticle and condensate measured in the setup of Clarke's works,<sup>70,71</sup> or through the effective chemical potential measured in the Josephson effect.<sup>23</sup>

*b. Charge-imbalance relaxation due to the electron-impurity scattering* In Fig. 7, it is anomalous to observe that after the pulse at  $\tau \approx 8$  ps, the induced effective chemical potential relaxes to zero. This indicates that there exist relaxation channels for the charge imbalance even in the presence of the elastic scattering in the isotropic *s*-wave superconductivity, which is in contrast to the previous studies.<sup>1,2,59,60</sup> To reveal the mechanism for the charge-imbalance relaxation, a simplified model in the *s*-wave superconducting QWs is set up with a *small* initially-given charge imbalance, in which  $\mathbf{p}_s$  is set to be zero and the HF self-energy is neglected. Accordingly, Eq. (A1) is simplified into

$$\partial_T \rho_{\mathbf{k}}^h + i[E_{\mathbf{k}}\tau_3, \rho_{\mathbf{k}}^h] + i[\mu_{\text{eff}}\tilde{\tau}_3, \rho_{\mathbf{k}}^h] = \partial_t \rho_{\mathbf{k}}|_{\text{scat}}^{\text{d}} + \partial_t \rho_{\mathbf{k}}|_{\text{scat}}^{\text{off}}. \quad (45)$$

Specifically, in Eq. (45), the off-diagonal terms in  $\mu_{\text{eff}}\tilde{\tau}_3$  induce the precession between the quasi-electron and quasi-hole states and hence the quasiparticle correlation;  $\partial_t \rho_{\mathbf{k}}|_{\text{scat}}^{\text{off}}$  directly breaks the conservation of the quasiparticle number<sup>54</sup> (more discussions are referred to Appendix A). The initial state in the quasiparticle space with a small quasiparticle charge imbalance is set to be

$$\rho_{\mathbf{k}}^{h,c} = \begin{pmatrix} f_0(E_{\mathbf{k}}^c) & 0 \\ 0 & 1 - f_0(E_{\mathbf{k}}^c) \end{pmatrix}. \quad (46)$$

In Eq. (46),  $E_{\mathbf{k}}^c = \sqrt{(\varepsilon_{\mathbf{k}} - \mu - \delta\mu_c)^2 + |\Delta|^2}$  with  $\delta\mu_c = 0.01\mu$  and  $f_0(E_{\mathbf{k}}^c) = \{\exp[E_{\mathbf{k}}^c/(k_B T_e)] + 1\}^{-1}$ . With  $|\delta\mu_c| \ll |\mu|$ ,

$$\rho_{\mathbf{k}}^{h,c} \approx \begin{pmatrix} f_0(E_{\mathbf{k}}) & 0 \\ 0 & 1 - f_0(E_{\mathbf{k}}) \end{pmatrix} - \frac{\partial f_0}{\partial E_{\mathbf{k}}} \frac{\zeta_{\mathbf{k}}}{E_{\mathbf{k}}} \delta\mu_c \tau_3. \quad (47)$$

With this initial state, the effective chemical potential for the condensate can be induced due to the charge neutrality condition [Eq. (33)]. Thus, Eqs. (45), (33) and Eq. (47) provide the consistent equations to study the charge-imbalance relaxation, which are solved first numerically and then analytically below.

In Fig. 8, the impurity-density dependencies of the charge-imbalance relaxation time (CIRT)  $\tau_C$  with  $\Delta = 0.8$  meV and  $0.4$  meV are plotted by the red solid curve with circles and blue dashed curve with squares. It is shown that the CIRT is finite with finite impurity density, indicating that the electron-impurity scattering surely can cause the charge-imbalance relaxation. Specifically, one sees in Fig. 8 that with the increase of the impurity density, the CIRT first decreases and then increases, showing similar features in the spin relaxation time (SRT) in the D'yakanov-Perel' (DP)<sup>119</sup> mechanism.<sup>73,120–126</sup> Furthermore, in the inset of Fig. 8, the temporal evolutions of the normalized effective chemical potential  $V/V_0$  are shown with different impurity densities  $n_i = 0$  (red solid curve),  $0.02n_0$  (green chain curve),  $n_0$  (blue dashed curve) and  $5n_0$  (yellow dashed curve). Specifically, when  $n_i = 0$ , the effective chemical potential does not relax to zero but to half of its initial value, indicating infinite charge-imbalance lifetime.

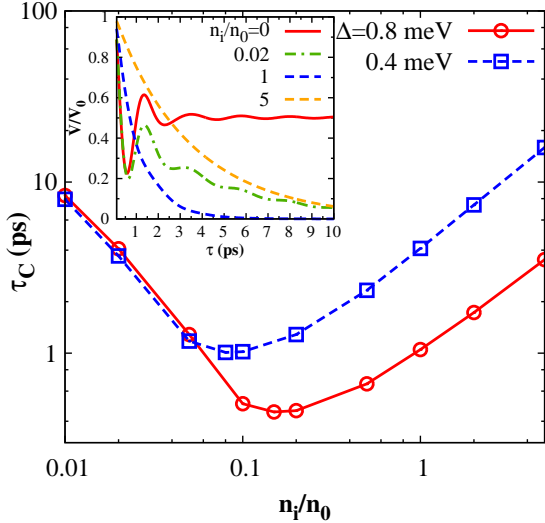


FIG. 8: (Color online) Impurity-density dependencies of the CIRT with  $\Delta = 0.8$  meV (red solid curve with circles) and  $0.4$  meV (blue dashed curve with squares), respectively. The finite CIRT shows that the electron-impurity scattering surely can cause the charge-imbalance relaxation. In the inset, the temporal evolutions of the normalized effective chemical potential  $V/V_0$  are shown with different impurity densities  $n_i = 0$  (red solid curve),  $0.02n_0$  (green chain curve),  $n_0$  (blue dashed curve), and  $5n_0$  (yellow dashed curve). Specially, when  $n_i = 0$ , the effective chemical potential does not relax to zero but to half of its initial value, indicating infinite charge-imbalance lifetime.

Although there exist similarities in the momentum-

scattering dependence of the relaxation rates, the DP mechanism<sup>73,120–126</sup> cannot simply explain the features revealed in the charge-imbalance relaxation. In the DP mechanism, the SOC acts as a momentum-dependent effective magnetic field  $\Omega(\mathbf{k})$ , around which the electron spins with different momenta process with different frequencies, i.e., the inhomogeneous broadening.<sup>73,127</sup> Without the momentum scattering, this inhomogeneous broadening can cause a free-induction decay due to the destructive interference. Whereas when there exists momentum scattering, the system can be divided into the weak and strong scattering regimes. In the weak scattering regime with  $|\Omega(\mathbf{k})|\tau_{\mathbf{k}} \gtrsim 1$ , the momentum scattering opens a spin relaxation channel and the electron SRT  $\tau_s$  is proportional to  $\tau_{\mathbf{k}}$ . Here,  $\tau_{\mathbf{k}}$  is the momentum relaxation time. In the strong scattering regime with  $|\Omega(\mathbf{k})|\tau_{\mathbf{k}} \ll 1$ , the momentum scattering suppresses the inhomogeneous broadening and  $\tau_s$  is inversely proportional to  $\tau_{\mathbf{k}}$ .<sup>73,120–126</sup> Nevertheless, when the SOC does not depend on the angle of momentum, the elastic scattering cannot provide the spin relaxation channel,<sup>73,128</sup> as long as the SOC is so weak that it can be neglected in the energy spectrum of the electron.<sup>129</sup>

It is interesting to see that although the effective chemical potential and quasiparticle excitation energy in the coherent term of Eq. (45) act as the effective SOC in the DP mechanism, they actually cannot provide the inhomogeneous broadening in the presence of the elastic scattering because of their momentum-angle independence.<sup>73,127,128</sup> Hence, the DP mechanism cannot explain the calculated charge-imbalance relaxation due to the electron-impurity scattering.<sup>73,128,129</sup> Moreover, one notes that even in the free situation, the CIRT is infinite, which is in contrast to the finite SRT in the DP mechanism.<sup>73,120–126</sup> Actually, a new mechanism is expected to be responsible for the charge-imbalance relaxation here. The concrete physical picture for the charge-imbalance relaxation can be obtained from the analytical analysis, which is presented as follows.

Due to the absence of the momentum angle in the coherent terms of Eq. (45), the calculation of the charge-imbalance relaxation can be markedly simplified. The density matrix can be expanded by its Fourier components, i.e.,  $\rho_{\mathbf{k}}^h = \rho_{\mathbf{k}}^h + \sum_{l=1}^{\infty} \rho_{\mathbf{k}}^{h,l} e^{il\theta_{\mathbf{k}}}$ . With the initial state Eq. (47), only the homogeneous component  $\rho_{\mathbf{k}}^h$  involves in the relaxation of the charge imbalance, whose kinetic equations are written as

$$\partial_T \rho_{\mathbf{k}}^h + i[\tilde{E}_{\mathbf{k}}\tau_3, \rho_{\mathbf{k}}^h] + i[\tilde{\mu}_{\text{eff}}\tau_1, \rho_{\mathbf{k}}^h] + (\rho_{\mathbf{k}}^h - \tau_3\rho_{\mathbf{k}}^h\tau_3)/\tau_{\mathbf{k}}^{\text{I}} - (\tau_1\tau_2\rho_{\mathbf{k}}^h - \tau_1\rho_{\mathbf{k}}^h\tau_3 + \text{h.c.})/\tau_{\mathbf{k}}^{\text{II}} = 0. \quad (48)$$

In Eq. (48),  $\tilde{E}_{\mathbf{k}} = E_{\mathbf{k}} + \mu_{\text{eff}}\zeta_{\mathbf{k}}/E_{\mathbf{k}}$ ,  $\tilde{\mu}_{\text{eff}} = -\mu_{\text{eff}}\Delta/E_{\mathbf{k}}$ ,

$$\frac{1}{\tau_{\mathbf{k}}^{\text{I}}} = \frac{n_i m^*}{2\pi} \int d\theta_{\mathbf{k}'-\mathbf{k}} |V_{\mathbf{k}-\mathbf{k}'}|^2 (u_{\mathbf{k}}^2 - v_{\mathbf{k}}^2)^2 \left| \frac{E_{\mathbf{k}}}{\zeta_{\mathbf{k}}} \right|, \quad (49)$$

$$\frac{1}{\tau_{\mathbf{k}}^{\text{II}}} = \frac{n_i m^*}{2\pi} \int d\theta_{\mathbf{k}'-\mathbf{k}} |V_{\mathbf{k}-\mathbf{k}'}|^2 (u_{\mathbf{k}}^2 - v_{\mathbf{k}}^2) u_{\mathbf{k}} v_{\mathbf{k}} \left| \frac{E_{\mathbf{k}}}{\zeta_{\mathbf{k}}} \right|, \quad (50)$$

with  $\theta_{\mathbf{k}}$  being the angle of momentum  $\mathbf{k}$ . It is noted that  $\tau_{\mathbf{k}}^I$  and  $\tau_{\mathbf{k}}^{II}$  in Eqs. (49) and (50) come from  $\partial_t \rho_{\mathbf{k}}^{\text{d}}|_{\text{scat}}$  and  $\partial_t \rho_{\mathbf{k}}^{\text{off}}|_{\text{scat}}$  in Eq. (45), respectively. Accordingly,  $\tau_{\mathbf{k}}^{54}$  directly breaks the quasiparticle-number conservation. Furthermore,  $\tau_{\mathbf{k}}^I$  and  $\tau_{\mathbf{k}}^{II}$  are different from the conventional momentum scattering time  $\tau_{\mathbf{k}}$ ,<sup>73,129</sup> although the former being in the same order as  $\tau_{\mathbf{k}}$ . Actually, from Eq. (50),  $\tau_{\mathbf{k}}^{II} > 0$  ( $\tau_{\mathbf{k}}^{II} < 0$ ) for the electron-like (hole-like) quasi-electron with  $|\mathbf{k}| > k_F$  ( $|\mathbf{k}| < k_F$ ).

By further expanding  $\rho_{\mathbf{k}}^h$  by the Pauli matrices in the Nambu space, i.e.,  $\rho_{\mathbf{k}}^h = \rho_{\mathbf{k},0}^h \tau_0 + \sum_{i=1}^3 \rho_{\mathbf{k},i}^h \tau_i$  with  $\tau_0 = \text{diag}\{1, 1\}$ , from Eq. (48), the kinetic equations for the components  $\rho_{\mathbf{k},i}^h$  ( $i = 1, 2, 3$ ) read

$$\frac{\partial}{\partial T} \begin{pmatrix} \rho_{\mathbf{k},1}^h \\ \rho_{\mathbf{k},2}^h \\ \rho_{\mathbf{k},3}^h \end{pmatrix} + \begin{pmatrix} 2/\tau_{\mathbf{k}}^I & 2\tilde{E}_{\mathbf{k}} & 0 \\ -2\tilde{E}_{\mathbf{k}} & 2/\tau_{\mathbf{k}}^I & 2\tilde{\mu}_{\text{eff}} \\ 4/\tau_{\mathbf{k}}^{II} & -2\tilde{\mu}_{\text{eff}} & 0 \end{pmatrix} \begin{pmatrix} \rho_{\mathbf{k},1}^h \\ \rho_{\mathbf{k},2}^h \\ \rho_{\mathbf{k},3}^h \end{pmatrix} = 0. \quad (51)$$

By using the components  $\rho_{\mathbf{k},i}^h$  of  $\rho_{\mathbf{k}}^h$ , the charge neutrality condition [Eq. (33)] becomes

$$n_0 = \sum_{\mathbf{k}} \left[ 1 - \frac{\zeta_{\mathbf{k}} + \mu_{\text{eff}}}{\sqrt{(\zeta_{\mathbf{k}} + \mu_{\text{eff}})^2 + \Delta^2}} + \frac{\zeta_{\mathbf{k}}}{E_{\mathbf{k}}} (1 + 2\rho_{\mathbf{k},3}^h) - \frac{2\Delta}{E_{\mathbf{k}}} \rho_{\mathbf{k},1}^h \right]. \quad (52)$$

Eq. (51) can be further analyzed in the near-equilibrium situation, in which the density matrix is composed of its equilibrium and deviation parts. By writing  $\rho_{\mathbf{k},i}^h = \bar{\rho}_{\mathbf{k},i}^h + \delta\rho_{\mathbf{k},i}^h$  with  $\bar{\rho}_{\mathbf{k},i}^h$  and  $\delta\rho_{\mathbf{k},i}^h$  being the equilibrium and deviation parts, Eq. (51) are linearized to be

$$\partial_T \delta\rho_{\mathbf{k},1}^h + 2\delta\rho_{\mathbf{k},1}^h/\tau_{\mathbf{k}}^I + 2E_{\mathbf{k}}\delta\rho_{\mathbf{k},2}^h = 0, \quad (53)$$

$$\partial_T \delta\rho_{\mathbf{k},2}^h - 2E_{\mathbf{k}}\delta\rho_{\mathbf{k},1}^h + 2\delta\rho_{\mathbf{k},2}^h/\tau_{\mathbf{k}}^I + \mu_{\text{eff}}\Delta/E_{\mathbf{k}} = 0, \quad (54)$$

$$\partial_T \delta\rho_{\mathbf{k},3}^h + 4\delta\rho_{\mathbf{k},1}^h/\tau_{\mathbf{k}}^{II} = 0. \quad (55)$$

The features of the charge-imbalance relaxation without and with impurities can be understood based on Eqs. (52) and (53-55). We first analyze the impurity-free limit with  $1/\tau_{\mathbf{k}}^I = 1/\tau_{\mathbf{k}}^{II} = 0$  in Eqs. (53-55). From Eq. (55), one observes that in the impurity-free limit,  $\delta\rho_{\mathbf{k},3}^h$  does not evolve with time, which contributes the charge imbalance due to the non-equilibrium quasiparticle population. Furthermore, in the steady state with the effective chemical potential denoted by  $\mu_{\text{eff}}^{\infty}$ , from Eqs. (53) and (54), one obtains  $\delta\rho_{\mathbf{k},2}^h = 0$  and  $\delta\rho_{\mathbf{k},1}^h = \mu_{\text{eff}}^{\infty}\Delta/(2E_{\mathbf{k}}^2)$ . Then from the charge neutrality condition [Eq. (52)], in the steady state,  $\sum_{\mathbf{k}} [-\frac{\Delta^2}{E_{\mathbf{k}}^2}(\mu_{\text{eff}}^0 - 2\mu_{\text{eff}}^{\infty})] = 0$  with  $\mu_{\text{eff}}^0$  being the initial effective chemical potential. Hence, the steady-state effective chemical potential  $\mu_{\text{eff}}^{\infty} = \mu_{\text{eff}}^0/2$ , which explains the steady state found in the numerical calculation (shown by the red solid curve in the inset of Fig. 7).

When there exists the momentum scattering, we first address the role of  $\tau_{\mathbf{k}}^I$  in the charge-imbalance relaxation. One notes that in Eq. (54),  $\delta\rho_{\mathbf{k},3}^h$  does not directly influence the evolutions of  $\delta\rho_{\mathbf{k},1}^h$  and  $\delta\rho_{\mathbf{k},2}^h$ , but rather influences them through the influence on  $\mu_{\text{eff}}$ . By neglecting

$1/\tau_{\mathbf{k}}^{II}$  in Eq. (55),  $\delta\rho_{\mathbf{k},3}^h$  still does not evolve with the time. Then from Eqs. (53) and (54), one obtains that in the steady state,  $\delta\rho_{\mathbf{k},1}^h = \frac{\Delta}{2E_{\mathbf{k}}^2}\mu_{\text{eff}}^{\infty}/[1 + \frac{1}{(E_{\mathbf{k}}\tau_{\mathbf{k}}^I)^2}]$ . Furthermore, from the charge neutrality condition [Eq. (52)], one obtains  $\sum_{\mathbf{k}} \{ -\frac{\Delta^2}{E_{\mathbf{k}}^2} [\mu_{\text{eff}}^0 - \mu_{\text{eff}}^{\infty} (1 + \frac{(E_{\mathbf{k}}\tau_{\mathbf{k}}^I)^2}{1 + (E_{\mathbf{k}}\tau_{\mathbf{k}}^I)^2})] \} = 0$ , which indicates that  $\mu_{\text{eff}}^0/2 < \mu_{\text{eff}}^{\infty} < \mu_{\text{eff}}^0$ . Specifically, this further indicates that when  $\langle E_{\mathbf{k}}\tau_{\mathbf{k}}^I \rangle \ll 1$ , the charge-imbalance relaxation can be suppressed by  $\tau_{\mathbf{k}}^I$  by suppressing the induction of  $\rho_{\mathbf{k},1}^h$ , i.e., the correlation between the quasi-electron and quasi-hole. Moreover, from Eq. (55), one finds that in the presence of  $\tau_{\mathbf{k}}^{II}$ , the induction of the quasiparticle correlation  $\delta\rho_{\mathbf{k},1}^h$  directly leads to the fluctuation of the quasiparticle number  $\delta\rho_{\mathbf{k},3}^h$ . Actually, this directly induces the annihilation of the extra quasiparticles in the quasi-electron and quasi-hole bands into the Cooper pairs.<sup>60,101-103</sup>

Therefore,  $\tau_{\mathbf{k}}^{II}$  can directly open a charge-imbalance relaxation channel by relaxing the charge imbalance due to the quasiparticle population, whose rate of change also depends on the value of the correlation between the quasi-electron and quasi-hole. Accordingly, there exists the competition between the scattering terms Eqs. (49) and (50), leading to the non-monotonic dependence on the momentum scattering for the CIRT. Specifically, in the weak scattering limit with  $\langle E_{\mathbf{k}}\tau_{\mathbf{k}}^I \rangle \gg 1$ , one expects that the momentum scattering due to  $\tau_{\mathbf{k}}^{II}$  can directly open a charge-imbalance relaxation channel with the CIRT proportional to the momentum scattering strength. In the strong scattering regime with  $\langle E_{\mathbf{k}}\tau_{\mathbf{k}}^I \rangle \ll 1$ , the induction of the quasi-electron and quasi-hole correlation can be directly suppressed by the impurity scattering, which can further suppress the charge-imbalance relaxation through the quasiparticle population. In this situation, the CIRT is enhanced with the increase of the momentum scattering strength. From this physical picture,  $\langle E_{\mathbf{k}}\tau_{\mathbf{k}}^I \rangle \approx \Delta \langle \tau_{\mathbf{k}}^I \rangle = 1$  labels the boundaries between the weak and strong scattering regimes. Thus, with  $\langle \tau_{\mathbf{k}}^I \rangle$  less influenced by the order parameter, the position of the boundaries between the weak and strong scattering regimes scales according to  $1/\Delta$  (refer to the blue dashed and red solid curves in Fig. 8).

Finally, we summarize the physical picture for the charge-imbalance relaxation channels provided by the elastic scattering. It is emphasized that the quasiparticle correlation between the quasi-electron and quasi-hole states, i.e.,  $\langle \alpha_{\mathbf{k}\uparrow} \beta_{\mathbf{k}\downarrow} \rangle$ , is responsible for the charge-imbalance relaxation, which is often overlooked in the previous studies.<sup>2,59,60</sup> Here, the existence of the non-equilibrium effective chemical potential itself can cause the precession between the quasi-electron and quasi-hole states, directly inducing the quasiparticle correlation. Once the quasiparticle correlation is induced, in the presence of the electron-impurity scattering, the process involving the annihilation of the quasi-electron and quasi-hole into the Cooper pairs, i.e.,  $\alpha_{\mathbf{k}\uparrow} \beta_{\mathbf{k}\downarrow} S^{\dagger}$ , is inevitably triggered [refer to Eq. (55)],<sup>54,60,101,102</sup> whose rate of change is directly determined by  $|\tau_{\mathbf{k}}^{II}|$  defined in Eq. (50).

This process has been schematically presented in Fig. 2. Consequently, the annihilation of the extra quasiparticles in the quasi-electron and quasi-hole bands directly causes the relaxation of charge imbalance for the quasiparticles and contributes to the fluctuation of the effective chemical potential for the condensate. Nevertheless, although the presence of the impurity scattering directly opens a charge-imbalance relaxation channel due to the quasiparticle population, it also suppresses the induction of the quasiparticle correlation. This competition between the relaxation channels due to the quasiparticle correlation and population leads to the non-monotonic dependence on the momentum scattering for the charge-imbalance relaxation. Accordingly, although there exist the similarities in the momentum-scattering dependence between the CIRT and SRT in the DP mechanism, their relaxation mechanisms are totally different.

### III. $(s+p)$ -WAVE SUPERCONDUCTING (100) QWS

In this section, we study the optical response to the THz pulses in the  $(s+p)$ -wave superconducting QWs, which can be realized in the strong spin-orbit coupled InSb (100) QWs in proximity to an  $s$ -wave superconductor.<sup>103,130</sup> In our previous work,<sup>103</sup> we have shown that in this configuration, due to the Rashba-like SOC, not only the  $p$ -wave triplet Cooper pairing but also the corresponding triplet order parameter can be induced, which are in  $(p_x \pm ip_y)$ -type. Moreover, we find that the  $\mathbf{l}$ -vector for the triplet anomalous correlation and

$\mathbf{d}$ -vector for the triplet order parameter are parallel to the effective magnetic field due to the SOC. Similar configuration can also be realized in CePt<sub>3</sub>Si superconducting film, which is a heavy-Fermion material.<sup>131–133</sup> Here, based on the understanding on the equilibrium properties of  $(s+p)$ -wave superconductor,<sup>103,130–133</sup> it is intriguing to explore their non-equilibrium properties, especially those of the triplet Cooper pairs. Below, we first present the Hamiltonian and then extend the gauge-invariant optical Bloch equations in the  $s$ -wave case to the  $(s+p)$ -wave one. Finally, we numerically calculate the optical response by solving the optical Bloch equations, focusing on the properties related to the spin dynamics of triplet Cooper pairs (Sec. III C 1). The features in the Higgs-mode excitation and charge-imbalance dynamics are also addressed (Sec. III C 2).

#### A. Hamiltonian

In the  $(s+p)$ -wave superconducting (100) QWs, the Hamiltonian is composed by the free BdG Hamiltonian  $\tilde{H}_0$  and the interaction Hamiltonian including the electron-electron Coulomb and electron-impurity interactions  $\tilde{H}_{ee}$  and  $\tilde{H}_{ei}$ . Here, the electron-phonon interaction is neglected due to its weak contribution at the low temperature (refer to Sec. II C). Specifically, the free BdG Hamiltonian in the presence of an optical field propagating along the  $\hat{z}$ -direction, in which the vector potential is assumed to be along the  $\hat{x}$ -direction, is written as<sup>54,133</sup>

$$\tilde{H}_0 = \int \frac{d\mathbf{r}}{2} \tilde{\Psi}^\dagger \begin{pmatrix} \frac{(\mathbf{p} - \frac{e}{c}\mathbf{A})^2}{2m^*} - \mu + e\phi(x) & -\alpha(k_x - \frac{eA_x}{c}) - i\alpha k_y & \frac{\Delta_p}{2} \{e^{i\zeta(x)}, e^{i\theta_{\mathbf{k}}}\} & \Delta_s e^{i\zeta(x)} \\ -\alpha(k_x - \frac{eA_x}{c}) + i\alpha k_y & \frac{(\mathbf{p} - \frac{e}{c}\mathbf{A})^2}{2m^*} - \mu + e\phi(x) & -\Delta_s e^{i\zeta(x)} & -\frac{\Delta_p}{2} \{e^{i\zeta(x)}, e^{-i\theta_{\mathbf{k}}}\} \\ \frac{\Delta_p}{2} \{e^{-i\zeta(x)}, e^{-i\theta_{\mathbf{k}}}\} & -\Delta_s e^{-i\zeta(x)} & -\frac{(\mathbf{p} + \frac{e}{c}\mathbf{A})^2}{2m^*} + \mu - e\phi(x) & -\alpha(k_x + \frac{eA_x}{c}) + i\alpha k_y \\ \Delta_s e^{-i\zeta(x)} & -\frac{\Delta_p}{2} \{e^{-i\zeta(x)}, e^{i\theta_{\mathbf{k}}}\} & -\alpha(k_x + \frac{eA_x}{c}) - i\alpha k_y & -\frac{(\mathbf{p} + \frac{e}{c}\mathbf{A})^2}{2m^*} + \mu - e\phi(x) \end{pmatrix} \tilde{\Psi}. \quad (56)$$

Here,  $\tilde{\Psi}(x) = (\psi_\uparrow(x), \psi_\downarrow(x), \psi_\uparrow^\dagger(x), \psi_\downarrow^\dagger(x))$  represents the field operator in the Nambu $\otimes$ spin space;  $\alpha = \gamma_D(\pi/a)^2$  for the infinitely deep well with  $\gamma_D$  being the Dresselhaus coefficient; and  $\Delta_p$  ( $\Delta_s$ ) is the magnitude of the  $p$ -wave triplet ( $s$ -wave singlet) order parameter. The electron-electron Coulomb and electron-impurity interactions are written as

$$\tilde{H}_{ee} = \int \frac{d\mathbf{r}d\mathbf{r}'}{8} U(\mathbf{r} - \mathbf{r}') [\tilde{\Psi}^\dagger(\mathbf{r}) \mathcal{T}_3 \tilde{\Psi}(\mathbf{r})] [\tilde{\Psi}^\dagger(\mathbf{r}') \mathcal{T}_3 \tilde{\Psi}(\mathbf{r}')], \quad (57)$$

$$\tilde{H}_{ei} = \frac{1}{2} \int d\mathbf{r} \tilde{\Psi}^\dagger(\mathbf{r}) V(\mathbf{r}) \mathcal{T}_3 \tilde{\Psi}(\mathbf{r}), \quad (58)$$

respectively, in which  $\mathcal{T}_3 = \text{diag}\{1, 1, -1, -1\}$ . Finally,

it is addressed that in this Hamiltonian [Eqs. (56), (57) and (58)], there exists similar gauge structure as the one in the  $s$ -wave superconductor [Eqs. (10-12)].

#### B. Optical Bloch Equations

In this part, we generalize the optical Bloch equations in the  $s$ -wave superconducting QWs to the ones in the  $(s+p)$ -wave situation. Here, in the  $\mathbf{p}_s$ -gauge, the optical

Bloch equations in the homogeneous situation read

$$\begin{aligned}
& \frac{\partial \rho_{\mathbf{k}}}{\partial T} + i \left[ \left( \frac{\mathbf{k}^2}{2m^*} - \Phi \right) \mathcal{T}_3 + h_{\mathbf{k}}^{\text{soc}}, \rho_{\mathbf{k}} \right] + \frac{1}{2} \left\{ \frac{\partial \mathbf{p}_s}{\partial T} \mathcal{T}_3, \frac{\partial \rho_{\mathbf{k}}}{\partial \mathbf{k}} \right\} \\
& + i \left[ \begin{pmatrix} 0 & -\alpha \mathbf{p}_s^x & 0 & 0 \\ -\alpha \mathbf{p}_s^x & 0 & 0 & 0 \\ 0 & 0 & 0 & \alpha \mathbf{p}_s^x \\ 0 & 0 & \alpha \mathbf{p}_s^x & 0 \end{pmatrix}, \rho_{\mathbf{k}}^{\text{off}} \right] + i \left[ \frac{\mathbf{p}_s^2}{2m^*} \mathcal{T}_3, \rho_{\mathbf{k}} \right] \\
& + i \left[ \begin{pmatrix} 0 & 0 & \Delta_p e^{i\phi_{\mathbf{k}}} & \Delta_s \\ 0 & 0 & -\Delta_s & -\Delta_p e^{-i\phi_{\mathbf{k}}} \\ \Delta_p e^{-i\phi_{\mathbf{k}}} & -\Delta_s & 0 & 0 \\ \Delta_s & -\Delta_p e^{i\phi_{\mathbf{k}}} & 0 & 0 \end{pmatrix}, \rho_{\mathbf{k}} \right] \\
& = \frac{\partial \rho_{\mathbf{k}}}{\partial t} \Big|_{\text{HF}} + \frac{\partial \rho_{\mathbf{k}}}{\partial t} \Big|_{\text{scat}}. \tag{59}
\end{aligned}$$

The details of the derivation have been outlined in Sec. II B. In Eq. (59),  $\rho_{\mathbf{k}}$  is the  $4 \times 4$  density matrix in the Nambu $\otimes$ spin space,<sup>54</sup>  $\Phi = \mu - \mu_{\text{eff}}$ ;  $h_{\mathbf{k}}^{\text{soc}} = -\alpha k_x \tau_0 \otimes \sigma_x + \alpha k_y \tau_3 \otimes \sigma_y$  represents the SOC Hamiltonian in the Nambu $\otimes$ spin space;  $\rho_{\mathbf{k}}^{\text{off}} = \frac{1}{2}(\rho_{\mathbf{k}} - \mathcal{T}_3 \rho_{\mathbf{k}} \mathcal{T}_3)$  only includes the off-diagonal blocks of the density matrix. Furthermore, in Eq. (59), in the left-hand side of the equation, the fourth term comes from the supercurrent-induced effective SOC, which can directly induce the dynamics of the Cooper-pair anomalous correlation; in the right-hand side of the equation, the HF and scattering terms are written as

$$\frac{\partial_t \rho_{\mathbf{k}}}{\Big|_{\text{HF}}} = i \sum_{\mathbf{k}'} U_{\mathbf{k}-\mathbf{k}'} \left[ \mathcal{T}_3 (\rho_{\mathbf{k}'} - \bar{\rho}_{\mathbf{k}'}) \mathcal{T}_3, \rho_{\mathbf{k}} \right], \tag{60}$$

$$\begin{aligned}
\frac{\partial_t \rho_{\mathbf{k}}}{\Big|_{\text{scat}}} &= -\pi n_i \sum_{\mathbf{k}'} \sum_{\eta_1, \eta_2=1}^4 |V_{\mathbf{k}-\mathbf{k}'}|^2 \delta(\mathcal{E}_{\mathbf{k}'\eta_1} - \mathcal{E}_{\mathbf{k}\eta_2}) \\
&\times \left[ \mathcal{T}_3 \tilde{\Gamma}_{\mathbf{k}'\eta_1} \mathcal{T}_3 \tilde{\Gamma}_{\mathbf{k}\eta_2} \rho_{\mathbf{k}} - \mathcal{T}_3 \rho_{\mathbf{k}} \tilde{\Gamma}_{\mathbf{k}'\eta_1} \mathcal{T}_3 \tilde{\Gamma}_{\mathbf{k}\eta_2} + \text{H.c.} \right]. \tag{61}
\end{aligned}$$

Specifically, in Eq. (60),  $\bar{\rho}_{\mathbf{k}}$  is the density matrix in the equilibrium state.<sup>103</sup> In Eq. (61),  $\mathcal{E}_{\mathbf{k}1} = E_{\mathbf{k}}^+$ ,  $\mathcal{E}_{\mathbf{k}2} = E_{\mathbf{k}}^-$ ,  $\mathcal{E}_{\mathbf{k}3} = -E_{\mathbf{k}}^+$  and  $\mathcal{E}_{\mathbf{k}4} = -E_{\mathbf{k}}^-$ , where  $E_{\mathbf{k}}^{\pm} = \sqrt{(\varepsilon_{\mathbf{k}}^{\pm} - \mu)^2 + \Delta_{\pm}^2}$  with  $\varepsilon_{\mathbf{k}}^{\pm} = \mathbf{k}^2/(2m^*) \pm \alpha k$  and  $\Delta_{\pm} = |\Delta_s \pm \Delta_p|$ . The projection operators  $\tilde{\Gamma}_{\mathbf{k}\eta} = \tilde{\mathcal{U}}_{\mathbf{k}} \tilde{Q}_{\mathbf{k}\eta} \tilde{\mathcal{U}}_{\mathbf{k}}^{\dagger}$  with  $\tilde{Q}_{\mathbf{k}1} = \text{diag}(1, 0, 0, 0)$ ,  $\tilde{Q}_{\mathbf{k}2} = \text{diag}(0, 1, 0, 0)$ ,  $\tilde{Q}_{\mathbf{k}3} = \text{diag}(0, 0, 1, 0)$  and  $\tilde{Q}_{\mathbf{k}4} = \text{diag}(0, 0, 0, 1)$  being the projection operators in the quasiparticle space. Here,  $\tilde{\mathcal{U}}_{\mathbf{k}}$  is the unitary transformation matrix from the particle space to the quasiparticle one, which is written as

$$\tilde{\mathcal{U}}_{\mathbf{k}} = \frac{\sqrt{2}}{2} \begin{pmatrix} u_{\mathbf{k}}^+ e^{-i\phi_{\mathbf{k}}} & -u_{\mathbf{k}}^+ & v_{\mathbf{k}}^+ & v_{\mathbf{k}}^+ e^{-i\phi_{\mathbf{k}}} \\ -u_{\mathbf{k}}^- & -u_{\mathbf{k}}^- e^{i\phi_{\mathbf{k}}} & v_{\mathbf{k}}^- e^{i\phi_{\mathbf{k}}} & -v_{\mathbf{k}}^- \\ v_{\mathbf{k}}^+ & -v_{\mathbf{k}}^+ e^{i\phi_{\mathbf{k}}} & -u_{\mathbf{k}}^+ e^{i\phi_{\mathbf{k}}} & -u_{\mathbf{k}}^+ \\ -v_{\mathbf{k}}^- e^{-i\phi_{\mathbf{k}}} & -v_{\mathbf{k}}^- & -u_{\mathbf{k}}^- & u_{\mathbf{k}}^- e^{-i\phi_{\mathbf{k}}} \end{pmatrix}. \tag{62}$$

In Eq. (62),  $u_{\mathbf{k}}^{\pm} = \sqrt{1/2 + \zeta_{\mathbf{k}}^{\pm}/(2E_{\mathbf{k}}^{\pm})}$  and  $v_{\mathbf{k}}^{\pm} = \sqrt{1/2 - \zeta_{\mathbf{k}}^{\pm}/(2E_{\mathbf{k}}^{\pm})}$  with  $\zeta_{\mathbf{k}}^{\pm} = \varepsilon_{\mathbf{k}}^{\pm} - \mu$ .

Finally, it is addressed that in Eq. (59),  $\mu_{\text{eff}}$  in  $\Phi$  is unspecified, which can also be determined by the charge neutrality condition from the self-consistent equation<sup>61,63-69</sup>

$$\begin{aligned}
N_0 &= \frac{1}{2} \sum_{\mathbf{k}} \left\{ 2 - \frac{\varepsilon_{\mathbf{k}}^+ - \Phi}{\sqrt{(\varepsilon_{\mathbf{k}}^+ - \Phi)^2 + \Delta_+^2}} - \frac{\varepsilon_{\mathbf{k}}^- - \Phi}{\sqrt{(\varepsilon_{\mathbf{k}}^- - \Phi)^2 + \Delta_-^2}} \right. \\
&\left. + \text{Tr} \left[ \tilde{\mathcal{U}}_{\mathbf{k}} (\rho_{\mathbf{k}}^h - \frac{1 - \mathcal{T}_3}{2} \tilde{\mathcal{U}}_{\mathbf{k}}^{\dagger} \mathcal{T}_3) \right] \right\}. \tag{63}
\end{aligned}$$

Here,  $N_0$  is the electron density in the QWs, and  $\rho_{\mathbf{k}}^h = \tilde{\mathcal{U}}_{\mathbf{k}}^{\dagger} \rho_{\mathbf{k}} \tilde{\mathcal{U}}_{\mathbf{k}}$  is the density matrix in the quasiparticle space. In the numerical calculation below,  $\mathbf{p}_s$  takes the same form as the one in Eq. (34).

### C. Numerical Results

In this subsection, we present the numerical results by solving the optical Bloch equations [Eqs. (59), (34) and (63)] in the specific material InSb (100) QWs in proximity to an  $s$ -wave superconductor. All parameters used in our computation are listed in Table II.<sup>109,134</sup>

TABLE II: Parameters used in the computation for InSb (100) QWs in proximity to an  $s$ -wave superconductor.<sup>109,134</sup>

$m^*/m_0$	0.015	$N_0$ (cm <sup>-2</sup> )	$8 \times 10^{14}$
$\kappa_0$	16.8	$\gamma_D$ (eV $\cdot$ $\text{\AA}^3$ )	389
$T_e$ (K)	5	$a$ (nm)	3
$\Delta_p$ (meV)	0.05	$\sigma_t$ (ps)	4

In our computation, the electron density is chosen to be  $n_e \leq 3N_0$ . With this density, electrons mainly populate at the lower branch of the energy band ( $\varepsilon_{\mathbf{k}}^-$ -band), as shown in Fig. 9 by the red solid curve.<sup>54</sup> In this situation, one sees in Fig. 9 that the Fermi ‘‘sphere’’ (the blue region) is in the shape of an annulus with the inner and outer Fermi surfaces represented by the yellow and black circles. Then some approximations can be made for the scattering term [Eq. (61)] to reduce the computation complication.<sup>129</sup> On one hand, with  $\mu \lesssim 0$  at low temperature, the scattering between  $\varepsilon_{\mathbf{k}}^+$ - and  $\varepsilon_{\mathbf{k}}^-$ -bands contributes marginally to the scattering process; on the other hand, the scattering between the inner and outer Fermi surfaces can be neglected, because in this process, large momentum magnitude needs to be changed.<sup>129</sup>

#### 1. Optical Excitation of Spin Polarization of Cooper Pairs

In our previous work,<sup>103</sup> it has been revealed that in the InSb (100) QWs in proximity to an  $s$ -wave superconductor, due to the Rashba-like SOC, the spin polarization of electrons in the momentum space is parallel

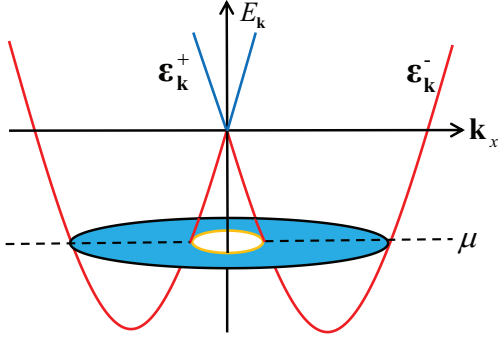


FIG. 9: (Color online) Schematic of the band structures of  $\varepsilon_{\mathbf{k}}^+$ - and  $\varepsilon_{\mathbf{k}}^-$ -bands, shown by the blue and red solid curves, respectively. The dashed line labeled by  $\mu$  corresponds to the chemical potential, with which only the lower band is efficiently populated. In this situation, one sees that the Fermi “sphere” (the blue region) is in the shape of an annulus with the inner and outer Fermi surfaces represented by the yellow and black circles.

to the effective magnetic field  $\mathbf{\Omega}(\mathbf{k})$  due to the SOC in the equilibrium state. This feature is all the same as the one in the normal state.<sup>54,129</sup> In the *normal* state, it has been well understood that when there exists electrical field, with the drift of electron states due to the applied field, this parallel relation is broken and hence the effective magnetic field  $\mathbf{\Omega}(\mathbf{k})$  can induce the momentum-dependent out-of-plane spin polarization, which accounts for the spin current of electrons.<sup>129</sup> Moreover, the center-of-mass momentum driven by the electrical field contributes to the effective magnetic field, which tends to polarize the electron states along this effective magnetic field.<sup>57,72,74,75</sup> In the superconducting state in our configuration, we show that both the spin polarization and spin current can be induced by the optical field, which oscillate with the same frequency of the optical field. Nevertheless, with our computation parameters, we find that the order parameters have little influence on the optical generations of the spin polarization and spin current. The details are presented in Appendix C.

Furthermore, in the superconducting InSb (100) QWs, we have revealed that there exists *p*-wave triplet Cooper pairing in  $(p_x \pm ip_y)$ -type.<sup>103</sup> With the frequency and momentum-dependent<sup>76,83,88,104</sup> Cooper pairing written as  $[f_s(\mathbf{k}, \omega) + \mathbf{f}(\mathbf{k}, \omega) \cdot \boldsymbol{\sigma}]i\sigma_y$ , it can be further shown that the  $\mathbf{f}$ -vector of the triplet Cooper pairing is also parallel to the effective magnetic field  $\mathbf{\Omega}(\mathbf{k})$  due to the SOC.<sup>103</sup> By analogy with the optical generation of the spin polarization addressed above, one expects that the  $\mathbf{f}$ -vector can also be controlled by the optical field. Actually, very recently, Tkachov indeed showed that in noncentrosymmetric superconductors, the driven center-of-mass momentum  $\mathbf{q}$  of the Cooper pairs can induce the nonunitary triplet pairing, which contributes to the spin polarization of the triplet Cooper pairs.<sup>83</sup> Specifically, with the spin polarization of Cooper pairs  $\mathbf{S}_{\mathbf{k}}^{\text{CP}}$  described by  $i\mathbf{f}(\mathbf{k}, \omega = 0) \times \mathbf{f}^*(\mathbf{k}, \omega = 0)$ , Tkachov showed

that with small superfluid velocity, the Cooper-pair spin polarization<sup>83</sup>

$$\mathbf{S}_{\mathbf{k}}^{\text{CP}} \propto \mathbf{\Omega}_{\mathbf{k}} \times [\mathbf{\Omega}_{\mathbf{k}} \times (\mathbf{q} \cdot \partial_{\mathbf{k}})\mathbf{\Omega}_{\mathbf{k}}]. \quad (64)$$

It is noted that Tkachov’s calculation is performed in the static situation, in which the supercurrent is induced from the proximity effect.<sup>83</sup> Nevertheless, with the superfluid velocity dynamically generated by the optical field, we expect that the Cooper-pair spin polarization can also be induced, which has not yet been reported in the literature. Particularly, the optical method can avoid the complexity when introducing the supercurrent by the proximity effect. Furthermore, the study of the dynamics of the Cooper-pair spin polarization can provide more understanding from the microscopic point of view. Actually, before the concrete calculation, the feature of Cooper-pair spin polarization in (100) InSb QWs can be roughly conjectured based on Eq. (64). Here, for the Dresselhaus SOC in the Rashba-like type, i.e.,  $\mathbf{\Omega}_{\mathbf{k}} = -\alpha k_x \hat{\mathbf{x}} + \alpha k_y \hat{\mathbf{y}}$ , with the center-of-mass momentum  $\mathbf{q} = q_x \hat{\mathbf{x}}$ , we conjecture from Eq. (64)

$$\mathbf{S}_{\mathbf{k}}^{\text{CP}} \propto \mathbf{\Omega}_{\mathbf{k}} \times [\mathbf{\Omega}_{\mathbf{k}} \times (\mathbf{q} \cdot \partial_{\mathbf{k}})\mathbf{\Omega}_{\mathbf{k}}] = q_x k_y^2 \hat{\mathbf{x}} + q_x k_x k_y \hat{\mathbf{y}}. \quad (65)$$

This indicates that the  $\hat{\mathbf{x}}$ -component ( $\hat{\mathbf{y}}$ -component) of the Cooper-pair spin polarization is even (odd) in momentum, which is proportional to  $k_y^2$  ( $k_x k_y$ ). Then the *total* Cooper-pair spin polarization, which is in sum of the momentum, is along the  $\hat{\mathbf{x}}$ -direction.

In our framework, in the density matrix, the information about the frequency has been integrated [Eq. (22)], in which the Cooper pairing is integrated to be the anomalous correlation.<sup>9,54,103</sup> Actually, it is reasonable to define the Cooper-pair spin polarization by using the anomalous correlation but not Cooper pairing at zero frequency.<sup>83</sup> Microscopically, the Cooper-pair spin polarization is calculated by the wavefunction of the triplet Cooper pairs [Eq. (3)], which does not depend on the relative temporal coordinate (refer to Ref. 9). Furthermore, the Fourier components of the Cooper-pair wavefunction are exactly the *anomalous correlation*,<sup>9</sup> which can be directly calculated by the optical Bloch equations. Here, the anomalous correlation of the Cooper pairs is conveniently expressed as

$$\begin{pmatrix} \rho_{13}(\mathbf{k}) & \rho_{14}(\mathbf{k}) \\ \rho_{23}(\mathbf{k}) & \rho_{24}(\mathbf{k}) \end{pmatrix} = [l_0(\mathbf{k})\sigma_0 + \mathbf{l}(\mathbf{k}) \cdot \boldsymbol{\sigma}]i\sigma_y, \quad (66)$$

in which the  $\mathbf{l}$ -vector ( $l_0$ ) describes the anomalous correlation of the triplet (singlet) Cooper pairs. Accordingly, from definition of the Cooper-pair spin polarization in Eq. (4), by using the  $\mathbf{l}$ -vector, the total spin polarization of the Cooper pair reads

$$\mathbf{P}_{\text{C}} = \frac{\sum_{\mathbf{k}} i\mathbf{l}(\mathbf{k}) \times \mathbf{l}^*(\mathbf{k})}{\sum_{\mathbf{k}} [|\mathbf{l}_x(\mathbf{k})|^2 + |\mathbf{l}_y(\mathbf{k})|^2 + |\mathbf{l}_z(\mathbf{k})|^2]}, \quad (67)$$

in which the denominator is introduced to act as the normalization factor.

Then the temporal evolution of  $\mathbf{P}_C$  is calculated by the optical Bloch equations, in which it is found that only the  $\hat{x}$ -component  $\mathbf{P}_C^x$  exists, in agreement with the analysis in Eq. (65). Specifically, in Fig. 10, the temporal evolutions of  $\mathbf{P}_C^x$  are plotted with different electron densities  $n_e = 3N_0$  (yellow dashed curve),  $2N_0$  (green chain curve) and  $N_0$  [red solid (blue dotted) curve in the absence (presence) of the impurity]. It is noted that for these three electron densities, the chemical potentials are about 4.2,  $-9.9$  and  $-15.6$  meV, respectively, which are larger than the minimal value of the energy spectra  $-m^*\alpha^2/2 \approx -17.9$  meV.<sup>103</sup> In Fig. 10, it can be seen that in the impurity-free situation, when  $n_e = 2N_0$  and  $N_0$ , the total spin polarizations of the Cooper pairs are significant, which oscillate with the frequency of the optical field. Whereas when  $n_e = 3N_0$ , corresponding to a positive chemical potential, the total Cooper-pair spin polarization is efficiently suppressed, whose oscillation does not show a particular pattern. This reveals that the low electron density with *single-band population* is in favor of the realization of significant Cooper-pair total spin polarization. This is in contrast to the optical excitation of the electron spin polarization, which is less influenced by the electron density (refer to Appendix C). Finally, we also calculate the total Cooper-pair spin polarization with the impurity density  $n_i = N_0$ , which is presented by the blue dotted curve in Fig. 10. One finds that the impurity can even enhance the optical excitation of the total Cooper-pair spin polarization.

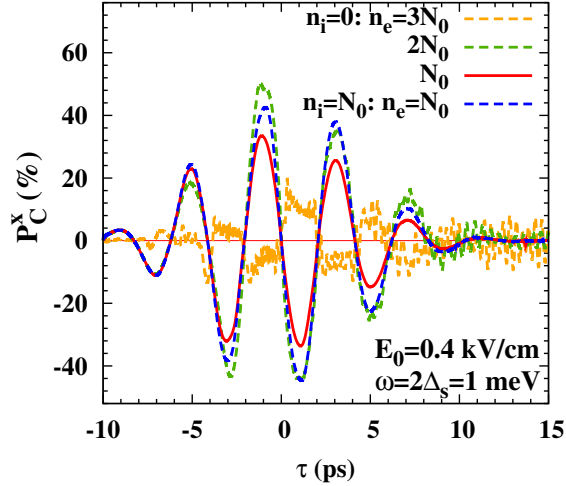


FIG. 10: (Color online) Temporal evolutions of the  $\hat{x}$ -component of the total Cooper-pair spin polarization  $\mathbf{P}_C^x$  with different electron densities  $n_e = 3N_0$  (yellow dashed curve),  $2N_0$  (green chain curve) and  $N_0$  [red solid (blue dotted) curve in the absence (presence) of the impurity].  $E_0 = 0.4$  kV/cm. The blue dotted curve denotes the total Cooper-pair spin polarization in the presence of the impurity with  $n_i = N_0$ .

To further reveal the dynamical features of  $\mathbf{P}_C$  from the microscopic viewpoint, we calculate the momentum distribution of the Cooper-pair spin vector  $\mathbf{n}(\mathbf{k}) \equiv$

$i\mathbf{l}(\mathbf{k}) \times \mathbf{l}^*(\mathbf{k})$  in the dynamical evolution. When  $n_e = N_0$  in the impurity-free situation, at a particular time  $\tau = 0.5$  ps with  $\mathbf{p}_s^x \approx -0.4k_F < 0$  ( $k_F = \sqrt{2\pi N_0}$ ), the  $\hat{x}$ - and  $\hat{y}$ -components of  $\mathbf{n}(\mathbf{k})$  in the momentum space are plotted in Figs. 11(a) and (b), respectively. With this electron density  $n_e = N_0$ , the Fermi “sphere” is in the shape of an annulus with the inner and outer Fermi surfaces (refer to Fig. 9). It can be seen that  $\mathbf{n}(\mathbf{k})$  is significant only around the inner and outer Fermi surfaces.<sup>54,103</sup> Moreover, one finds that  $\mathbf{n}_x(\mathbf{k}) \propto -k_y^2$  and  $\mathbf{n}_y(\mathbf{k}) \propto -k_x k_y$  in both the inner and outer Fermi surfaces, in agreement with Eq. (65). Thus, only  $\mathbf{n}_x(\mathbf{k})$  contributes to the total Cooper-pair spin polarization after the sum of momentum. Furthermore, a specific feature is found by comparing the Cooper-pair spin vectors in the inner and outer Fermi surfaces. It is intriguing to observe that both  $\mathbf{n}_x(\mathbf{k})$  and  $\mathbf{n}_y(\mathbf{k})$  are larger in the inner Fermi surface than those in the outer one. These numerical results can be understood from the analytical analysis in the following.

It is convenient to set up simplified kinetic equations for  $l_0$  and  $\mathbf{l}$ -vector from the optical Bloch equations [Eq. (59)], which can be used to analyze the dynamics of Cooper pairing directly. Moreover, from the simplified kinetic equations, the kinetic equations for the Cooper-pair spin vectors can be obtained. Specifically, with the third, fifth and sixth terms in the left-hand side and the HF-term in the right-hand side of Eq. (59) neglected, (which have been checked to be unimportant in the excitation of Cooper-pair spin polarization by the numerical calculations), the kinetic equations for  $l_0$  and  $\mathbf{l}$ -vector become

$$\begin{aligned} \partial_T(l_0 + \mathbf{l} \cdot \boldsymbol{\sigma}) + i\{\zeta_{\mathbf{k}} - \alpha k_x \sigma_x + \alpha k_y \sigma_y, l_0 + \mathbf{l} \cdot \boldsymbol{\sigma}\} \\ + i[-\alpha \mathbf{p}_s^x \sigma_x, l_0 + \mathbf{l} \cdot \boldsymbol{\sigma}] = 0. \end{aligned} \quad (68)$$

In the matrix form,

$$\begin{aligned} \partial_T \begin{pmatrix} l_0 \\ \mathbf{l}_k^x \\ \mathbf{l}_k^y \\ \mathbf{l}_k^z \end{pmatrix} + 2i \begin{pmatrix} \zeta_{\mathbf{k}} & -\alpha k_x & \alpha k_y & 0 \\ -\alpha k_x & \zeta_{\mathbf{k}} & 0 & 0 \\ \alpha k_y & 0 & \zeta_{\mathbf{k}} & i\alpha \mathbf{p}_s^x \\ 0 & 0 & -i\alpha \mathbf{p}_s^x & \zeta_{\mathbf{k}} \end{pmatrix} \begin{pmatrix} l_0 \\ \mathbf{l}_k^x \\ \mathbf{l}_k^y \\ \mathbf{l}_k^z \end{pmatrix} \\ = 0. \end{aligned} \quad (69)$$

In Eq. (69), one finds that  $l_0$  is coupled to the  $\mathbf{l}$ -vector due to the SOC. It is noted that in the equilibrium state, the  $\mathbf{l}$ -vector of the triplet Cooper correlation is parallel to the effective magnetic field  $\boldsymbol{\Omega}(\mathbf{k})$  due to the SOC in the momentum space. When the optical field with in-plane vector potential is applied to the superconducting system, the superconducting velocity is induced, which directly contributes to the effective SOC, i.e.,  $\pm i\alpha \mathbf{p}_s^x$ , in Eq. (69). This effective SOC can cause the precession of the  $\mathbf{l}$ -vectors, with the component perpendicular to  $\boldsymbol{\Omega}(\mathbf{k})$  induced. Thus, from the definition  $\mathbf{n}(\mathbf{k}) = i\mathbf{l}(\mathbf{k}) \times \mathbf{l}^*(\mathbf{k})$ ,<sup>83</sup> the Cooper-pair spin polarization  $\mathbf{n}(\mathbf{k})$  is expected.

To make this point more concrete, from Eq. (69), the kinetic equations for the  $\mathbf{n}$ -vector can be derived, written

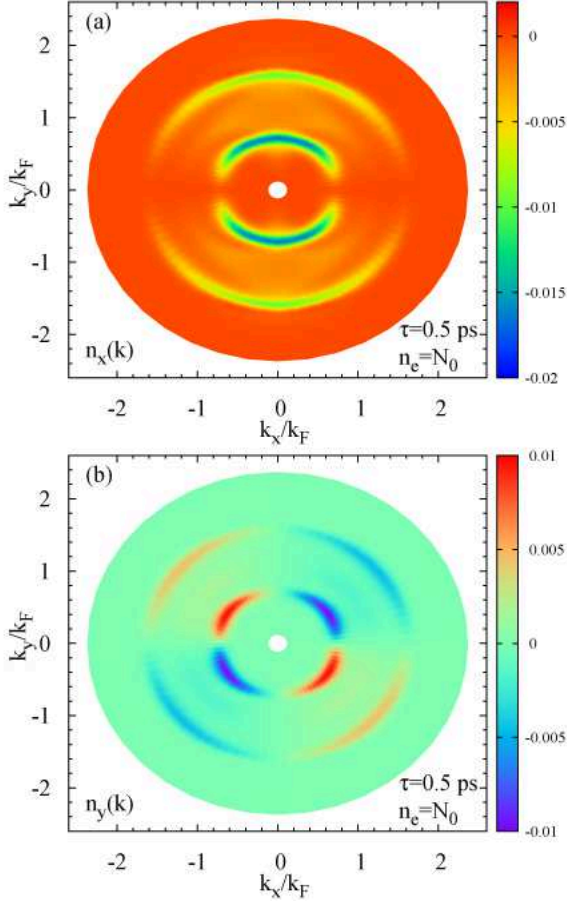


FIG. 11: (Color online) Momentum distributions of the Cooper-pair spin vectors  $\mathbf{n}_x(\mathbf{k})$  [(a)] and  $\mathbf{n}_y(\mathbf{k})$  [(b)] at  $\tau = 0.5$  ps when  $n_e = N_0$  and  $n_i = 0$ .  $E_0 = 0.4$  kV/cm. At this particular time  $\tau = 0.5$  ps,  $\mathbf{p}_s^x \approx -0.4k_F < 0$  with  $k_F = \sqrt{2\pi N_0}$ . In the figures, it can be seen that  $\mathbf{n}_x(\mathbf{k}) \propto -k_y^2$  and  $\mathbf{n}_y(\mathbf{k}) \propto -k_x k_y$  in both the inner and outer Fermi surfaces, in agreement with Eq. (65). One further observes that both  $\mathbf{n}_x(\mathbf{k})$  and  $\mathbf{n}_y(\mathbf{k})$  are larger in the inner Fermi surface than the those in the outer Fermi one.

as

$$\partial_T^2 \mathbf{n}_x + 4\alpha^2 k_y (k_x \mathbf{n}_y + k_y \mathbf{n}_x) + 4\alpha^2 k_y \mathbf{p}_s^x (\mathbf{l}_y^* l_0 + \mathbf{l}_y l_0^*) = \mathbf{0} \quad (70)$$

$$\partial_T \mathbf{n}_y = (k_x/k_y) \partial_T \mathbf{n}_x + 2\alpha \mathbf{p}_s^x \mathbf{n}_z, \quad (71)$$

$$\partial_T^2 \mathbf{n}_z + 4\alpha^2 k^2 \mathbf{n}_z + 2\alpha \mathbf{p}_s^x \partial_T \mathbf{n}_y + 4\alpha^2 k_x \mathbf{p}_s^x (\mathbf{l}_z^* l_0 + \mathbf{l}_z l_0^*) = \mathbf{0} \quad (72)$$

From Eqs. (70-72), it is concluded that  $\mathbf{n}_x \propto \mathbf{p}_s^x$ ,  $\mathbf{n}_y \propto \mathbf{p}_s^x$ , and  $\mathbf{n}_z \propto (\mathbf{p}_s^x)^2$ . This is because in the equilibrium state,  $\bar{\mathbf{l}}_z = 0$  (“bar” labels the equilibrium state), whose first order deviation is proportional to  $\mathbf{p}_s^x$ . By only keeping the quantities in the first order of  $\mathbf{p}_s^x$ , one obtains from Eq. (71) that

$$k_y \mathbf{n}_y = k_x \mathbf{n}_x, \quad (73)$$

which satisfies the numerical results presented in Figs. 11(a) and (b). Thus, from Eq. (70), one obtains

$$\partial_T^2 \mathbf{n}_x + 4\alpha^2 k^2 \mathbf{n}_x + 8\alpha^2 k_y \mathbf{p}_s^x \bar{\mathbf{l}}_y l_0 = 0, \quad (74)$$

whose solution reads

$$\mathbf{n}_x(\mathbf{k}) \approx \frac{8\alpha^2 k_y \bar{\mathbf{l}}_y l_0}{\omega^2 - 4\alpha^2 k^2} \mathbf{p}_s^x. \quad (75)$$

Here,  $\bar{l}_0(\mathbf{k})$  and  $\bar{\mathbf{l}}_y(\mathbf{k})$  in the equilibrium state are<sup>54,103</sup>

$$\bar{l}_0 = u_{\mathbf{k}}^+ v_{\mathbf{k}}^+ [2f_0(E_{\mathbf{k}}^+) - 1] + u_{\mathbf{k}}^- v_{\mathbf{k}}^- [2f_0(E_{\mathbf{k}}^-) - 1], \quad (76)$$

$$\bar{\mathbf{l}}_y = \frac{k_y}{k} \{u_{\mathbf{k}}^+ v_{\mathbf{k}}^+ [2f_0(E_{\mathbf{k}}^+) - 1] - u_{\mathbf{k}}^- v_{\mathbf{k}}^- [2f_0(E_{\mathbf{k}}^-) - 1]\} \quad (77)$$

It is noted that when  $\omega$  tends to zero, Eq. (75) directly recovers the static results in the work of Tkachov.<sup>83</sup> Furthermore, Eq. (75) also describes the dynamical situation especially at the high frequency. Moreover, it is expected that the Cooper-pair spin polarization can be resonantly excited for particular momenta around  $k^* \equiv \omega/(2\alpha)$ . Nevertheless, this resonance is pronounced only when  $k^* \approx k_F$ , at which the anomalous correlation in the equilibrium state  $\bar{l}_0(\mathbf{k})$  and  $\bar{\mathbf{l}}(\mathbf{k})$  are significant.

The features for the dynamics of Cooper-pair spin polarization revealed in the numerical calculation can be understood based on Eq. (75). Specifically, from Eqs. (73), (75-77), one obtains that  $\mathbf{n}_x(\mathbf{k}) \propto k_y^2 \mathbf{p}_s^x$  and  $\mathbf{n}_y(\mathbf{k}) \propto k_x k_y \mathbf{p}_s^x$ , confirming the conjecture in Eq. (65). Furthermore, it is observed that in Eq. (77), the contributions of the anomalous correlation from the lower and upper bands are opposite, which is relatively large in the situation with *single-band population*<sup>103</sup> (refer to Fig. 10). Thus, the induced total Cooper-pair polarization is significant when only the lower-band is populated. It is noted when  $n_e \geq N_0$ ,  $\omega \ll \alpha k$ . Thus,

$$\mathbf{n}_x(\mathbf{k}) \approx -2(k_y/k^2) \bar{\mathbf{l}}_y l_0 \mathbf{p}_s^x, \quad (78)$$

which is inversely proportional to the momentum. This relation naturally explains the calculated results that the induced Cooper-pair spin vector is larger in the inner Fermi surface than the one in the outer Fermi surface (refer to Fig. 11). Finally, it is addressed that from Eq. (75), it is obtained that the Cooper-pair spin polarization is stabilized by the superconducting momentum.

## 2. Higgs Mode and Charge Imbalance

In this part, we consider the dynamics of the Higgs mode and charge imbalance excited by the THz pulses in the (*s+p*)-wave superconducting InSb (100) QWs. In this configuration, although there exists strong SOC, most features for the dynamics of the Higgs mode and charge imbalance are revealed to be similar to those in the *s*-wave one (refer to Sec. II). Nevertheless, a novel regime with  $|\mathbf{p}_s|$  larger than the Fermi momentum can be realized without destroying the superconductivity. One notes that the regime with  $|\mathbf{p}_s|$  larger than the Fermi momentum is hard to be realized in the QWs with a single Fermi surface, e.g., the *s*-wave superconducting GaAs QWs considered in Sec. II, in which the superconductivity can be destroyed when  $|\mathbf{p}_s| \gtrsim k_F$ . Nevertheless, with



typical electron densities  $n_e \lesssim 3N_0$ , in InSb (100) QWs, the specific band structure results in two Fermi surfaces due to the strong SOC, which are labeled by the yellow and black circles in Fig. 9. It is observed that the Fermi momentum of the inner Fermi surface (inner Fermi momentum) can be much smaller than one of the outer Fermi surface (outer Fermi momentum). Thus, in InSb QWs, the superconducting momentum can be tuned to be larger than the inner Fermi momentum but smaller than the outer one, but without destroying the superconductivity.

Particularly, compared to the situation in the  $s$ -wave superconducting GaAs QWs, when  $|\mathbf{p}_s|$  is tuned to be larger than the inner Fermi momentum in InSb QWs, some new features in the excitation of the Higgs mode and creation of the charge imbalance are expected. For the excitation of the Higgs mode, in GaAs QWs, we have shown that the pump effect plays a marginal role (refer to Sec. II C 1). Nevertheless, it is estimated that the pump effect influences the excitation of the Higgs mode as long as  $|\mathbf{p}_s|$  is larger than the Fermi momentum. Accordingly, with  $|\mathbf{p}_s|$  larger than the inner Fermi momentum in InSb (100) QWs, the pump of the quasiparticles around the inner Fermi surface is now expected. For the creation of the charge imbalance, in GaAs QWs, we have found that the pump effect still has significant contribution (refer to Sec. II C 2). Furthermore, it is revealed that the charge imbalance is contributed by the pump and drive effects separately, through influencing the quasiparticle correlation and quasiparticle population, respectively (refer to Fig. 7). This fact indicates that in GaAs QWs, the system still lies in the “linear” regime without any interplay between the pump and drive effects. Nevertheless, when  $|\mathbf{p}_s|$  is tuned to be larger than the inner Fermi momentum in InSb QWs, the interplay between the pump and drive effects is expected.

*a. Higgs mode* We first focus on the Higgs mode. As with the electron densities we considered ( $n_e \leq 3N_0$ ), the triplet order parameter and its fluctuation are much smaller than the singlet one,<sup>54</sup> here we focus on the Higgs mode contributed by the singlet order parameter  $|\delta\Delta_s|$ . In Fig. 12, the temporal evolutions of the Higgs mode  $|\delta\Delta_s|$  are plotted with different optical-field frequencies  $\omega = 2\Delta_s$  (green dashed curve) and  $4\Delta_s$  (red solid curve) when  $n_e = N_0$ . The electrical field strength is taken to be relatively large  $E_0 = 0.4$  kV/cm, with which the peak value of  $\mathbf{p}_s$  is about  $0.6\tilde{k}_F$  ( $0.3\tilde{k}_F$ ) when  $\omega = 2\Delta_s$  ( $\omega = 4\Delta_s$ ). Here,  $\tilde{k}_F = \sqrt{2\pi N_0}$ . With this electric field, the peak value of  $\eta \approx 2$  meV when  $\omega = 2\Delta_s$ , is larger than  $2\Delta_s = 1$  meV, indicating that the system lies in the strong-pump regime. It can be seen in Fig. 12 that the Higgs modes  $|\delta\Delta_s|$  oscillate with twice the frequency of the optical field and plateaus appear after the optical pulse. These features are similar to the ones in the  $s$ -wave superconducting QWs.

However, it is observed that the pump effect can have significant contribution to the excitation of the Higgs mode when  $\omega = 2\Delta_s$ , in contrast to the situation in the

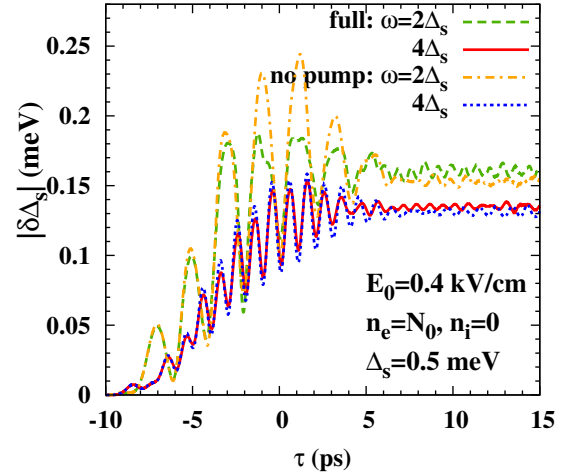


FIG. 12: (Color online) Temporal evolutions of the Higgs mode for the singlet order parameter  $|\delta\Delta_s|$  with different frequencies  $\omega = 2\Delta_s$  (green dashed curve) and  $4\Delta_s$  (red solid curve) when  $n_e = N_0$  and  $n_i = 0$ .  $E_0 = 0.4$  kV/cm. When the pump effect is neglected,  $|\delta\Delta_s|$  are plotted for  $\omega = 2\Delta_s$  (yellow chain curve) and  $4\Delta_s$  (blue dotted curve). By comparing the green dashed (red solid) curve with the yellow chain (blue dotted) curve, one finds that when  $\omega = 2\Delta_s$  ( $\omega = 4\Delta_s$ ), the pump effect can have significant (marginal) role in the excitation of the Higgs mode.

$s$ -wave superconducting QWs (refer to Sec. II C 1). It is shown in Fig. 12 that with the pump effect neglected in the calculation, when  $\omega = 2\Delta_s$  the yellow chain curve is markedly different from the green dashed curve; nevertheless, when  $\omega = 4\Delta_s$ , the blue dotted curve still almost coincides with the red solid one. These can be understood as follows. It is noted that when  $n_e = N_0$  here, the Fermi momentum of the inner (outer) Fermi surface  $k_F^< \approx 0.5\tilde{k}_F$  ( $k_F^> \approx 1.4\tilde{k}_F$ ). Thus, when  $\omega = 2\Delta_s$ ,  $|\mathbf{p}_s| \lesssim 0.6\tilde{k}_F$  can be comparable to the Fermi momentum of the inner Fermi surface, indicating that the system lies in the regime with  $|\mathbf{p}_s| \gtrsim k_F^<$ . In this regime, it has been estimated that the pump effect can survive from the Pauli blocking due to the drive effect and hence contribute to the excitation of the Higgs mode (refer to Sec. II C 1 c). Furthermore, by comparing the yellow chain and green dashed curves, one observes that the pump effect actually suppresses, rather enhances, the excitation of the Higgs mode.

*b. Charge imbalance* Then we analyze the optical excitation of the charge imbalance. The temporal evolutions of the effective chemical potential are shown in Fig. 13 in the free situation. In the calculation, the electron density  $n_e = 2N_0$  and  $\omega = 2\Delta_s = 1$  meV. The electric field strength is relatively large with  $E_0 = 0.4$  kV/cm, with which the system lies not only in the strong-pump regime but also in the regime with  $|\mathbf{p}_s| \gtrsim k_F^<$ . In Fig. 13, the blue dashed curve denotes the full calculation with both the drive and pump effects included, whereas the red solid (green chain) curve represents the calculated results with only the drive (pump) effect re-

tained. It can be seen that the effective chemical potential is always positive, and no longer equals to the sum of the ones contributed by the drive and pump effects separately. This is in contrast to the features revealed in the  $s$ -wave superconducting GaAs QWs, indicating that there exists significant interplay between the pump and drive effects. Moreover, our calculated results indicate that in the competition between the pump and drive effects in the creation of the charge imbalance, the drive effect is dominant.

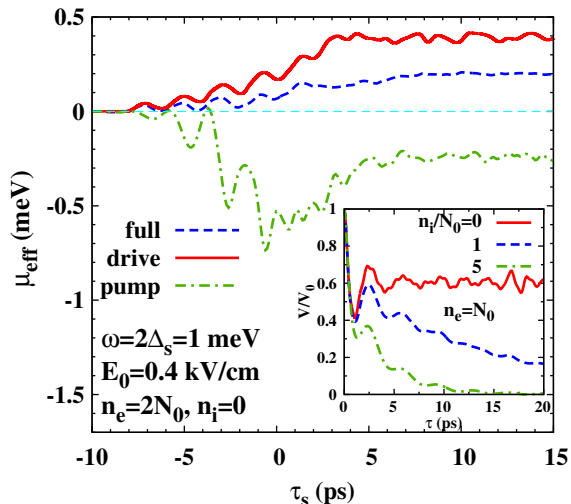


FIG. 13: (Color online) Temporal evolutions of the effective chemical potential in the free situation. The electron density  $n_e = 2N_0$  and  $\omega = 2\Delta_s \approx 1.15$  THz. The electric field strength is relatively large with  $E_0 = 0.4$  kV/cm, with which the system lies in the strong-pump and strong-drive regimes. In the figure, the blue dashed curve denotes the full calculation with both the drive and pump effects included, whereas the red solid (green chain) curve represents the calculated results with only the drive (pump) effect retained. In the inset, the temporal evolution of the charge imbalance is presented with  $n_e = N_0$  with different impurity densities  $n_i = 0$  (the red solid curve),  $n_i = N_0$  (the blue dashed curve) and  $n_i = 5N_0$  (the green chain curve), respectively.

Finally, it is addressed that the electron-impurity scattering can still provide the charge-imbalance relaxation channel in the  $(s+p)$ -wave superconducting QWs, whose features are similar to the situation in the  $s$ -wave one (refer to Sec. II C 2). This can be seen in the inset of the Fig. 13 that when  $n_i = 0$ , the normalized effective chemical potential  $V/V_0$  does not relax to zero, represented by the red solid curve; whereas when there exists impurities, the relaxation channel for the charge imbalance can be opened, as shown by the blue dashed ( $n_i = N_0$ ) and green chain ( $n_i = 5N_0$ ) curves.

#### IV. CONCLUSION AND DISCUSSION

In conclusion, we have investigated the optical response to the THz pulses in both the  $s$ -wave and  $(s+p)$ -wave superconducting semiconductor QWs. We set up the gauge-invariant optical Bloch equations via the gauge-invariant nonequilibrium Green function approach,<sup>94,97,98</sup> with the gauge structure revealed by Nambu explicitly retained.<sup>30</sup> In the gauge-invariant Green function approach, the gauge-invariant Green function with the Wilson line is constructed.<sup>100</sup> By choosing the  $\mathbf{p}_s$ -gauge, in the gauge-invariant optical Bloch equations, not only can the microscopic description for the quasiparticle dynamics be realized, but also the dynamics of the condensate is included, with the superfluid momentum  $\mathbf{p}_s$  and the effective chemical potential  $\mu_{\text{eff}}$  naturally incorporated. It is addressed that  $\mathbf{p}_s$  directly contributes to the center-of-mass momentum and  $\mu_{\text{eff}}$  corresponds to the collective excitation revealed by Nambu,<sup>30,32,35,36</sup> evolving with time in the homogeneous limit. We show that  $\mathbf{p}_s$  plays an important role in the dynamics of quasiparticles. Its nonlinear term  $\propto \mathbf{p}_s^2$  contributes to the pump of the quasiparticles (pump effect), and its rate of change  $\partial_t \mathbf{p}_s$  acts as a drive field to drift the quasiparticles (drive effect). Specifically, the drive effect can contribute to the formation of the blocking region<sup>48–55</sup> for the quasiparticle, which directly suppresses the anomalous correlation of Cooper pairs (refer to Fig. 1). It is found that both the pump and drive effects contribute to the excitation of the Higgs mode, which oscillates with twice the frequency of the optical field. However, it is shown that the contribution from the drive effect to the excitation of Higgs mode is dominant as long as the driven superconducting momentum is less than the Fermi momentum. This is because in this condition, the pump of the quasiparticle population is efficiently suppressed thanks to the Pauli blocking. This is in sharp contrast to the conclusions obtained from the Liouville<sup>37,38,40</sup> or Bloch<sup>39,41–44,46</sup> equations in the literature, in which the drive effect is overlooked with only the pump effect considered. Actually, in these treatments,<sup>37–44,46</sup> the contribution of the Cooper-pair center-of-mass momentum to the suppression of the anomalous correlation of Cooper pairs is overlooked. In our framework, the role of the electron-impurity scattering on the excitation of the superconducting state is also revealed, which is found to further suppress the Cooper pairing on the basis of the drive effect.

In the gauge-invariant optical Bloch equations, the charge neutrality condition is self-consistently considered based on the two-component model for the charge. In this model, the deviation from the equilibrium state for the quasiparticle, i.e., the charge imbalance, can cause the fluctuation of the effective chemical potential  $\mu_{\text{eff}}$  for the condensate.<sup>1–4,59–61</sup> This consideration is actually consistent with the one in the determination of the collective mode based on the gauge structure and charge conservation for the superconductivity.<sup>30,32,35,36</sup> We predict that

during the optical process, the charge imbalance can be created by both the pump and drive effects, with the former arising from the AC Stark effect and the latter coming from the breaking of Cooper pairs by the electrical field. Specifically, when  $|\mathbf{p}_s|$  is much smaller than the Fermi momentum, the charge imbalance is contributed by the pump and drive effects separately, through influencing the quasiparticle correlation and quasiparticle population, respectively.

The induction of the charge imbalance of quasiparticles directly causes the fluctuation of the effective chemical potential of the condensate. This fluctuation of the effective chemical potential is found to directly provide a charge-imbalance relaxation channel even with the elastic scattering due to impurities. This is in contrast to the previous understanding in the literature that in the isotropic  $s$ -wave superconductivity, the impurity scattering cannot cause any charge-imbalance relaxation.<sup>2,59,60</sup> Actually, the previous understanding is based on the framework with quasiparticle-number conservation but not the charge conservation, in which the charge-imbalance relaxation is induced by the direct scattering of quasiparticles between the electron- and hole-like branches in the presence of the impurities (refer to Fig. 2). This inter-branch scattering is forbidden for the electron-impurity scattering in the isotropic  $s$ -wave superconductivity thanks to the coherence factor ( $u_{\mathbf{k}}u_{\mathbf{k}'} - v_{\mathbf{k}}v_{\mathbf{k}'}$ ) in the scattering potential.<sup>2,59,60</sup> Furthermore, the momentum-scattering dependence of the charge-imbalance relaxation is revealed. When the momentum scattering is weak (strong), the charge-imbalance relaxation is enhanced (suppressed) by the momentum scattering.

Although the above momentum-scattering dependencies of the charge-imbalance relaxation seemingly resemble the ones in the DP mechanism,<sup>73,119–126</sup> we point out that the DP mechanism cannot explain the charge-imbalance relaxation in the presence of the elastic scattering.<sup>73,128,129</sup> In fact, a new mechanism is revealed to be responsible for the charge-imbalance relaxation here. We demonstrate that the charge-imbalance relaxation here is caused by the direct annihilation of the quasiparticles in the quasi-electron and quasi-hole bands (refer to Fig. 2), in which the quasiparticle-number conservation is *broken*. The source of the breaking of quasiparticle-number conservation is the quasiparticle correlation between the quasi-electron and quasi-hole states,<sup>54</sup> which is contributed by the quasiparticle precession induced by the non-equilibrium chemical potential of the condensate. Then, due to the electron-impurity scattering, the induction of the quasiparticle correlation further triggers the process of the condensation with two quasiparticles binding into one Cooper pair in the condensate, or vice versa.<sup>60,101,102</sup>

These processes can directly cause the annihilation of the extra quasiparticles in the quasi-electron or quasihole bands, due to which the charge-imbalance relaxation for the quasiparticles is induced. Meanwhile, with the con-

densation or breaking of the Cooper pairs in the condensate, the fluctuation of the effective chemical potential is also induced. Thus, through the quasiparticle correlation, the electron-impurity scattering opens a charge-imbalance relaxation channel due to the fluctuation of the quasiparticle population. Based on this picture, it is emphasized that the creation and relaxation of charge imbalance is a unique feature for the superconductivity with non-zero order parameter, in which the particle-number or quasiparticle-number fluctuation inherently exists due to the breaking of the global  $U(1)$  symmetry. It is further found that the induction of the quasiparticle correlation by  $\mu_{\text{eff}}$  is directly suppressed by the impurity scattering. Consequently, the competition between the relaxation channels due to the quasiparticle correlation and population leads to the non-monotonic dependence on the momentum scattering for the charge-imbalance relaxation.

By using the optical Bloch equations, the optical creation of the spin polarization for the Cooper pairs is investigated in the  $(s+p)$ -wave superconducting InSb (100) QWs. We predict that when the optical field with the in-plane vector potential applied, the total spin polarization of triplet Cooper pairs can be induced, which is shown to be parallel to the vector potential and oscillates with the frequency of the optical field. This can be understood as follows. In the equilibrium state, in the InSb superconducting (100) QWs with the Rashba-like SOC, the  $\mathbf{l}$ -vector of the anomalous correlation for the triplet Cooper pairs is parallel to the effective magnetic field  $\mathbf{\Omega}(\mathbf{k})$  due to the SOC.<sup>103</sup> Here,  $\mathbf{l}$ -vector is defined from  $[\mathbf{l}(\mathbf{k}) \cdot \boldsymbol{\sigma}]i\sigma_y = \begin{pmatrix} F_{\uparrow\uparrow}(\mathbf{k}) & F_{\uparrow\downarrow}(\mathbf{k}) \\ F_{\uparrow\downarrow}^*(\mathbf{k}) & F_{\downarrow\downarrow}(\mathbf{k}) \end{pmatrix}$  with  $F(\mathbf{k})$  representing the Fourier components of triplet Cooper-pair wavefunction in spatial space.<sup>9</sup> When the optical field with the in-plane vector potential is applied to this superconducting system, the superconducting velocity is induced, which is shown to contribute to an effective SOC. This induced effective SOC can cause the precession of the  $\mathbf{l}$ -vectors, with the component perpendicular to  $\mathbf{\Omega}(\mathbf{k})$  induced. Thus, the Cooper-pair spin vector can be induced by its definition  $\mathbf{n}(\mathbf{k}) = i\mathbf{l}(\mathbf{k}) \times \mathbf{l}^*(\mathbf{k})$ ,<sup>83</sup> whose summation by momentum contributes to the total spin polarization of Cooper pairs  $\mathbf{P}_C$  [Eq. (4)]. It is demonstrated that the induced Cooper-pair spin vector  $\mathbf{n}(\mathbf{k})$  is inversely proportional to the momentum. Moreover, it is revealed that the Cooper-pair spin polarization is proportional to the superconducting velocity, which oscillates with the frequency of the optical field. This shows that the Cooper-pair spin polarization is directly stabilized by the superconducting momentum.

Although our calculations are performed in the two-dimensional superconducting semiconductor QWs in particular materials with small and simple Fermi surfaces, the obtained predictions can still shed light on the optical response in the film of the superconducting metal, even with complex Fermi surfaces. In our set up, the

optical field and the correspondingly-induced superconducting velocity are treated to be homogeneous in the whole material. This is because with our material parameters, the London penetration depth  $\lambda_L \approx \sqrt{m^*/(\rho_s e^2)}$  for the magnetic field<sup>16</sup> is in the order of micrometer, much larger than the well width of the QWs. In this situation, the Meissner effect can be neglected and hence the optical field can efficiently penetrate into the material. Actually, even in the superconducting film of metal, the efficient penetration of the optical field is often considered to be satisfied,<sup>20–29</sup> to which the framework used in this work can be extended.

From the experimental point of view, we remark the possible experimental detections for our predictions, including the Higgs mode induced by the drive effect, the induction of the charge imbalance by the optical method, the novel relaxation channel for the charge imbalance due to the elastic scattering and the induction of the Cooper-pair spin polarization by the optical technique. Specifically, for the Higgs mode induced by the drive effect, our calculation shows that its oscillation amplitude is suppressed and plateau value after the pulse is enhanced by the electron-impurity scattering. Particularly, the latter feature is in contrast to the ones in the influence of the impurity on the pump effect.<sup>135</sup> Thus, the experimental observation on the impurity-density dependence of the Higgs-mode oscillation can help to distinguish the contribution to the Higgs mode from the drive and pump effects. For the charge imbalance induced by the optical method, it can be directly detected either through the voltage between the quasiparticle and condensate measured in the setup of Clarke's works,<sup>70,71</sup> or through the effective chemical potential measured in the Josephson effect.<sup>23</sup> These techniques with time resolution can also be used to measure the charge-imbalance relaxation due to the impurity scattering, which should be performed at low temperature with significant impurity density. As to the Cooper-pair spin polarization induced by the optical method, its direct observation is not as easy as the spin polarization of electrons. Nevertheless, it was proposed by Tkachov that the Cooper-pair spin polarization can be detected by the magnetoelectric Andreev effect.<sup>83</sup>

Finally, we remark the physical origin of the effective chemical potential from another point of view, which has been presented based on the consideration of the charge conservation in the two-component model for the charge.<sup>1–4,59–62</sup> From the gauge structure in the superconductivity, the effective chemical potential originates from the rate of change of the superconducting phase. Actually, based on the work of Ambegaokar and Kadanoff,<sup>32</sup> in the long-wave limit, the excited superconducting phase in the optical process is exactly the collective mode revealed by Nambu with the consideration of the gauge invariance in the superconductivity,<sup>30</sup> which is referred to as the Nambu-Goldstone mode in the field theory.<sup>31,100</sup> In both the experiment<sup>136,137</sup> and theory,<sup>138</sup> the Nambu-Goldstone mode was reported to directly contribute to the optical absorption, especially when the photon en-

ergy is below the superconducting gap. Based on this understanding, we conjecture that the effective chemical potential is contributed by the temporal variations of the Nambu-Goldstone mode, which is excited by the optical pulse. Therefore, the study on the effective chemical potential not only helps to reveal the dynamics of the charge imbalance, but also can shed light on the understanding of the optical excitation for the Nambu-Goldstone mode.

### Acknowledgments

This work was supported by the National Natural Science Foundation of China under Grant No. 11334014 and 6141136001. One of the authors (T.Y.) would like to thank M. Q. Weng for helpful discussions.

### Appendix A: OPTICAL BLOCH EQUATIONS IN QUASIPARTICLE SPACE

It is convenient to perform the analytical analysis for the dynamical process of the *quasiparticle* by the optical Bloch equations in the quasiparticle space. Here, we transform the optical Bloch equations in the particle space, i.e., Eq. (25), into the ones in the quasiparticle space by the unitary transformation Eq. (30), which are written as

$$\begin{aligned}
& \frac{\partial \rho_{\mathbf{k}}^h}{\partial T} + i \left[ E_{\mathbf{k}} \tau_3, \rho_{\mathbf{k}}^h \right] + i \left[ \mu_{\text{eff}} \tilde{\tau}_3, \rho_{\mathbf{k}}^h \right] + i \left[ \frac{\mathbf{p}_s^2}{2m^*} \tilde{\tau}_3, \rho_{\mathbf{k}}^h \right] \\
& + \frac{1}{2} \left\{ \frac{\partial \mathbf{p}_s}{\partial T} \tilde{\tau}_3, \frac{\partial \rho_{\mathbf{k}}^h}{\partial \mathbf{k}} \right\} + \frac{1}{2} \left\{ \frac{\partial \mathbf{p}_s}{\partial T} \tilde{\tau}_3, \left[ \rho_{\mathbf{k}}^h, \frac{\partial \mathcal{U}_{\mathbf{k}}}{\partial \mathbf{k}} \mathcal{U}_{\mathbf{k}}^\dagger \right] \right\} \\
& = i \sum_{\mathbf{k}'} U_{\mathbf{k}-\mathbf{k}'} \left[ (\mathcal{U}_{\mathbf{k}} \tau_3 \mathcal{U}_{\mathbf{k}'}^\dagger) (\rho_{\mathbf{k}'}^h - \rho_{\mathbf{k}'}^{h,0}) (\mathcal{U}_{\mathbf{k}'} \tau_3 \mathcal{U}_{\mathbf{k}}^\dagger), \rho_{\mathbf{k}}^h \right] \\
& - \pi n_i \sum_{\mathbf{k}' \eta = \pm} |V_{\mathbf{k}-\mathbf{k}'}|^2 \delta(E_{\mathbf{k}'\eta} - E_{\mathbf{k}\eta}) \left[ (\mathcal{U}_{\mathbf{k}} \tau_3 \mathcal{U}_{\mathbf{k}'}^\dagger) Q_\eta (\mathcal{U}_{\mathbf{k}'} \tau_3 \mathcal{U}_{\mathbf{k}}^\dagger) \right. \\
& \left. \times Q_\eta \rho_{\mathbf{k}}^h - (\mathcal{U}_{\mathbf{k}} \tau_3 \mathcal{U}_{\mathbf{k}'}^\dagger) \rho_{\mathbf{k}'}^h Q_\eta (\mathcal{U}_{\mathbf{k}'} \tau_3 \mathcal{U}_{\mathbf{k}}^\dagger) Q_\eta + \text{H.c.} \right], \quad (\text{A1})
\end{aligned}$$

whose structure is analyzed as follows.

In the second and third terms in Eq. (A1), the diagonal terms in  $\tilde{\tau}_3$  renormalize the quasiparticle excitation energy; whereas the off-diagonal terms cause the precession between the quasi-electron and quasi-hole states, which act as the pump term similar to the inter-band optical excitation in the semiconductor.<sup>94–96</sup> Specifically, it can be seen that the fluctuation of the condensate, i.e.,  $\mu_{\text{eff}}$ , can also contribute to the pump term, which definitely influences the dynamics of the quasiparticle. Moreover, in the quasiparticle space, the drive term is contributed by the fourth and fifth terms, with the latter originating from the Berry phase effect.<sup>115–117</sup> Finally, in the scattering term, only the electron-impurity scattering is presented here with the electron-phonon one [Eq. (29)] negligible at the low temperature.  $Q_\pm = 1/2 \pm \tau_3/2$  are the projection operators in the quasiparticle space. It is noted that the derived scattering term here is different from the one

used in the Boltzmann equation for the Bogoliubov quasiparticle, in which the contribution from the off-diagonal terms in  $\mathcal{U}_{\mathbf{k}}\tau_3\mathcal{U}_{\mathbf{k}'}^\dagger = (u_{\mathbf{k}}u_{\mathbf{k}'} - v_{\mathbf{k}}v_{\mathbf{k}'})\tau_3 - (u_{\mathbf{k}}v_{\mathbf{k}'} + v_{\mathbf{k}}u_{\mathbf{k}'})\tau_1$  is neglected by neglecting the correlation between the quasi-electron and quasi-hole states.<sup>2,5,54,60</sup>

Specifically, in the scattering term, the contributions from the diagonal and off-diagonal terms in  $\mathcal{U}_{\mathbf{k}}\tau_3\mathcal{U}_{\mathbf{k}'}^\dagger$  can be separated, which are represented by  $\partial_t\rho_{\mathbf{k}}^{\text{d}}|_{\text{scat}}$  and  $\partial_t\rho_{\mathbf{k}}^{\text{off}}|_{\text{scat}}$ , respectively. For the diagonal contribution,

$$\begin{aligned} \partial_t\rho_{\mathbf{k}}^{\text{d}}|_{\text{scat}} &= -2\pi n_i \sum_{\mathbf{k}'} |V_{\mathbf{k}-\mathbf{k}'}|^2 (u_{\mathbf{k}}u_{\mathbf{k}'} - v_{\mathbf{k}}v_{\mathbf{k}'})^2 \\ &\times \delta(E_{\mathbf{k}'} - E_{\mathbf{k}}) (\rho_{\mathbf{k}}^h - \tau_3\rho_{\mathbf{k}'}^h\tau_3), \end{aligned} \quad (\text{A2})$$

which recovers to the scattering term used in the Boltzmann equation for the Bogoliubov quasiparticle when the off-diagonal term in  $\rho_{\mathbf{k}}^h$  is neglected.<sup>2,5,54,60</sup> For the off-diagonal contribution,

$$\begin{aligned} \partial_t\rho_{\mathbf{k}}^{\text{off}}|_{\text{scat}} &= \pi n_i \sum_{\mathbf{k}'} |V_{\mathbf{k}-\mathbf{k}'}|^2 (u_{\mathbf{k}}u_{\mathbf{k}'} - v_{\mathbf{k}}v_{\mathbf{k}'}) (u_{\mathbf{k}}v_{\mathbf{k}'} + u_{\mathbf{k}'}v_{\mathbf{k}}) \\ &\times \delta(E_{\mathbf{k}'} - E_{\mathbf{k}}) (\tau_1\tau_3\rho_{\mathbf{k}}^h - \tau_1\rho_{\mathbf{k}'}^h\tau_3 + \text{H.c.}), \end{aligned} \quad (\text{A3})$$

Obviously, for the equilibrium distribution for the quasiparticle  $\rho_{\mathbf{k},0}^h = 1/2 + [f_0(E_{\mathbf{k}}) - 1/2]\tau_3$ , Eqs. (A2) and (A3) are exactly zero.

## Appendix B: QUASIPARTICLE AND SUPER-FLUID DENSITIES

In this part, we present the calculated quasiparticle and super-fluid densities under the optical THz pulse in the  $s$ -wave superconducting GaAs QWs. In Fig. 14, the temporal evolutions of the quasiparticle density  $\rho_q$  are plotted with different impurity densities  $n_i = 0$  (blue dashed curve),  $0.2n_0$  (red solid curve) and  $0.5n_0$  (green chain curve). It is shown that after the pulse  $\tau \gtrsim 5$  ps, there exist plateaus in the quasiparticle density, whose values increase with the increase of the impurity density. This is because the existence of the impurity density can enhance the optical absorption. These populations of the hot quasiparticles can efficiently suppress the Cooper pairing.

Then the normal-fluid and super-fluid densities  $\rho_n$  and  $\rho_s$  after the pulse are *estimated* based on the two-fluid model in the equilibrium state.<sup>16,107</sup> Specifically, for the order parameter  $\Delta = |\Delta|e^{i\mathbf{q}\cdot\mathbf{r}}$  with the center-of-mass momentum  $\mathbf{q} = 2m^*\mathbf{v}_s$  along the  $\hat{\mathbf{x}}$ -direction, the momentum supercurrent is calculated to be<sup>16,54</sup>

$$\begin{aligned} \mathbf{J}_s &= 2m^*\mathbf{v}_s \sum_{\mathbf{k}} \left[ v_{\mathbf{k}}^2 + (u_{\mathbf{k}}^2 - v_{\mathbf{k}}^2)f_0(\mathbf{k}\cdot\mathbf{v}_s + \sqrt{\Gamma_{\mathbf{k}}^2 + |\Delta|^2}) \right] \\ &+ 2 \sum_{\mathbf{k}} \mathbf{k}f_0(\mathbf{k}\cdot\mathbf{v}_s + \sqrt{\Gamma_{\mathbf{k}}^2 + |\Delta|^2}). \end{aligned} \quad (\text{B1})$$

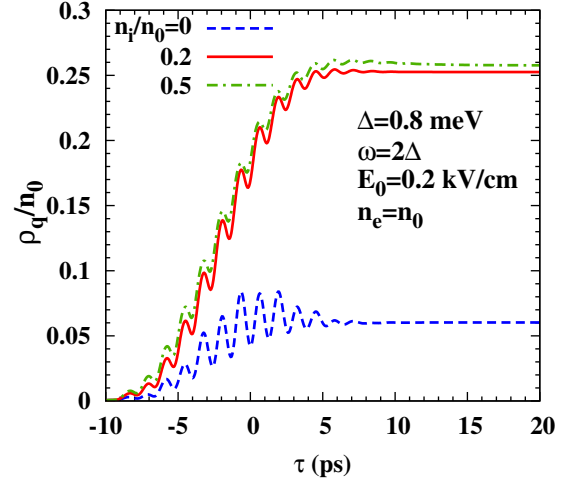


FIG. 14: (Color online) Temporal evolutions of the quasiparticle density  $\rho_q$  in the  $s$ -wave superconducting GaAs QWs under the optical THz pulse with different impurity densities  $n_i = 0$  (blue dashed curve),  $0.2n_0$  (red solid curve) and  $0.5n_0$  (green chain curve).  $E_0 = 0.2$  kV/cm and  $\omega = 2\Delta \approx 2.3$  THz.

with  $\Gamma_{\mathbf{k}} = k^2/(2m^*) - \mu + m^*\mathbf{v}_s^2/2$ . For the linear response,  $\mathbf{q}$  is small, hence,

$$\mathbf{J}_s \approx 2\mathbf{v}_s \sum_{\mathbf{k}} \left[ k_x^2 \frac{\partial f_0(E_{\mathbf{k}})}{\partial E_{\mathbf{k}}} + m^*v_{\mathbf{k}}^2 + m^*(u_{\mathbf{k}}^2 - v_{\mathbf{k}}^2)f_0(E_{\mathbf{k}}) \right]. \quad (\text{B2})$$

Thus, with  $\mathbf{J}_s \equiv \mathbf{v}_s m^* \rho_s$ , one obtains

$$\rho_s = 2 \sum_{\mathbf{k}} \left[ \frac{k_x^2}{m^*} \frac{\partial f_0(E_{\mathbf{k}})}{\partial E_{\mathbf{k}}} + v_{\mathbf{k}}^2 + (u_{\mathbf{k}}^2 - v_{\mathbf{k}}^2)f_0(E_{\mathbf{k}}) \right]. \quad (\text{B3})$$

For the normal parts, by assuming the drift distribution  $f_0(E_{\mathbf{k}} - \mathbf{k}\cdot\mathbf{v}_n)$  with  $\mathbf{v}_n = v_n\hat{\mathbf{x}}$ ,<sup>107</sup> the momentum normal-current reads

$$\mathbf{J}_n = 2 \sum_{\mathbf{k}} \mathbf{k}f_0(E_{\mathbf{k}} - \mathbf{k}\cdot\mathbf{v}_n) \approx 2v_n\hat{\mathbf{x}} \left[ - \sum_{\mathbf{k}} k_x^2 \frac{\partial f_0(E_{\mathbf{k}})}{\partial E_{\mathbf{k}}} \right].$$

Consequently, for the linear response with  $\mathbf{J}_n = \mathbf{v}_n m^* \rho_n$ , one has

$$\rho_n = -2 \sum_{\mathbf{k}} \frac{k_x^2}{m^*} \frac{\partial f_0(E_{\mathbf{k}})}{\partial E_{\mathbf{k}}}. \quad (\text{B4})$$

Obviously, from Eqs. (B3) and (B4),  $\rho_s + \rho_n = 2 \sum_{\mathbf{k}} \left[ v_{\mathbf{k}}^2 + (u_{\mathbf{k}}^2 - v_{\mathbf{k}}^2)f_0(E_{\mathbf{k}}) \right]$ , which is exactly the total particle density conserved due to the charge neutrality [Eq. (33)].

It is noticed that Eqs. (B3) and (B4) are established for the equilibrium state with  $f_0(E_{\mathbf{k}})$  representing the equilibrium quasiparticle distribution.<sup>16,107</sup> To estimate the super-fluid and normal-fluid densities at the non-equilibrium state, Eqs. (B3) and (B4) are extended with  $f_0(E_{\mathbf{k}})$  replaced by the non-equilibrium quasiparticle distribution calculated by optical Bloch equations [Eq. (25)],

which is isotropic in the momentum space after the pulse.<sup>20–22,24</sup> This extension is based on the fact that after the pulse, the quasiparticle distribution can be effectively described by an effective temperature.<sup>112–114</sup>

In Fig. 15, the impurity density dependencies of superfluid density after the pulse are plotted with different electrical fields  $E_0 = 0.05$  kV/cm (blue dashed curve with squares), 0.1 kV/cm (red solid curve with squares) and 0.2 kV/cm (green chain curve with squares). It is

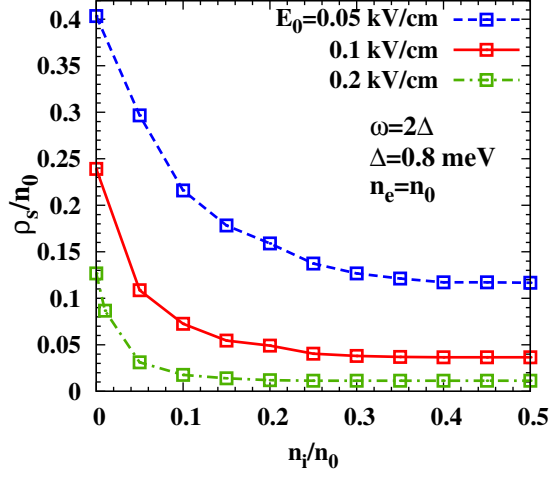


FIG. 15: (Color online) Impurity density dependence of the superfluid density  $\rho_s$  after the pulse, estimated from Eq. (B3), with different electrical fields  $E_0 = 0.05$  kV/cm (blue dashed curve with squares), 0.1 kV/cm (red solid curve with squares) and 0.2 kV/cm (green chain curve with squares).

shown that with the increase of the impurity density, the superfluid density decreases. This is consistent with the fact that with the optical pulse, the presence of the impurity can further suppress the Cooper pairing [refer to Fig. 4(c)]. Specifically, one sees that although there exists a significant order parameter after the pulse, the superfluid density can be extremely small at the non-equilibrium state.

### Appendix C: OPTICAL GENERATIONS OF SPIN POLARIZATION AND SPIN CURRENT

We first define the spin polarization and spin current in the ( $s+p$ )-wave superconducting (100) QWs. The temporal evolution of the total spin polarization of the system is calculated by<sup>54,139</sup>

$$\mathbf{P} \equiv (P_x, P_y, P_z) = (1/2) \sum_{\mathbf{k}} \text{Tr}(\rho_{\mathbf{k}} \boldsymbol{\alpha}) / n_0, \quad (\text{C1})$$

in which

$$\boldsymbol{\alpha} = \frac{1 + \tau_3}{2} \otimes \boldsymbol{\sigma} + \frac{1 - \tau_3}{2} \otimes \sigma_y \boldsymbol{\sigma} \sigma_y. \quad (\text{C2})$$

The velocity operator is calculated by the Heisenberg equation  $\hat{\mathbf{v}} = -i[\hat{\mathbf{r}}, \hat{H}_0(\mathbf{A} = 0)]$ . Specifically,

$$v_y = \begin{pmatrix} k_y/m^* & -i\alpha & \Delta_p f(\mathbf{k}) & 0 \\ i\alpha & k_y/m^* & 0 & -\Delta_p f^*(\mathbf{k}) \\ \Delta_p f^*(\mathbf{k}) & 0 & -k_y/m^* & i\alpha \\ 0 & -\Delta_p f(\mathbf{k}) & -i\alpha & -k_y/m^* \end{pmatrix}, \quad (\text{C3})$$

with  $f(\mathbf{k}) = (-k_x k_y + i k_x^2) / k^3$ . Then the spin current is defined as<sup>129,140–143</sup>

$$\mathbf{J}_{\hat{\mathbf{v}}}^{\hat{\alpha}} = \sum_{\mathbf{k}} \text{Tr}(\{\mathbf{v}, \boldsymbol{\alpha}\} \rho_{\mathbf{k}}) / 2. \quad (\text{C4})$$

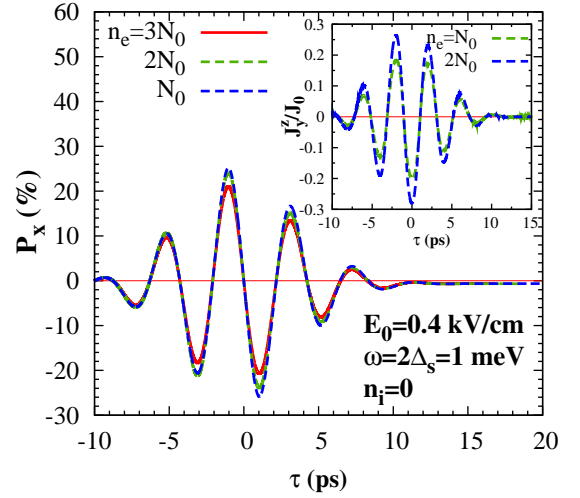


FIG. 16: (Color online) Temporal evolutions of optically-generated spin polarization with different electron densities  $n_e = N_0$  (red solid curve),  $2N_0$  (green dashed curve) and  $3N_0$  (blue dashed curve).  $E_0 = 0.4$  kV/cm. The optically-generated spin polarization is along the  $\hat{x}$ -direction, i.e., in parallel to the optically-induced supercurrent, and oscillates with the same frequency of the optical field. The spin current is presented in the inset, which is calculated according to Eq. (C4).  $J_0 = n_e k_F (k_B T_e / E_F)$  with  $k_F = \sqrt{2\pi n_e}$  and  $E_F = \pi n_e / m^*$ .

According to Eq. (C1), the temporal evolutions of the optically-generated spin polarization are shown in Fig. 16 with different electron densities  $n_e = N_0$  (red solid curve),  $2N_0$  (green dashed curve) and  $3N_0$  (blue dashed curve). It is shown that the optically-generated spin polarization is along the  $\hat{x}$ -direction, i.e., in parallel to the optically-induced supercurrent, and oscillates with the same frequency of the optical field. This is consistent with the previous studies in the system with Rashba SOC.<sup>57,72,74</sup> Furthermore, the calculated results with different electron densities show that the generated spin polarization is less influenced by the electron density. In the inset of Fig. 16, the spin current is presented, which is calculated according to Eq. (C4). It is shown

that the induced spin current is perpendicular to the total electrical current with the spin polarization being along the  $\hat{z}$ -direction, oscillating with the frequency of the optical field. By noticing that the spin current is divided by  $J_0 = n_e k_F (k_B T_e / E_F) \propto \sqrt{n_e}$  with  $k_F = \sqrt{2\pi n_e}$  and  $E_F = \pi n_e / m^*$ , our calculation further shows that the

induced spin current is also insensitive to the electron density. Finally, it is addressed that with our material parameter, the numerical calculations indicate that the superconducting order parameter has little influence on the optical generations of both the spin polarization and spin current (not shown in Fig. 16).

\* Electronic address: taoyuphy@mail.ustc.edu.cn

† Electronic address: mwww@ustc.edu.cn

- 1 M. Tinkham, *Introduction to Superconductivity* (McGraw-Hill, New York, 1975).
- 2 C. J. Pethick and H. Smith, *J. Phys. C* **13**, 6313 (1980).
- 3 *Non-Equilibrium Superconductivity*, edited by D. N. Langengerg and A. Larkin (North-Holland, Amsterdam, 1980).
- 4 *Nonequilibrium Superconductivity, Phonons, and Kapitza Boundaries*, edited by K. E. Gray (Plenum Press, New York, 1981).
- 5 N. Kopnin, *Theory of Nonequilibrium Superconductivity* (Oxford University Press, New York, 2001).
- 6 V. Chandrasekhar, in *The Physics of Superconductors*, edited by K. H. Bennemann and J. B. Ketterson (Springer-Verlag, Berlin, 2004), Vol. II.
- 7 F. S. Bergeret, A. F. Volkov, and K. B. Efetov, *Rev. Mod. Phys.* **77**, 1321 (2005).
- 8 A. I. Buzdin, *Rev. Mod. Phys.* **77**, 935 (2005).
- 9 A. J. Leggett, *Quantum Liquids* (Oxford University Press, Oxford, 2006).
- 10 Y. X. Liao and M. S. Foster, *Phys. Rev. A* **92**, 053620 (2015).
- 11 Y. Dong, L. Dong, M. Gong, and H. Pu, *Nat. Commun.* **6**, 6103 (2015).
- 12 Y. Z. Chou, Y. X. Liao, and M. S. Foster, *Phys. Rev. B* **95**, 104507 (2017).
- 13 R. A. Barankov, L. S. Levitov, and B. Z. Spivak, *Phys. Rev. Lett.* **93**, 160401 (2004).
- 14 R. A. Barankov and L. S. Levitov, *Phys. Rev. Lett.* **96**, 230403 (2006).
- 15 D. C. Mattis and J. Bardeen, *Phys. Rev.* **111**, 412 (1958).
- 16 J. R. Schrieffer, *Theory of Superconductivity* (W. A. Benjamin, New York, 1964).
- 17 S. B. Nam, *Phys. Rev.* **156**, 470 (1967); *Phys. Rev. B* **2**, 3812 (1970).
- 18 S. D. Brorson, R. Buhleier, I. E. Trofimov, J. O. White, C. Ludwig, F. F. Balakirev, H. U. Habermeier, and J. Kuhl, *J. Opt. Soc. Am. B* **13**, 1979 (1996).
- 19 Z. Dai and P. A. Lee, *Phys. Rev. B* **95**, 014506 (2017).
- 20 R. A. Kaindl, M. A. Carnahan, J. Orenstein, D. S. Chemla, H. M. Christen, H. Y. Zhai, M. Paranthaman, and D. H. Lowndes, *Phys. Rev. Lett.* **88**, 027003 (2001).
- 21 J. Demsar, R. D. Averitt, A. J. Taylor, V. V. Kabanov, W. N. Kang, H. J. Kim, E. M. Choi, and S. I. Lee, *Phys. Rev. Lett.* **91**, 267002 (2003).
- 22 R. A. Kaindl, M. A. Carnahan, D. S. Chemla, S. Oh, and J. N. Eckstein, *Phys. Rev. B* **72**, 060510(R) (2005).
- 23 R. Kaneko, I. Kawayama, H. Murakami, and M. Tonouchi, *Appl. Phys. Express* **3**, 042701 (2010).
- 24 A. Glossner, C. Zhang, S. Kikuta, I. Kawayama, H. Murakami, P. Müller, and M. Tonouchi, arXiv:1205.1684.
- 25 M. Beck, M. Klammer, S. Lang, P. Leiderer, V. V. Kabanov, G. N. Gol'tsman, and J. Demsar, *Phys. Rev. Lett.* **107**, 177007 (2011).
- 26 R. Matsunaga and R. Shimano, *Phys. Rev. Lett.* **109**, 187002 (2012).
- 27 R. Matsunaga, Y. I. Hamada, K. Makise, Y. Uzawa, H. Terai, Z. Wang, and R. Shimano, *Phys. Rev. Lett.* **111**, 057002 (2013).
- 28 R. Matsunaga, N. Tsuji, H. Fujita, A. Sugioka, K. Makise, Y. Uzawa, H. Terai, Z. Wang, H. Aoki, and R. Shimano, *Science* **345**, 1145 (2014).
- 29 R. Matsunaga, N. Tsuji, K. Makise, H. Terai, H. Aoki, and R. Shimano, arXiv:1703.02815.
- 30 Y. Nambu, *Phys. Rev.* **117**, 648 (1960).
- 31 Y. Nambu, *Rev. Mod. Phys.* **81**, 1015 (2009).
- 32 V. Ambegaokar and L. P. Kadanoff, *Il Nuovo Cimento* **22**, 914 (1961).
- 33 A. Altland and B. Simons, *Condensed Matter Field Theory* (Cambridge University Press, Cambridge, England, 2010).
- 34 P. W. Anderson, *Rev. Mod. Phys.* **38**, 298 (1966).
- 35 C. P. Enz, *Rev. Mod. Phys.* **46**, 705 (1974).
- 36 R. Côté and A. Griffin, *Phys. Rev. B* **48**, 10404 (1993).
- 37 T. Papenkort, V. M. Axt, and T. Kuhn, *Phys. Rev. B* **76**, 224522 (2007).
- 38 T. Papenkort, T. Kuhn, and V. M. Axt, *Phys. Rev. B* **78**, 132505 (2008).
- 39 N. Tsuji and H. Aoki, *Phys. Rev. B* **92**, 064508 (2015).
- 40 A. F. Kemper, M. A. Sentef, B. Moritz, J. K. Freericks, and T. P. Devereaux, *Phys. Rev. B* **92**, 224517 (2015).
- 41 M. Dzero, M. Khodas, and A. Levchenko, *Phys. Rev. B* **91**, 214505 (2015).
- 42 H. Krull, N. Bittner, G. S. Uhrig, D. Manske, and A. P. Schnyder, *Nat. Commun.* **7**, 11921 (2016).
- 43 M. Lu, H. W. Liu, P. Wang, and X. C. Xie, *Phys. Rev. B* **93**, 064516 (2016).
- 44 N. Tsuji, Y. Murakami, and H. Aoki, *Phys. Rev. B* **94**, 224519 (2016).
- 45 T. Cea, C. Castellani, and L. Benfatto, *Phys. Rev. B* **93**, 180507(R) (2016).
- 46 Y. Murotani, N. Tsuji, and H. Aoki, *Phys. Rev. B* **95**, 104503 (2017).
- 47 P. W. Anderson, *Phys. Rev.* **112**, 1900 (1958).
- 48 P. Fulde and R. A. Ferrell, *Phys. Rev.* **135**, 550 (1964).
- 49 A. I. Larkin and Yu. N. Ovchinnikov, *Zh. Eksp. Teor. Fiz.* **47**, 1136 (1964) [*Sov. Phys. JETP* **20**, 762 (1965)].
- 50 S. Takada and T. Izuyama, *Prog. Theor. Phys.* **41**, 635 (1969).
- 51 I. Khavkine, H. Y. Kee, and K. Maki, *Phys. Rev. B* **70**, 184521 (2004).
- 52 G. Tkachov and V. I. Fal'ko, *Phys. Rev. B* **69**, 092503 (2004).
- 53 F. Rohlfing, G. Tkachov, F. Otto, K. Richter, D. Weiss, G. Borghs, and C. Strunk, *Phys. Rev. B* **80**, 220507(R) (2009).

- (2009).
- <sup>54</sup> T. Yu and M. W. Wu, Phys. Rev. B **94**, 205305 (2016).
- <sup>55</sup> F. Yang and M. W. Wu, Phys. Rev. B **95**, 075304 (2017).
- <sup>56</sup> L. D. Landau and E. M. Lifshitz, *Fluid Mechanics*, 2nd ed., Vol. 6, Course of Theoretical Physics (Pergamon, Oxford, 1993).
- <sup>57</sup> J. H. Jiang, M. W. Wu, and Y. Zhou, Phys. Rev. B **78**, 125309 (2008).
- <sup>58</sup> M. J. Stephen, Phys. Rev. **139**, A197 (1965).
- <sup>59</sup> M. Tinkham and J. Clarke, Phys. Rev. Lett. **28**, 1366 (1972).
- <sup>60</sup> M. Tinkham, Phys. Rev. B **6**, 1747 (1972).
- <sup>61</sup> S. Takahashi and S. Maekawa, J. Phys. Soc. Jpn. **77**, 031009 (2008).
- <sup>62</sup> J. Clarke and M. Tinkham, Phys. Rev. Lett. **44**, 106 (1980).
- <sup>63</sup> S. Takahashi and S. Maekawa, Phys. Rev. Lett. **88**, 116601 (2002).
- <sup>64</sup> H. Kontani, J. Goryo, and D. S. Hirashima, Phys. Rev. Lett. **102**, 086602 (2009).
- <sup>65</sup> S. Takahashi and S. Maekawa, Jpn. J. Appl. Phys. **51**, 010110 (2012).
- <sup>66</sup> T. Wakamura, H. Akaike, Y. Omori, Y. Niimi, S. Takahashi, A. Fujimaki, S. Maekawa, and Y. Otani, Nat. Mater. **14**, 675 (2015).
- <sup>67</sup> H. L. Zhao and S. Hershfield, Phys. Rev. B **52**, 3632 (1995).
- <sup>68</sup> S. Li, A. V. Andreev, and B. Z. Spivak, Phys. Rev. B **92**, 100506(R) (2015).
- <sup>69</sup> A. G. Aronov, Yu. M. Galperin, V. L. Gurevich, and V. I. Kozub, in *Nonequilibrium Superconductivity*, edited by D. N. Langenberg and A. I. Larkin (Elsevier, New York, 1986)
- <sup>70</sup> J. Clarke, Phys. Rev. Lett. **28**, 1363 (1972).
- <sup>71</sup> J. Clarke, B. R. Fjordbøge, and P. E. Lindelof, Phys. Rev. Lett. **43**, 642 (1979).
- <sup>72</sup> J. L. Cheng and M. W. Wu, Appl. Phys. Lett. **86**, 032107 (2005).
- <sup>73</sup> M. W. Wu, J. H. Jiang, and M. Q. Weng, Phys. Rep. **493**, 61 (2010).
- <sup>74</sup> L. E. Golub and E. L. Ivchenko, New J. Phys. **15**, 125003 (2013).
- <sup>75</sup> T. Misawa, T. Yokoyama, and S. Murakami, Phys. Rev. B **84**, 165407 (2011).
- <sup>76</sup> M. Sgrist and K. Ueda, Rev. Mod. Phys. **63**, 239 (1991).
- <sup>77</sup> M. Eschrig, Phys. Today **64**, 43 (2011).
- <sup>78</sup> J. Linder and T. Yokoyama, Phys. Rev. B **83**, 012501 (2011).
- <sup>79</sup> I. Kulagina and J. Linder, Phys. Rev. B **90**, 054504 (2014).
- <sup>80</sup> J. Linder and J. W. A. Robinson, Nat. Phys. **11**, 307 (2015).
- <sup>81</sup> M. Eschrig, Rep. Prog. Phys. **78**, 104501 (2015).
- <sup>82</sup> S. H. Jacobsen, I. Kulagina, and J. Linder, Sci. Rep. **6**, 23926 (2016).
- <sup>83</sup> G. Tkachov, Phys. Rev. Lett. **118**, 016802 (2017).
- <sup>84</sup> F. S. Bergeret and I. V. Tokatly, Phys. Rev. Lett. **110**, 117003 (2013); Phys. Rev. B **89**, 134517 (2014).
- <sup>85</sup> A. D. Bernardo, S. Diesch, Y. Gu, J. Linder, G. Divitini, C. Ducati, E. Scheer, M. G. Blamire, and J. W. A. Robinson, Nat. Commun. **6**, 8053 (2015).
- <sup>86</sup> Y. Kalcheim, O. Millo, A. D. Bernardo, A. Pal, and J. W. A. Robinson, Phys. Rev. B **92**, 060501(R) (2015).
- <sup>87</sup> V. L. Berezinskii, JETP Lett **20**, 287 (1974).
- <sup>88</sup> A. J. Leggett, Rev. Mod. Phys. **47**, 331 (1975).
- <sup>89</sup> H. Takayanagi and T. Kawakami, Phys. Rev. Lett. **54**, 2449 (1985).
- <sup>90</sup> T. Akazaki, H. Takayanagi, J. Nitta, and T. Enoki, Appl. Phys. Lett. **68**, 418 (1996).
- <sup>91</sup> K. M. H. Lenssen, M. Matters, and C. J. P. M. Harmans, Appl. Phys. Lett. **63**, 2079 (1993).
- <sup>92</sup> T. D. Moore and D. A. Williams, Phys. Rev. B **59**, 7308 (1999).
- <sup>93</sup> Z. Wan, A. Kazakov, M. J. Manfra, L. N. Pfeiffer, K. W. West, and L. P. Rokhinson, Nat. Commun. **6**, 7426 (2015).
- <sup>94</sup> H. Haug and A. P. Jauho, *Quantum Kinetics in Transport and Optics of Semiconductors* (Springer, Berlin, 1996).
- <sup>95</sup> V. M. Axt and S. Mukamel, Rev. Mod. Phys. **70**, 145 (1998).
- <sup>96</sup> F. Rossi and T. Kuhn, Rev. Mod. Phys. **74**, 895 (2002).
- <sup>97</sup> P. Lipavský, V. Špička, and B. Velický, Phys. Rev. B **34**, 6933 (1986).
- <sup>98</sup> M. Levanda and V. Fleurov, J. Phys.: Condens. Matter **6**, 7889 (1994).
- <sup>99</sup> B. Y. Sun and M. W. Wu, New J. Phys. **15**, 083038 (2013).
- <sup>100</sup> M. E. Peskin and D. V. Schroeder, *An Introduction to Quantum Field Theory* (Addison-Wesley, New York, 1995).
- <sup>101</sup> J. Bardeen, G. Rickayzen, and L. Tewordt, Phys. Rev. **113**, 982 (1959).
- <sup>102</sup> B. D. Josephson, Phys. Lett. **1**, 251 (1962).
- <sup>103</sup> T. Yu and M. W. Wu, Phys. Rev. B **93**, 195308 (2016).
- <sup>104</sup> A. D. Hillier, J. Quintanilla, B. Mazidian, J. F. Annett, and R. Cywinski, Phys. Rev. Lett. **109**, 097001 (2012).
- <sup>105</sup> P. Vogl, in *Physics of Nonlinear Transport in Semiconductor*, edited by K. Ferry, J. R. Barker, and C. Jacoboni (Plenum, New York, 1980).
- <sup>106</sup> J. Zhou, J. L. Cheng, and M. W. Wu, Phys. Rev. B **75**, 045305 (2007).
- <sup>107</sup> K. Huang, *Statistical Mechanics*, 2nd. ed. (John Wiley & Sons, New York, 1987).
- <sup>108</sup> L. P. Kadanoff and G. Baym, *Quantum Statistical Mechanics* (W. A. Benjamin, Inc., New York, 1962).
- <sup>109</sup> *Semiconductors*, Landolt-Börnstein, New Series, Vol. 17a, ed. by O. Madelung (Springer, Berlin, 1987).
- <sup>110</sup> F. Yang and M. W. Wu, arXiv:1704.00409.
- <sup>111</sup> S. Takada, Prog. Theor. Phys. **43**, 27 (1970).
- <sup>112</sup> E. M. Lifshitz and L. P. Pitaevskii, *Physical Kinetics* (Pergamon, London, 1981); G. E. Uhlenbeck, G. W. Ford, and E. W. Montroll, *Lectures in Statistical Mechanics* (American Mathematical Society, Providence, 1963), Chap. IV; V. F. Gantmakher and Y. B. Levinson, *Carrier Scattering in Metals and Semiconductors* (North-Holland, Amsterdam, 1987), Chap. 6.
- <sup>113</sup> H. Fröhlich and B. V. Paranjape, Proc. Phys. Soc. London, Sect. B **69**, 21 (1956); K. Hess, in *Physics of Nonlinear Transport in Semiconductors*, edited by D. K. Ferry, J. R. Barker, and C. Jacoloni (Plenum, New York, 1980), p. 1; D. K. Ferry, in *Physics of Nonlinear Transport in Semiconductors*, edited by D. K. Ferry, J. R. Barker, and C. Jacoloni (Plenum, New York, 1980), p. 117; K. Seeger, *Semiconductor Physics* (Springer-Verlag, Berlin, 1982).
- <sup>114</sup> T. Yu and M. W. Wu, J. Phys.: Condens. Matter **27**, 255001 (2015).
- <sup>115</sup> N. Nagaosa, J. Sinova, S. Onoda, A. H. MacDonald, and N. P. Ong, Rev. Mod. Phys. **82**, 1539 (2010).
- <sup>116</sup> N. A. Sinitsyn, J. Phys.: Condens. Matter **20**, 023201



- (2008).
- <sup>117</sup> S. Murakami, Phys. Rev. B **69**, 241202(R) (2004).
- <sup>118</sup> G. E. Blonder, M. Tinkham, and T. M. Klapwijk, Phys. Rev. B **25**, 4515 (1982).
- <sup>119</sup> M. I. D'yakanov and V. I. Perel', Zh. Eksp. Teor. Fiz. **60**, 1954 (1971) [Sov. Phys. JETP **33**, 1053 (1971)].
- <sup>120</sup> *Optical Orientation*, edited by F. Meier and B. P. Zakharchenya (North-Holland, Amsterdam, 1984).
- <sup>121</sup> *Semiconductor Spintronics and Quantum Computation*, edited by D. D. Awschalom, D. Loss, and N. Samarth (Springer, Berlin, 2002).
- <sup>122</sup> I. Žutić, J. Fabian, and S. D. Sarma, Rev. Mod. Phys. **76**, 323 (2004).
- <sup>123</sup> J. Fabian, A. M. Abiague, C. Ertler, P. Stano, and I. Žutić, Acta Phys. Slov. **57**, 565 (2007).
- <sup>124</sup> *Spin Physics in Semiconductors*, edited by M. I. D'yakonov (Springer, Berlin, 2008).
- <sup>125</sup> T. Korn, Phys. Rep. **494**, 415 (2010).
- <sup>126</sup> *Handbook of Spin Transport and Magnetism*, edited by E. Y. Tsympal and I. Žutić (Boca Raton, FL: CRC press, 2011).
- <sup>127</sup> M. W. Wu and C. Z. Ning, Eur. Phys. J. B **18**, 373 (2000); M. W. Wu, J. Phys. Soc. Jpn. **70**, 2195 (2001).
- <sup>128</sup> L. Wang and M. W. Wu, Phys. Rev. B **89**, 115302 (2014).
- <sup>129</sup> T. Yu and M. W. Wu, Phys. Rev. B **93**, 045414 (2016).
- <sup>130</sup> L. P. Gor'kov and E. I. Rashba, Phys. Rev. Lett. **87**, 037004 (2001).
- <sup>131</sup> E. Bauer, G. Hilscher, H. Michor, Ch. Paul, E. W. Scheidt, A. Griбанov, Yu. Seropegin, H. Noël, M. Sigrist, and P. Rogl, Phys. Rev. Lett. **92**, 027003 (2004).
- <sup>132</sup> T. Yokoyama, Y. Tanaka, and J. Inoue, Phys. Rev. B **72**, 220504(R) (2005).
- <sup>133</sup> Y. Tanaka, T. Yokoyama, A. V. Balatsky, and N. Nagaosa, Phys. Rev. B **79**, 060505(R) (2009).
- <sup>134</sup> J. M. Jancu, R. Scholz, E. A. de Andrada e Silva, and G. C. La Rocca, Phys. Rev. B **72**, 193201 (2005).
- <sup>135</sup> Actually, in our framework beyond the Boltzmann equation, even without the drive effect, the electron-impurity scattering also suppresses the oscillation amplitude of the Higgs mode due to the pump effect. This is because in the electron-impurity scattering terms, i.e., Eqs. (A2) and (A3), both the quasiparticle correlation and population are still influenced by the impurity. The details are addressed in Sec. II C 2.
- <sup>136</sup> O. Klein, E. J. Nicol, K. Holczer, and G. Grüner, Phys. Rev. B **50**, 6307 (1994).
- <sup>137</sup> T. Cea, D. Bucheli, G. Seibold, L. Benfatto, J. Lorenzana, and C. Castellani, Phys. Rev. B **89**, 174506 (2014).
- <sup>138</sup> U. S. Pracht, T. Cea, N. Bachar, G. Deutscher, E. Farber, M. Dressel, M. Scheffler, C. Castellani, A. M. Garcia-Garcia, and L. Benfatto, arXiv:1705.03252.
- <sup>139</sup> H. Shiba, Prog. Theor. Phys. **40**, 435 (1968).
- <sup>140</sup> J. Sinova, D. Culcer, Q. Niu, N. A. Sinitsyn, T. Jungwirth, and A. H. MacDonald, Phys. Rev. Lett. **92**, 126603 (2004).
- <sup>141</sup> A. Khaetskii, Phys. Rev. B **73**, 115323 (2006).
- <sup>142</sup> M. Glazova and A. Kavokin, J. Lumin. **125**, 118 (2007).
- <sup>143</sup> K. Shen, R. Raimondi, and G. Vignale, Phys. Rev. B **90**, 245302 (2014).